

UNU FILE COPY

AD A073559

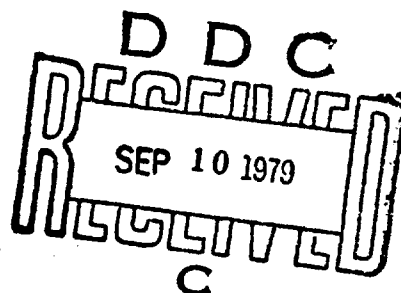
LEVEL II

1062.981

AFOSR Grant Number: 77 - 3440

DEVELOPMENT OF IMPROVED HIGH STRENGTH ALUMINUM
POWDER METALLURGY PRODUCTS

EOARD-TR-79-3



by

David P. Voss
Materials Research Institute
German Aerospace Research Establishment (DFVLR)
Köln, Germany

Progress Report # 2

31 December 1978

This report is intended only for internal management use.

Prepared for

Deutsche Forschungs- und Versuchsanstalt für Luft- und Raumfahrt
(DFVLR), Institut für Werkstoff-Forschung, 5000 Köln, Germany

and

This document has been approved
for public release and sale; its
distribution is unlimited.

European Office of Aerospace Research and Development,
London, England

79 09 6 012

EOARD TR-79-3

14 August 1979

This report has been reviewed by the Information Office (EOARD/CMI) and is releasable to the National Technical Information Service (NTIS). At NTIS it will be releasable to the general public, including foreign nationals.

This technical report has been reviewed and is approved for publication.

John T. Milton

JOHN T. MILTON
Scientific and Technical
Information Officer

Gordon L. Hermann

GORDON L. HERMANN
Lt Colonel, USAF
Chief, Structures and Materials

FOR THE COMMANDER

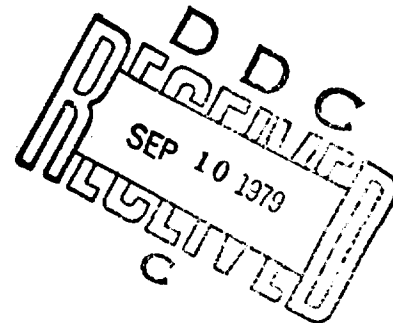
Gordon L. Hermann

GORDON L. HERMANN
Lt Colonel, USAF
Deputy Commander

DFVLR Deutsche Forschungs- und Versuchsanstalt
für Luft- und Raumfahrt e.V.

- Institut für Werkstoff-Forschung -
Linder Höhe, 5000 Köln 90, Germany

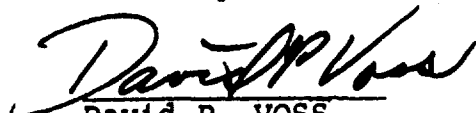
U.S. Air Force
AFOSR Grant No. 77-3440
EOARD P.R. No. G77-0004



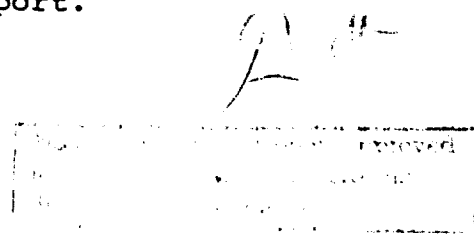
Development of Improved High Strength
Aluminum P/M Products

Second Progress Report
for the period
June 1, 1978 to December 31, 1978

This progress report was prepared for management purposes. It is a preliminary report of information generated during the initial phase of this investigation, and as such, the data and conclusions reported may be subject to major change. This report will be replaced by a Final Report.


David P. VOSS
Project Engineer


Dr. G. Wirth
Chief, Materials Technology and
High Temperature Strengths



79 09 6 012

REPORT DOCUMENTATION PAGE		READ INSTRUCTIONS BEFORE COMPLETING FORM
1. Report Number EDARD TR-79-3	2. Govt Accession No.	3. Recipient's Catalog Number
4. Title (and Subtitle) DEVELOPMENT OF IMPROVED HIGH STRENGTH ALUMINUM POWDER METALLURGY PRODUCTS	5. Type of Report & Period Covered Progress Report. # 10-2 1 June 1978 - December 31, 1978	6. Performing Org. Report Number DFVLR-IB-354 - 78/11
7. Author(s) DAVID P. VOSS (USAF)	8. Contract or Grant Number AFOSR Grant - 77 - 3440 EDARD - 77 - 0024	9. Program Element, Project, Task Area & Work Unit Numbers P.E. 61102 F Proj Task 2301/D1
10. Performing Organization Name and Address Institute for Materials Research DFVLR Postfach 90 60 58 D-5000 Cologne 90	11. Controlling Office Name and Address European Office of Aerospace Research and Development/LNM Box 14 FPO New York 09510	12. Report Date 31 December 1978
13. Monitoring Agency Name and Address DL	14. Number of Pages 145	15. 2301
16. & 17. Distribution Statement Approved for public release; distribution unlimited.		
18. Supplementary Notes Research was also supported with DFVLR money and facilities.		
19. Key Words Rapidly Solidified Powders, Atomization, Prealloyed Aluminum Powder, Powder Metallurgy, Aluminum Powder Alloys, Vacuum Degassing, Vacuum Hot Pressing, Extrusion, P/M Mechanical Properties, 2024, 7075, Fatigue		
20. Abstract: An investigation of high strength aluminum 2024 and 7075 alloys was conducted. Both powder metallurgy (P/M) and conventional ingot metallurgy (I/M) extrusion products were examined with particular attention devoted to fatigue behavior. The P/M alloys were produced from prealloyed, air atomized powders of various average particle diameters (APD) using carefully controlled fabrication procedures. The most significant step was a full vacuum preheat treatment of 80% dense compacts which controlled hydrogen contents of the P/M products, thereby producing equivalent hydrogen contents in both the P/M and I/M alloy products. Laboratory ingots were also produced with chemical compositions and processing parameters identical to those of P/M products. Notch K_t=3 HCF testing (R=0.1) was conducted to maximize the likelihood that HCF differences, if they occurred, would be statistically and metallurgically significant. Fatigue tests were conducted in lab air to simulate service environment, however, testing frequency (100 Hz) would tend to reduce any environmental effect.		

The products investigated included: (1) unidirectional, isothermally vacuum hot-pressed (610 MPa with 10 min dwell at 733 K for 7075 and 753 K for 2024) P/M billets, and (2) extrusions of the I/M and hot-pressed P/M billets (extrusion - preheat 643 K with 10:1 and 25:1 direct extrusion ratios). Extrusion parameters were selected based on the previously reported P/M processing study [1]. Typical longitudinal properties for the 7075 products are shown below.

	UTS (MPa)	0.2%YS (MPa)	R.A. (%)	e(4D) (%)	NTS/YS	S_{10^7} (MPa)
P/M* hot-pressed (T6)	584	510	9.1	6.5	1.09	---
P/M* hot-pressed and 25:1 extruded (T6510)	671	622	14.5	14.0	1.20	145
I/M 25:1 extruded (T6510)	679	627	17.3	12.6	1.30	105

*88 μ m APD powder which was vacuum canned prior to hot-pressing.

The 7075 alloy 25:1 direct extrusions were produced with equivalent yield strengths in the artificially aged T6510 condition; the notch HCF strength ($N=10^7$ cycles) of the P/M product showed a 38 % improvement over the I/M alloy product and a 45 % improvement over literature values of an extruded commercial ingot tested under similar conditions.

The strength, fracture toughness (NTS/YS), ductility, and $K_{t=3}$ notch HCF strength for the longitudinal direction of P/M 2024-T3510 extrusions produced from powders of various APDs (36-117 μ m) did not show a significant variation with APD. Similarly the transverse strength, fracture toughness (NTS/YS), and ductility properties are also independent of the initial powder APD over the range 44-117 μ m. The strengths of extruded P/M 2024 alloy products in the artificially aged condition are equivalent to the I/M alloy. However, the extrusion - preheat temperature appeared to slightly influence the strength of the artificially aged P/M products: for example, the longitudinal strength increased by an average of 21 MPa (5 % increase) for extrusions given a 643 K extrusion - preheat versus 753 K. The transverse mechanical properties of 10:1 P/M 2024-T4 extrusions given a 643 K extrusion-preheat, shown below, reveal the combined level of deformation and hydrogen/contaminant removal is sufficient to produce a sound P/M product.

	UTS (MPa)	0.2%YS (MPa)	R.A. (%)	e(4D) (%)	NTS/YS*
P/M (82 μ m APD)	506	355	26.0	23.5	1.75
I/M	470	305	14.8	20.7	1.90

*products tested with reduced specimens and exceeded the ASTM 1.3 NTS/YS rule for validity, some yielding was observed.

The naturally aged, unrecrystallized 2024-T3510 extrusion products show a definite grain size-yield strength relationship for grain sizes below a threshold grain width value of 8 μ m. The most significant grain size variations are obtained from processing variations and not from initial powder APD variations.

Table of Contents

	Page
Abstract (Form 1473)	i
Index to Symbols	iv
Alloy and Heat Treatments	vii
List of Illustrations	viii
List of Tables	xiii
Objective	1
Introduction	2
Procedures	7
Results	10
Discussion	40
Conclusion	52
Appendix A	55
Future Research Effort	57
References	58
Acknowledgements	58
Illustrations (Figures)	69
Tables	107

Accession For	
NTIS GRA&I	<input checked="" type="checkbox"/>
DDC TAB	<input type="checkbox"/>
Unannounced	<input type="checkbox"/>
Justification	
By	
Distribution	
Accession for	
Dist	

Index to Symbols/Abbreviations

A	area of cross-section
A_0	initial area
A_f	area at fracture
APD	average particle diameter of powder by weight
ASTM	American Society for Testing Materials
B	thickness of compact specimen
C_{vol}	compression ratio of powder (compaction ratio)
δ_4	see e
D	diameter
ϕ	diameter
DCS	dendritic cell size
da/dN	fatigue crack growth rate
E	modulus of elasticity
e	engineering elongation, measured over a length equal to four times the diameter of the specimen (tabulated values are elongation at fracture)
ϵ	true strain = $\ln(1+e)$ or $\ln(A_0/A)$
ϵ_f	true fracture strain
f	frequency
g_{\perp}	average subgrain size perpendicular to extrusion direction
$g_{//}$	average subgrain size parallel to extrusion direction
G_{\perp}	average grain size perpendicular to extrusion direction
$G_{//}$	average grain size parallel to extrusion direction
$G_{//}/G_{\perp}$	average grain size aspect ratio
h	hour
HCF	high cycle fatigue
HERF	high energy rate forming
HIP	hot isostatic press

[Hz]	frequency (cycles per second)
I/M	ingot metallurgy
ITMT	intermediate thermal mechanical treatment
[K]	temperature in degrees Kelvin
ΔK	stress intensity factor
K_C	plane stress fracture toughness
K_{IC}	plane strain fracture toughness
K_Q	candidate plane strain fracture toughness (after ASTM E399)
K_t	theoretical stress concentration factor ($= \alpha_K$)
k	strength coefficient (true stress at true strain of unity)
L	longitudinal (extrusion) direction
\bar{L}_p	mean particle intercept length
\bar{l}_g	mean grain intercept length
\bar{l}_s	mean subgrain intercept length
LCF	low cycle fatigue
λ	mean free distance between particles (straight line) spacing parameter
[MPa]	[N/mm ²]
n	strain-hardening coefficient
N	number of cycles
NTS	notch tensile strength
NTS/YS	notch tensile strength yield strength ratio
0.2%CYS	0.2 % compressive yield strength
0.2%YS	0.2 % yield strength (tensile)
Ω	grain shape parameter (degree of orientation)
p_x	partial pressure of x
P	probability of failure [%] or total pressure [Pa]
P/M	powder metallurgy
ψ	see R.A.

ρ	density
R	stress ratio (minimum/maximum)
R.A.	reduction in area
R_B	Rockwell hardness - B scale
RT	room temperature
S or σ	stress
σ'	true stress
σ_B	see UTS
σ_f	true stress at fracture
σ_p	mean center to center particle spacing
σ_{BK}	see NTS
S_N	mean fatigue strength at N cycles
S_N^P	mean fatigue strength at N cycles for P percent failure.
SEM	scanning electron microscope
SHT	solution heat treatment
ST	short transverse direction
S_v	grain boundary area per unit volume
T	transverse direction or temperature [K]
TEM	transmission electron microscope
TMT	thermal mechanical treatment
U	average solidification rate
UTS	ultimate tensile strength
v/o (vol.%)	volume percent
VPCP	volume percent coarse (constituent) particles
VPSP	volume percent second phase
YS	yield strength
w/o (wt.%)	weight percent

Alloy and Heat Treatment Designations
(after Aluminum Association)

2000 (or 2XXX) type aluminum alloys based on Al-Cu-Mg

7000 (or 7XXX) " " " " " Al-Zn-Mg-Cu

Alloy and Temper	Solution ^{a,b)} Heat Treatment Temperature	Water Quench Temperature	Stress ^{c,d)} Relief or TMT	Aging Treatment
2024-T3510	766 K	RT	1½ % stretch	7-10 days RT (natural age)
-T4	"	"	none	"
-T6	"	"	none	12 h at 464 K (artificial age)
-T8510	"	"	1½ % stretch	11 h at 464 K (artificial age)
-T85X0	"	"	X % " (TMT)	"
-T8570	"	"	7-8 % " "	8 h at 464 K (artificial age)
7X75 (includes 7475 and 7075)				
-T6	743 K	RT	none	3-5 days RT+24 h 394 K
-T611	"	373 K	none	" + "
-T6510	"	RT	1½ % stretch	" + "
-T6510X	"	"	"	" +70 h 394 K
-T652	"	"	3-4 % compression	" +24 h 394 K
-T73510	"	"	1½ % stretch	" + 6 h 394 K + 8 h 450 K

a) Time as per MIL-H-6088 E Specification, Heat Treatment of Aluminum Alloys

- 1 h in salt or 1½ h in air for 10:1 and 25:1 extrusion products
- 3½ h in air for vacuum hot-pressed ø 70 mm products prior to compaction

b) SHT in salt unless otherwise noted

c) Within 1 hour after quench and without any additional straightening

d) Without stress relief: T4 and T6

LIST OF ILLUSTRATIONS

FIGURE 1

Mechanical properties of 7X75 type aluminum alloys ...

FIGURE 2

Indication of strength variation and mechanical property anisotropy for 7075-T6 P/M and I/M extrusion products

FIGURE 3

Notch $K_t = 3$ constant load amplitude axial fatigue response of P/M 7075-T6510 extrusions which were produced with identical chemical composition to control I/M 7075 extrusions

FIGURE 4

Notch $K_t = 3$ constant load amplitude axial fatigue response of control I/M 7075-T6510 extrusions which were produced with identical chemical composition to P/M 7075 extrusions

FIGURE 5

Notch $K_t = 3$ constant load amplitude axial fatigue response of P/M and control I/M 7075-T6510 extrusion products produced and tested under identical conditions - 25:1 extrusion ratio with 643 K extrusion-preheat ..

FIGURE 6

Notch $K_t = 3$ constant load amplitude axial fatigue response of P/M and I/M 7075-T6510 extrusions

FIGURE 7

Notch $K_t = 3$ constant load amplitude axial fatigue response of vacuum hot-pressed P/M 7075-T6

FIGURE 8

Back-reflection pinhole X-ray patterns for 7075 (a) I/M and (b) P/M 25:1 extrusion products with 643 K extrusion-preheat

LIST OF ILLUSTRATIONS (CONTINUED)

FIGURE 9

Optical micrographs under polarized light of solution heat treated, lightly polished and unetched surface of 7075

FIGURE 10

Optical micrographs of lightly polished and unetched surfaces shown in Figure 9, under unpolarized light, of 7075

FIGURE 11

Representative optical micrographs of lightly etched 7075 aluminum alloy 10:1 extrusions

FIGURE 12

EDAX patterns of intensity vs the element's characteristic energy level for representative iron containing Al-Fe-Cu second phase particles in 7075-T6510 extrusions

FIGURE 13

Representative optical micrographs of 7075-T6510 P/M 25:1 Direct Extrusions, with 643 K extrusion-preheat, parallel to extrusion direction

FIGURE 14

Representative optical micrograph of 7075-T6510 I/M 25:1 Direct Extrusions, with 643 K extrusion-preheat, parallel to extrusion direction

FIGURE 15

Representative optical micrograph of 7075-T6510 I/M 25:1 Direct Extrusions, with 643 K extrusion-preheat, parallel to extrusion direction

FIGURE 16

Transmission electron micrographs of an as-extruded 7075 I/M 25:1 extrusion produced with a 643 K extrusion-preheat

LIST OF ILLUSTRATIONS (CONTINUED)

FIGURE 17

Transmission electron micrographs of a as-extruded
7075 P/M 25:1 extrusion produced with a 643 K
extrusion-preheat

FIGURE 18

Transmission electron micrograph of a solution heat
treated 7075 I/M 25:1 extrusion produced with a
643 K extrusion-preheat

FIGURE 19

Transmission electron micrograph of a solution heat
treated 7075 P/M 25:1 extrusion produced with a
643 K extrusion-preheat

FIGURE 20

Scanning electron fractographs of a tensile fracture
surface. The tensile specimen was machined from the
transverse direction of a 10:1 P/M 7075-T6 extrusion
produced with a 643 K extrusion-preheat

FIGURE 21

Scanning electron fractographs of a tensile fracture
surface. The tensile specimen was machined from the
transverse direction of a 10:1 I/M 7075-T6 extrusion
produced with a 643 K extrusion-preheat

FIGURE 22

Scanning electron fractographs of a tensile fracture
surface. The tensile specimen was machined from the
transverse direction of a 5.54:1 P/M 7075-T6 extru-
sion produced with a 643 K extrusion-preheat

FIGURE 23

Mechanical properties of 2024 type aluminum alloys ..

FIGURE 24

Aging response of P/M and I/M 2024 extrusion product
and effect of extrusion-preheat temperature on aging
response of the P/M extrusion products

LIST OF ILLUSTRATIONS (CONTINUED)

FIGURE 25

Notch $K_t = 3$ constant load amplitude axial fatigue response of P/M 2024-T3510 extrusions which were produced with identical chemical composition to control I/M 2024 extrusions

FIGURE 26

Notch $K_t = 3$ constant load amplitude axial fatigue response of control I/M 2024-T3510 Alloy C extrusions which were produced with identical chemical composition to P/M 2024 extrusions

FIGURE 27

Notch $K_t = 3$ constant load amplitude axial fatigue response of P/M and I/M 2024-T3510 extrusion products

FIGURE 28

Normalized notch $K_t = 3$ constant load amplitude axial fatigue response of P/M and I/M 2024-T3510 extrusion products

FIGURE 29

Notch $K_t = 3$ constant load amplitude axial fatigue response of a P/M 2024-T3510 extrusion product manufactured from powder with a 117 μm APD and with a 753 K extrusion-preheat

FIGURE 30

Notch $K_t = 3$ constant load amplitude axial fatigue response of a P/M 2024-T3510 extrusion product manufactured from powder with a 82 μm APD and with a 753 K extrusion-preheat

FIGURE 31

Notch $K_t = 3$ constant load amplitude axial fatigue response of a P/M 2024-T3510 extrusion product manufactured from powder with a 36 μm APD and with a 753 K extrusion-preheat

FIGURE 32

Representative optical micrographs of the grain structure of 2024-T3510 I/M 25:1 direct extrusions ..

LIST OF ILLUSTRATIONS (CONTINUED)

FIGURE 33

Representative optical micrograph of the grain
structure of a 2024-T3510 P/M 26.1:1 direct
extrusion

FIGURE 34

Representative optical micrographs of the grain
structure of 2024-T3510 P/M 25:1 direct extrusions

FIGURE 35

Longitudinal yield strength of 2024-T3510 extrusion
products as a function of the reciprocal of the long
transverse grain width

LIST OF TABLES

TABLE 1

Chemical analysis of powder and ingot materials as determined from the wrought aluminum products

TABLE 2

Mechanical properties of 7X75-T6 extrusions with 643 K extrusion-preheat

TABLE 3

Longitudinal mechanical properties of 7X75-T6510 extrusions with 643 K extrusion-preheat

TABLE 4

Mechanical properties of vacuum hot-pressed 7075-T6 and 2024-T351 products produced from air atomized, pre-alloyed powder.

TABLE 5

Effect of direction on the 0.2 % compressive yield stress of 7X75-T6 extrusions

TABLE 6

Influence of elevated solution heat treatment temperature on the mechanical properties of 7075-T6 extrusions

TABLE 7

Density measurements of 7075 P/M and I/M products

TABLE 8

Quantitative metallographic characterization of the coarse intermetallic particles for P/M and I/M 7X75 aluminum alloy 10:1 extrusion products

LIST OF TABLES (CONTINUED)

TABLE 9

Influence of relative amount of volume percent second phase on fracture toughness, as measured by notch tensile strength to yield strength ratio for various 7X75 aluminum alloy extrusion products

TABLE 10

Quantitative metallographic values for the grain morphology of 7X75-T6510 aluminum alloy 25:1 extrusion products

TABLE 11

Influence of evacuation-preheat environment

TABLE 12

Characterization of 2024 alloy powders investigated for this report

TABLE 13

Natural aging response of P/M and I/M 2024-T3510 aluminum alloy extrusion products manufactured with various extrusion-preheat temperatures and extrusion ratios ...

TABLE 14

Natural aging response of P/M and I/M 2024-T4 extrusions manufactured with various extrusion-preheat temperatures and extrusion ratios

TABLE 15

Artificial aging response of P/M and I/M 2024-T6 aluminum alloy extrusion products manufactured with a 25:1 extrusion ratio and various extrusion-preheat temperatures

TABLE 16

Artificial aging response of P/M and I/M 2024-T8510 aluminum alloy extrusion products manufactured with various extrusion-preheat temperatures and extrusion ratios

LIST OF TABLES (CONTINUED)

TABLE 17

Response P/M and I/M 2024 aluminum alloy extrusion products manufactured with 643 K extrusion-preheat and various extrusion ratios, to thermal mechanical treatments of 2 and 4 % tensile plastic deformation before artificial aging

TABLE 18

Response of P/M and I/M 2024 aluminum alloy extrusion products manufactured with a 25:1 extrusion ratio and various extrusion-preheat temperatures, to thermal mechanical treatment of 7-8 % tensile plastic deformation before artificial aging

TABLE 19

Longitudinal mechanical properties of P/M 2024-T4 extrusion products

TABLE 20

Transverse mechanical properties of P/M 2024-T4 extrusion products

TABLE 21

Quantitative metallographic characterization of the coarse intermetallic particles for P/M and I/M 2024 aluminum alloy 25:1 extrusion products

TABLE 22

Quantitative metallographic values for the grain morphology of P/M and I/M 2024-T3510 aluminum alloy extrusion products

TABLE 23

Effect of microstructure on longitudinal mechanical properties of 2024-T3510 extrusion products, with 25:1 ratio for round and 25.78:1 for the channel

OBJECTIVE

The objective of this investigation is to develop an understanding of the effect of processing on the microstructure and mechanical properties of high strength P/M aluminum alloys, and to establish the degree to which the P/M approach influences the ultimate performance of high strength aluminum products under fatigue limiting conditions. Fabrication processes, mechanical properties, and microstructures of 2024 and 7075 aluminum alloy P/M products are characterized in order to develop this understanding and also to establish an optimum processing scheme for producing high strength aluminum alloy P/M products with the best possible fatigue behavior.

INTRODUCTION

The work reported herein is part of a continuing investigation [1] aimed at the development of an understanding of the processing-microstructure-mechanical property interrelationships for high strength aluminum powder metallurgy (P/M) alloys. Particular emphasis is devoted to the study of the effects of processing and microstructure on the fatigue responses of the 2024 (AlCuMg2) and 7075 (AlZnMgCu1.5) P/M alloys and their respective conventional ingot metallurgy (I/M) alloys.

Over the total spectrum of aluminum P/M alloys, only a few investigations of the fatigue behavior of these alloys have been reported, and of these a limited number have studied the microstructure-fatigue relationship. These investigations are summarized below.

Grosch and Jäniche [2] reported smooth S-N fatigue strength of extruded (12.7:1) and unannealed aluminum (99.5 %) P/M and I/M products at 10^8 cycles. The P/M products showed about a 30 % improvement in fatigue strength over the I/M products. When the fatigue strengths were normalized with ultimate tensile strength, the smooth fatigue improvement was found to be due to the P/M product's strength increase.

Lyle et al. [3] investigated the smooth and notch S-N fatigue behavior of two aluminum P/M alloys with compositions similar to I/M alloys 2014 and 6061. The P/M products were produced from blends of atomized, elemental powders which were liquid phase sintered in a protective atmosphere and hot-worked. This processing developed P/M products with strength properties and fatigue endurance limits ($5 \cdot 10^8$ cycles) comparable to their respective I/M counterparts. Subsequent fatigue behavior examinations [4-10] have been directed at investigating the effect of processing improvements and alloying, and have not investigated the fatigue behavior of the same I/M and air atomized P/M alloy processed in the same manner.

The effect of alloying was investigated by Lyle and Cebulak [4],

and Cebulak and Truax [5] using prealloyed 7XXX (Al-Zn-Mg-Cu) type aluminum alloy powders produced by air atomization. For P/M extrusion products fabricated from powder compacts preheated in flowing argon, they reported improved smooth S-N fatigue behavior over I/M 7075 at equal tensile and yield strengths, as well as an improved smooth fatigue response for P/M products with increased strength properties greater than those of 7075-T6. However, the notch S-N fatigue behavior of the 7XXX type P/M alloy products was only equal to the I/M 7075 alloy. With alloy optimization, i.e. 7XXX type P/M alloys with 0.4 wt.% or 1.5 wt.% Co, Cebulak et al. [6,7] reported a significant improvement in the notch fatigue ($K_t = 3$) behavior of these alloys over the behavior of an extruded laboratory ingot (7075-T6) and a commercial extrusion product (7075-T651). However, these findings are based on limited testing, from which very few test specimens from each of the three P/M products investigated (1.5 wt.% Co: lab billet with argon preheat and 10:1 extrusion, and 1400 kg billet with full vacuum preheat and 12.1:1 extrusion; 0.4 wt.% Co: 1392 kg billet with full vacuum preheat and 12.1:1 extrusion) did not fail, but which did show significantly longer lives to failure at each stress level investigated. If one does assume the highest stress level for which no failure occurred below $N = 2 \cdot 10^7$ cycles as the endurance limit (S_N), normalization of the endurance limit with the product's tensile yield strength shows a significant improvement in the fatigue response beyond that resulting from the P/M product's yield strength improvement. Indeed, if the required substantial testing [6] confirms the improvement in fatigue behavior shown below,

			$S_N(\text{MPa}) / \sigma_{0.2\%}(\text{MPa})$
P/M	1.5 wt.% Co	lab billet	152/655 = 0.232
P/M	1.5 wt.% Co	mill billet	138/550 = .251
P/M	0.4 wt.% Co.	mill billet	124/515 = .241
I/M	7075-T6	-	120/600 = .200

a significant increase in fatigue performance will have been attained through alloying and extension of solid solubility afforded by P/M processing. Otto [8] has investigated production

parameters (composition and processing) controlling the fatigue crack growth (FCG) in these two Co containing alloys, and a continuing investigation [9] is being conducted to optimize these production parameters and study the reproducibility of the FCG data base for these alloys.

Koczak et al. [10] are presently conducting a study of the fatigue-microstructure relationship of Al-Zn-Mg-Cu P/M alloy forgings (with and without Co) which supplements the work of Otto. Unlike the earlier investigations discussed above, this research is directed at relating the forged microstructure to fatigue response in various environments. However, the effect of microstructure on the long life fatigue strength (endurance limit) of these alloys does not appear to be an integral part of the investigation.

Lebo and Grant [11] and Sankaran [12] have investigated the fatigue-microstructure relationship of products fabricated from splat cooled (solidification rate of 10^6 K/sec) 2024 and 2024+Li powders, respectively. Products made from splat cooled powders, which were given a vacuum preheat, were extruded 20:1 at 573 K followed by a 50 % cold reduction by swaging in order to obtain recrystallization upon solution heat treatment at 768 K. This recrystallization treatment was necessary to reduce the amount of delamination which resulted from the fine dispersion of oxides along prior powder particle boundaries. Even though a grain size coarser than 2024 I/M products resulted, an increase in strength and smooth S-N fatigue behavior without loss of ductility was reported. The fatigue study did not investigate the long life fatigue strength of these products, however, normalization of the fatigue strength at $2 \cdot 10^6$ cycles showed that the reported fatigue improvement was directly related to the strength increase. Since up to 95 % of the smooth S-N fatigue life may be representative of crack initiation [13, 14], the reported increase in fatigue life could result from the increased crack initiation resistance due to the increased strength. The fine dispersion of constituent CuMgAl_2 particles, suppression of AlCuFeMn constituent particle nucleation, and increase in solid solubility are all reported as being responsible

for the increased strength without loss of ductility, as well as possibly increasing the crack initiation resistance of the P/M product over its I/M counterpart. With respect to the lithium containing, splat quenched 2024 P/M alloys, significant yield strength improvements in the T-6 temper, along with the density decrease and modulus increase associated with Li alloying in aluminum, were reported. The P/M 2024+Li has an improved S-N fatigue response although the FCG rate was increased by the significant volume fraction of insoluble second phase particles resulting from the lower solubility of Cu in Li containing aluminum alloy.

Previous attempts to increase the notch fatigue strength of high strength aluminum products without additional alloying, such as thermal mechanical treatment, were unsuccessful [15,16] even though increases in the strength parameters could be developed. However, current results demonstrate that it is possible through controlled P/M processing to produce P/M 7075 extrusions with notch S-N fatigue strength equivalent to that reported for the Co containing aluminum P/M alloy extrusions. Normalization of the notch fatigue strength at 10^7 cycles with both tensile and yield strength reveals that fatigue behavior improvements are not proportionate to strength. Similar notch fatigue results have been reported [1] earlier for P/M 2024-T3510 fatigue extrusion products and are also summarized below.

		S_N^*/σ_{UTS} [MPa/MPa]	$S_N^*/\sigma_{0.2\%}$
7075-T6510	P/M ¹	145/683 = 0.212	145/630 = 0.230
	I/M ¹	105/671 = 0.156	105/622 = 0.169
2024-T3510	P/M ¹	140/587 = 0.239	140/460 = 0.304
	I/M ¹	105/491 = 0.214	105/368 = 0.285

* S_{10^7} values pending statistical analysis

¹ extrusions fabricated with a 643 K extrusion-preheat and a 25:1 extrusion ratio

The current work seeks to determine the metallurgical effects of alloy chemistry, processing, and powder particle size distribution on tensile and fatigue properties of products fabricated from air atomized powders. Characterization of the fatigue behavior via notch ($K_t = 3$) fatigue testing has been utilized as a survey technique. Notch fatigue was selected because the recent history of fatigue testing of high performance aluminum alloy products has shown that even though improvements in smooth S-N fatigue response could be demonstrated, its application by the aerospace industry for fatigue critical components was limited unless an associated improvement in notch fatigue properties was developed. In addition, for damage-tolerant design the FCG properties are more important than crack initiation. Consequently, notch fatigue testing was selected as a survey technique because it normally reflects more of the FCG influence on the total S-N fatigue life than smooth fatigue testing [17].

PROCEDURE

As the experimental procedures for production of the various P/M products and the technique/methods for examination of these products have been previously reported [1], detailed procedures will not be repeated. The following supplementary information is provided as an amendment to the procedures in [1].

- (1) A full vacuum-preheat treatment was given to all P/M products reported in [1] and in this report, unless otherwise clearly noted. In some instances the word "preheat" may be confusing as it is used to describe both the green compact evacuation treatment (vacuum-preheat) and treatment of the billet prior to hot working (extrusion-preheat). Consequently in this report an effort has been made to clearly distinguish between the two cases.

Full vacuum-preheat as used in this investigation is the evacuation of a canned green compact, and vacuum hot pressing of the compact into a near 100 % dense billet before the canning material is removed. The distinction is therefore made between full vacuum-preheat versus selective atmosphere (inert or self-generated hydrogen) green compact preheat followed by vacuum hot pressing. For full vacuum-preheating and compaction, the processing sequence is as follows:

- (1) cold isostatic pressing of the powder to approximately a density of 80 %, (2) canning of the green compact, (3) homogenization and degassing of the compact under a dynamic vacuum until a pressure of 10^{-4} Pa at the alloy's respective solution heat treatment temperature is reached, (4) welding the can's evacuation tube shut, (5) uniaxial hot-pressing of the evacuated, canned green compact at a temperature just below the solution heat treatment temperature, and (6) removal of the canning material. The homogenization treatment which was conducted during degassing, was identical to the homogenization treatment given to the control ingot materials: 2024 alloy C - 24 h at 766 K, and 7075 alloy H - 16 h at 733 K plus 24 h at 743 K. Danilkin et al. [18] have reported that vacuum degassing is the only preheat environment which

can reduce the hydrogen level of aluminum P/M compacts to equivalent I/M levels.

Current additional processing studies are aimed at investigating the time - temperature - microstructure - hydrogen content - mechanical property interrelationship for the 2024 and 7075 P/M alloys. Because fatigue crack growth rate and fracture toughness properties are sensitive to the dispersoid particle size and distribution [19], a degassing/homogenization treatment for the powder compacts must reduce hydrogen content and volume percent coarse intermetallic particles while maintaining an optimum dispersoid size and distribution.

- (2) Extrusion products with a 10:1 extrusion ratio have a cross section of 10 x 50 mm. These extrusions were fabricated with the same procedures as those used for the 25:1 extrusions.

Extrusion is accomplished with the extrusion cylinder and billet preheated to the extrusion-preheat temperature.

Extrusions fabricated from the 2024 I/M alloys A and B, Table 1, were purchased as commercial products in the as-extruded condition. Heat treatment and testing of these products were accomplished with the same practices employed for the 2024 I/M control alloy C and P/M alloy extrusion products.

- (3) Sharp Notch Tension testing was conducted according to procedures outlined in ASTM Standards, Part 10, Designation: E602-76T, with the exception of specimens from 10:1 extrusions. In this case, a comparative measure of plane-strain fracture toughness was obtained with a mini specimen which was proportionally reduced from the small ASTM specimen in accordance with Munz [20] with the notch radius $\leq 50 \mu\text{m}$. The dimensions of the mini specimen are total length: $L = 50$; threads: M 10 with 10 mm thread length; diameter (ϕ): notch 6.00 mm, and non-yield section 8.60 mm, so ϕ notch/ ϕ section = 0.7. In several cases the results of tests with the mini specimen exceed the $\text{NTS/YS} \leq 1.3$ ASTM rule for reduced specimens, and in some of these cases, yielding could be observed from the load-displacement diagram.

- (4) Longitudinal tensile and notch tensile specimens from 10:1 extrusions, were taken from the $\frac{1}{8}$ and $\frac{3}{8}$ width points along the long transverse direction. Tensile specimens from the 10:1 extrusion were machined with a diameter $\phi = 4.0$ mm and total length = 50 mm with M 10 threads of 10 mm length (or in conjunction with the diagram for tensile specimens in [1]: A = ϕ 4, B = 10, C = 50, D = R5 mm).
- (5) The fatigue testing reported was constant amplitude, axial stressed in the longitudinal (extrusion) direction. All testing was conducted on the same axial resonance machine in an ambient laboratory air environment.

RESULTS

The mechanical property evaluation of the I/M and P/M products whose chemical compositions are listed in Table 1 was completed during this reporting period. These products were produced in accordance with the processing parameters already detailed [1]. Alloy M which contains extremely low iron and silicon impurity levels has been incorporated into this investigation in order to ascertain the influence of these impurity elements on the mechanical properties of the 7075 I/M (control) and P/M extrusions. The alloy M thick plate material was purchased from Alcan as a high purity 7075 product; however, its chemical analysis and refined microstructure indicate that the material is a specially processed 7475 commercial ingot. Consequently, extrusions produced from alloy M material have been designated 7475.

The long time vacuum degassing yielded P/M products with hydrogen contents equivalent to those of their respective I/M products, Table 1. In addition, the long time vacuum degassing of the compact at the solution heat treatment temperature provided sufficient time for solid state precipitation of the dispersoid particles in both the 2024 and 7075 P/M products. Therefore, identical dispersoid particle size and distribution in the I/M and P/M alloys were obtained prior to hot working.

1. 7075

1.1 Processing (Summarized from Results in [1])

All 7075 P/M products were produced from 88 μm APD powder (26 % - 325 mesh) which was vacuum-preheated. The 80 % dense powder compacts were compacted via either vacuum hot pressing (610 MPa at 743 K with a 10 minute dwell) or hot impact vacuum compaction (5.61×10^6 Joules/m² at 743 K in a high energy rate forming Dynapak machine). Both compacting operations were uniaxial in nature. Extrusion products were produced from the vacuum hot-pressed billets by direct extrusion utilizing a 643 K extrusion-preheat. I/M extrusion products were also fabricated with a 643 K extrusion-preheat.

1.2 Mechanical Properties

Both the I/M (alloy H and M) and P/M (alloy L) extrusions' tensile properties in the T6510 heat treatment are equivalent. Although the fracture toughness of the two I/M products is higher, the NTS/YS ratio for the P/M product indicates that its fracture toughness is equivalent to typical values for 7075 I/M extrusions, figure 1. The most significant difference between the I/M and P/M products occurs in the notch fatigue behavior. A complete listing of tensile properties for various extrusion parameters is given in Tables 2 and 3.

1.2.1 Hot-Working

The effect of the degree of hot-working on tensile properties is shown in Table 2 where it can be seen that a 81.9 % (5.54:1) reduction in cross section area via direct extrusion is sufficient to produce outstanding longitudinal mechanical properties. In comparison to other round P/M extrusions, the results shown in Table 3 for 25:1 extruded P/M products show that only slight further increase in longitudinal strength can be obtained with significantly increased extrusion reduction. Good strength values are also developed for P/M products after 5.54:1 extrusion in the transverse direction; however, these values are only equivalent to the vacuum hot-pressed product's strength properties, Table 4. The vacuum hot-pressed product displays enhanced ductility values compared to the transverse ductility values of the 5.54:1 extrusion, but lower ductility compared to the longitudinal ductility of the 5.54:1 extrusion. Mechanical properties of vacuum hot-pressed products are given in Table 4, and are summarized below for comparison with the 5.54:1 and 10:1 extrusion product's transverse mechanical properties.

7075-T6		mechanical properties				
P/M product form	property direction	UTS (MPa)	0.2%YS (MPa)	R.A. %	elong. %	NTS/YS
vacuum hot-pressed	isotropic	584	510	9.1	6.6	1.09
extruded 5.54:1 (81.9 %)	transverse	579	516	4.8	5.0	-
extruded 10:1 (90 %)	transverse	610	543	18.9	14.4	1.14

For extrusion products, these values indicate that in order to obtain good transverse ductility, reductions on the order of at least 10:1 or better are required. Extrusion ratios on the order of 6:1 probably do not provide sufficient shear flow during extrusion for the oxide surface to be completely broken up and for complete, sound welding of the virgin metal surfaces to take place. This processing deficiency, which must also be present in the vacuum hot-pressed product, is aligned mostly parallel to the extrusion direction. Consequently, these defects do not significantly affect longitudinal properties of extrusions, but limit the extrusion's transverse properties because the tensile axis is perpendicular to these aligned weak zones.

1.2.2 Vacuum Hot Compaction

1.2.2.1 Hot-Pressing

As shown in the microstructure section, no porosity can be metallographically found for the vacuum hot-pressed product. The mechanical properties of this P/M product are comparable to the typical I/M extrusion mechanical properties in Figure 1, and are in sharp contrast to those of Gurney et al. [22] for 7075 rotating electrode powder (REP). They reported that their REP vacuum hot-pressed billet was incapable of sustaining machining stresses. The round REP powders probably did not experience sufficient shearing deformation during hot compaction to close voids and develop sound particle to particle welding. However, because of the irregular shape of air atomized powder particles, hot-pressing results in good particle to particle welding due to the shorter metal flow distance that is required with the irregular shaped particles.

1.2.2.2 Hot Impact Compaction

Similar to the findings for the P/M 2024 alloy E [1], hot impact vacuum compaction of the P/M 7075 alloy produced mechanical properties (prior to hot-working) which were inferior to those produced by vacuum hot-pressing. Tensile specimens from the impact compacted product showed a brittle behavior with tensile

strengths ranging from 256 to 509 MPa and ductility parameters from 0 % to only 4.2 %. The specimen with a 509 MPa tensile strength was the only specimen of the three which displayed a 0.2 % yield strength (493 MPa) and ductility. These properties are significantly below those obtained from vacuum hot-pressing. Consequently, further work with impact compaction was not pursued.

1.2.3 Texture

The degree of mechanical property anisotropy between P/M and I/M products was investigated with compressive yield strength specimens. The results of this investigation are given in Table 5 and displayed graphically in Figure 2. The results indicate that the I/M extrusion product's mechanical properties are more anisotropic than those of the P/M material in the 45° and transverse directions, while the longitudinal compressive yield strengths of the two products are essentially equivalent. This equivalency in the longitudinal direction indicates that the extrusion textures for both products are similar. However, the effect of the P/M product's finer grain size (P/M - 5 μ m and I/M - 22 μ m) could be responsible for the better isotropy in the P/M extrusion product. Final discussion of texture strengthening will have to wait for the results of X-ray texture analyses which are in progress.

1.2.4 Solution Heat Treatment

A supplementary mechanical property investigation to determine the effect of solution heat treatment temperature on strength and ductility of 7075 P/M products may be found in Appendix A. The aim of this supplementary investigation was to determine if higher evacuation-preheat temperatures would adversely affect mechanical properties.

1.2.5 S-N Fatigue

The S-N fatigue behavior was characterized in air with longitudinal specimens from 25:1 extrusions. Testing was performed with

notch $K_t = 3$ specimens subjected to constant amplitude axial loading ($R = 0.1$). The 7075-T6510 P/M product, Figure 3, has a 145 MPa fatigue strength at 10^7 cycles compared to a 105 MPa fatigue strength at 10^7 cycles for the control I/M product, Figure 4. This 38 % improvement is presently being evaluated for statistical significance according to the method described by Maennig [27]. The fatigue behavior of I/M and P/M products is shown in Figure 5 for comparison.

Although the S-N fatigue behavior displayed in Figure 5 allows one to immediately visualize the improved high cycle fatigue (HCF) response of the P/M product, two factors may not be immediately apparent. First, the data scatter occurring in the I/M product's response (Figure 4) is significantly greater than that for the P/M product (Figure 3). Second, extrapolation of the individual fatigue curves indicates that the low cycle fatigue (LCF) response of the P/M product is possibly not as good as that of the I/M product.

The fatigue results found in this investigation are compared to those of Kaufman et al. [28] for commercially processed 7075-T6510 I/M extrusions which were tested under similar conditions. This data, shown in figure 6, reveals that special I/M processing can improve the notch S-N fatigue properties of I/M extrusion products; however, the improvement via I/M technology is small in comparison to the 45 % improvement in fatigue strength afforded by the P/M approach.

Fatigue results of specimens taken from other high strength P/M extrusions which were processed with different extrusion-preheat temperatures, are also shown in figure 6. These additional results confirm the HCF improvement and the flatness of the P/M extrusion product's notch fatigue behavior. These additional P/M produced specimens were of equivalent strength to the specimens from the 643 K extrusion-preheat product and show that the extrusion preheat temperature for P/M 7075 is not critical.

The notch S-N fatigue behavior of the 7075-T6 vacuum hot-pressed product was also investigated, Figure 7. These limited results

indicate the vacuum hot-pressed product has the potential to at least match the improved HCF behavior of the extruded P/M product. Thus products made from the 7075 vacuum hot-pressed P/M billets should provide the same improved notch fatigue behavior, independent of degree of hot-working (forging or direct pressing), as has been found for the heavily deformed P/M extrusion products. The notch fatigue behavior shown in Figure 7 gives further evidence to the increased limit and flat S-N response of the P/M products. In comparing the fatigue results in Figure 7 to those for P/M extrusions in Figure 6 it must be mentioned that residual quench stresses could be a factor in the vacuum hot-pressed response. Specimens were quenched with \varnothing 16 mm, and subsequently machined to a \varnothing 6.4 mm notch. Consequently, if significant residual stress remains after machining, it should be tensile in nature [29].

Recrystallization and the degree thereof have also been shown to have an impact on degrading the fatigue response of high-strength aluminum products [30, 31]. However, for the fatigue response reported, the degree of recrystallization is not a factor. Back-reflection pinhole X-ray patterns of 25:1 I/M and P/M extrusion products do not show any indications of recrystallization, Figure 8.

1.3 Microstructure

1.3.1 Porosity

In comparison to the control I/M product, density measurements revealed that the vacuum hot-pressed billets and extrusions fabricated from these billets were 100 % dense, Table 7. A supplementary examination for possible residual porosity in these P/M products was conducted metallographically using polarized light. Examination of unetched surfaces employing the scanning electron microscope (SEM) did not provide the capability to distinguish between possible porosity and pits or voids resulting from dislodgement of intermetallic particles, that is afforded by optical metallographic techniques.

The initial comparison between vacuum hot-pressed and 25:1 P/M extrusion products, Figure 9a and 9b, did not reveal any measurable difference. Thus the similar defect structure in both products resulted from either dislodgement of intermetallic particles or similar porosity produced from release of residual hydrogen in both the P/M products. It is important to note here that all products examined for residual porosity were solution treated and quenched. These treatments have been shown to exaggerate porosity through release of residual hydrogen [32]. Consequently, to eliminate the possible damaging influence of residual hydrogen, the P/M products were compared to an I/M product of equivalent volume percent second phase, Figure 9c. The results indicate that no residual porosity could be found, and that the defect structure is a void/pit structure resulting from dislodged intermetallic particles.

Metallographic specimens were not final polished or etched for fear of dislodging a greater number of particles. Consequently, the polishing scratches are readily observed in Figure 9.

The comparative micrographs in Figure 10 taken with unpolarized light further demonstrate the relationship between particles and the void structure. The locations shown in Figures 9 and 10 are not representative of a typical polished surface location. However, they are representative of locations with a defect structure. Most of the polished surface was defect free.

1.3.2 Intermetallic (soluble and insoluble) Particles

Three different types of particles/precipitates form in the 7X75 alloy. These particles may be characterized by their size and the manner in which they form.

- a. Coarse intermetallic (constituent) particles $\sim 0.1 - 30 \mu\text{m}$ are formed during solidification from the impurity elements iron and silicon combining with aluminum and the major alloying elements zinc, magnesium, and copper. These particles may be characterized as equilibrium or nonequilibrium and further divided as soluble or insoluble. No definite distinction in

size may be made between these various particles.

- b. Intermediate precipitates or chromium dispersoid particles
0.05 to 0.5 μm are formed by solid state precipitation during the homogenization treatment. The dispersoid (E-phase) $\text{Al}_{12}\text{Mg}_2\text{Cr}/\text{Al}_{18}\text{Mg}_3\text{Cr}_2$ particle is incoherent with the matrix. In the case of the P/M products the amorphous oxide particles $(\text{MgAlZnCu})_x \text{O}_y$ also fit into this size range [33, 34].
- c. Fine precipitates 0.001 to 1 μm are formed by solid state precipitation. These range from the 0.001 μm coherent Guinier-Preston (GP) zones, which are the predominant hardening precipitate to the metastable, partially coherent MgZn_2' (η'), and finally to the incoherent large grain boundary precipitates which are thought to be the $\text{MgZn}_2(\eta)$ phase. The latter being relatively nonhardening particles which form up to 1 μm in size during slow quenching or drastic overaging.

1.3.2.1 Volume Percent Second Phase

The volume percent of the constituent intermetallic particles (VPCP) of several 7X75 aluminum alloy extrusion products was determined by the ASTM point count method [35]. The point count was taken on SEM micrographs [36] which provided contrast and good resolution of the particle boundaries. Because of the resolution, VPCP determination was based on particle sizes of 0.1 μm and greater. The resolution error associated with the particle perimeter, or perimetral effect, has been shown by El-Soudani and Pelloux [37] to be 10 % when optical micrographs are used instead of SEM micrographs. Representative optical micrographs for several I/M and P/M homogenization treatments, Figure 11, clearly demonstrate the need to resolve the particle boundaries, as well as providing an indication of the size and distribution of these particles.

Results of the VPCP determination, Table 8, show a good correlation with the NTS/YS values given in Table 3, with the assumption that there is no significant change in VPCP between the 25:1 and 10:1 extrusion products. The extrusion product with the

lowest VPCP provides the highest indication of plane strain fracture toughness, these results being consistent with the findings of others [19 , 24, 38, 39]. The finer distribution in the P/M products is indicative of the smaller dendrite cell size of these products, and is reflected in the completely dimple rupture fracture surface of P/M tensile and notch tensile specimens.

The application of the standard I/M 7075 homogenization treatment (Treatment A) to the I/M and P/M products resulted in their having essentially equivalent VPCP values but different average particle size values, Table 8. This suggests that the high solidification rate experienced by the powder was capable of altering the size and distribution of the intermetallics, but was unable to significantly suppress their formation. The green compact which was homogenized at 793 K (homogenization Treatment C) and has a 1.7 VPCP, shows that a considerable amount of the particles are soluble. Therefore, an elevated temperature homogenization period which is insufficient to cause coarsening of the chromium dispersoid phase particles, or a thermal-mechanical processing [40] similar to that used on the I/M 7475 alloy (0.4 VPCP), would substantially reduce the VPCP of the P/M products and thereby increase their fracture toughness properties.

Abson et al. [41] have shown for 7075 REP powder that 2 h at 700 K is sufficient to precipitate the chromium dispersoid phase to a distribution equivalent to that of commercially homogenized I/M 7075. In addition, based on current transmission electron microscopy observations and the findings of Haarr [26] concerning the chromium dispersoid phase distribution, it can be assumed that both the I/M and P/M products presented in Table 8, have an equivalent chromium particle distribution. Therefore, even when a volume percent second phase (VPSP) value would be determined which includes the dispersoid phase, the difference in magnitude between the VPSP of the I/M alloys and the VPSP of the P/M alloy would remain the same as the difference in VPCP. However, for the P/M products the oxide distribution must also be considered. Assuming all oxygen to be present as either MgO or Al_2O_3 , after Lyle and Cebulak [33], and distributed as 60 %

MgO, after Otto [34], a prediction of 0.3 vol.% MgO and 0.17 vol.% Al_2O_3 can be made. Thus an indication of the oxide volume percent of 0.47 vol.% is obtained, and a relative measure of the total volume percent second phase versus the NTS/YS fracture toughness values from Tables 2 and 3 can be made. From such a comparison, as provided in Table 9, the effect of second phase on fracture toughness and the reason why the fracture toughness of the P/M 7075 is lower than the I/M extrusion products becomes clearer. Because these constituent particles are brittle, they either fracture or separate from the matrix when the local plastic strain amplitude reaches a critical value, as in fast crack growth ($da/dn > 10^{-6}$ m/cycle) or unstable crack growth at fracture. The alloy with a higher VPSP can therefore be predicted to have a lower resistance to unstable crack growth (lower NTS/YS). The data in Table 9 fit this trend as well as showing that the relationship is not linear.

It is noteworthy to discuss the microstructure-property relationship between the two I/M products in order to obtain an understanding of why the I/M products' mechanical properties are improved over typical mechanical properties for these alloys. Both the I/M extrusions (alloy H and M) have a fine microstructure which is the primary factor controlling the property improvements found for these two products in comparison to the typical I/M values shown in Figure 1. In addition to having an initial high purity base, direct chill (DC) casting of the 10 kg, \varnothing 80 mm alloy H ingot yielded a fine 20 μ m average dendrite cell size (DCS) which further refined the alloy's constituent particle distribution. The special commercial processing of the high purity alloy M ingot was responsible for the refined microstructure in the alloy M extrusion.

1.3.2.2 Particle Chemistry

The lattice parameters for the I/M and P/M products were measured with a Siemens Fine Structure Goniometer using $Cu K_{\alpha}$ radiation, $2\theta = 0.02^{\circ}$ step scan, and gold powder calibration. Intensity measurements were taken from the (422) reflection on I/M and P/M specimens which had been solution heat treated, air cooled, and

electrolytically polished. The accuracy of the reported parameter is estimated to be better than 0.0002 m^{-10} . The decrease in lattice parameter from $4.0559 \times 10^{-10} \text{ m}$ for I/M alloy H to $4.0545 \times 10^{-10} \text{ m}$ for the P/M product given the same homogenization treatment (Treatment A, Table 8), suggests that the higher solidification rate experienced by the powders led to a slightly supersaturated final P/M product. Results of the lattice parameter investigation given in Table 8 are within values published elsewhere: Van Horn [43] $4.056 \times 10^{-10} \text{ m}$ for nonartificially aged I/M 7075 products, and Durand et al. [44] $4.049 \times 10^{-10} \text{ m}$ for air atomized 7075 powders. Published values for the change in the aluminum lattice parameter from binary solid solution additions [43] indicates that silicon, copper, chromium, titanium, and beryllium could be the elements predominantly responsible for the lattice parameter difference between I/M alloy H and P/M alloy L. Iron additions up to its equilibrium solid solubility limit in aluminum are reported to leave the lattice parameter practically unchanged [45]. Beryllium, which is usually added to the melt to reduce oxidation, titanium and silicon are not present in the P/M product in sufficient quantity to account for the lattice parameter change alone. In addition, there is no detectable difference in the chromium particle distribution between the I/M and P/M products.

The constituent particles were examined in a scanning electron microscope (SEM) with an energy dispersive X-ray analysis (EDAX) capability. Display of the results of this examination are in the form of X-ray intensity counts plotted against the energy (keV) of the X-rays emitted from the area being analyzed. This method provides a qualitative chemical analysis of the constituent particles through comparison of the relative intensities for the different elements.

A random survey of particles did not show any difference in particle chemistry for the I/M and P/M products which had been given the standard 7075 homogenization treatment (Treatment A, Table 8). Particles were of Al-Mg-Cu-Zn and Al-Mg-Fe-Cu-Zn-Cr chemical compositions, indicating $\text{Cu}(\text{Mg}, \text{Zn})\text{Al}_2$ and $\text{Al}_7\text{Cu}_2\text{Fe}$ type particles respectively. The 7475 I/M product contained

Al-Mg-Cu-Zn and Al-Fe-Cu-Zn particles as well as many large Al-Fe-Cu-Cr-Mn particles. The ratio of Fe to Cu was altered for the latter particle type with significantly more Fe present. Similarly, the P/M product given homogenization treatment C (high temperature homogenization) contained particles of increased Fe content.

No Mg_2Si particles or high intensity peaks for Si were found except for the P/M alloy given treatment A, where small amounts of Si were associated with Al-Mg-Cu-Zn particles. This indicates that a significant portion of the small amount of silicon present in these alloys could have remained in solid solution. However, if the total silicon content had remained in solid solution the lattice parameter would have only been reduced by 1.19×10^{-14} m. In addition, since the Mg_2Si particles did not form, magnesium was not removed from its strengthening role of forming the intermediate η' precipitate.

Representative pictures of the EDAX display are shown in Figure 12 for the iron containing particles from (1) P/M 7075 treatment A, (b) I/M 7475, and (c) P/M 7075 treatment C. Of particular interest is the increase of the Fe peak height to the Cu peak height for the P/M treatment C in comparison to treatment A. This change indicates that increased solubility of copper is probably the main element responsible for the change in lattice parameter. Since silicon, copper and iron are weak solid solution strengthening elements in the 7XXX series aluminum alloys [46 - 48], the fact that no change in strength occurred with a changing lattice parameter can be understood.

No attempt has been made to systematically determine the chemistry of constituent particles, this work may be found elsewhere from the examination of fractured surfaces [49]. The information obtained from the current particle chemistry examination helps to understand why the lattice parameter changed without affecting the strength. In addition, insight has also been gained concerning the mechanism by which the copper is taken into solid solution. Since the lattice parameter for the short time homogenization (Treatment B) is very similar to that of the

I/M product and since the lattice parameters for the P/M products given the long time (Treatment A) or high temperature (Treatment C) homogenization are equivalent, the total copper content is not maintained in solid solution directly by the rapid solidification. That portion of copper content which was rejected during solidification, can dissolve more quickly into the matrix of the P/M product because the distance required for diffusion has been shortened due to the smaller dendritic cell size. The quicker resolution of the initially rejected copper in the powder product is therefore an indirect product of the rapid solidification.

1.3.3 Optical Microstructure

Optical micrographs for the three alloys examined are presented in Figures 13 - 15 for the 25:1 extrusions. The grain morphology is one of small, unrecrystallized elongated grains containing a well defined hot-worked substructure. Table 10 provides a listing of the grain and subgrain parameters determined by quantitative metallographic techniques [42, 50].

Both the I/M products have a coarser grain size in comparison to the P/M product, however, the grain size of the I/M products is much smaller than the typical grain size range for commercial I/M products. The mean grain intercept length (\bar{L}) for the P/M product is 26 % of the mean grain intercept length of both the I/M products. The 20 - 30 μm grain size range of the I/M products is equivalent to I/M products which have been subjected to some type of intermediate thermal mechanical treatment (ITMT) [51], and is a factor of 2 to 4 times smaller than a typical commercial product [32]. The P/M product's grain size is therefore an order of magnitude smaller than typical I/M products.

In addition to optical measurements, X-ray line broadening analysis [52] was employed to quantitatively investigate the substructure of the P/M and I/M products. The results of this analysis showed that there is no measurable difference for the 2 μm range and below, in the lattice distortion between the I/M and P/M extrusion products. Both products showed significant line broadening which was indicative of the fine substructure

shown in the higher magnification micrographs of Figures 13 and 14.

1.3.4 Transmission Electron Microscopy (TEM)

A TEM examination of the I/M and P/M extrusion products' microstructure in the as-extruded (Figures 16 and 17) and in the as-extruded plus solution heat treated (Figures 18 and 19) conditions revealed no differences other than size of the subgrains.

The as-extruded structure for both the I/M and P/M products is a well defined polygonized substructure as a result of dynamic recovery, Figures 16 and 17. A considerable volume fraction of larger particles is evident in both of these microstructures, with a high frequency of occurrence in the boundaries. These particles are probably forms of the equilibrium phases $MgZn_2$, $CuMgAl_2$, $Mg_3Zn_3Al_2$ and $Al_{18}Mg_3Cr_2$ (M, S, T, and E phases respectively), and are responsible for limiting the degree of recovery in the as-extruded products as well as influencing the fine subgrain size in the solution heat treated product. No recrystallized grains or differences in the $Al_{18}Mg_3Cr_2$ chromium dispersoid phases' sizes or distributions were observed for either product.

After solution heat treatment the volume fraction of large particles, the M, S, and T equilibrium phases, is significantly reduced, Figures 18 and 19. Recrystallization has not occurred in either product, however, the substructure of the I/M extrusion product is slightly coarsened in comparison to that of the P/M product. Both structures appear to be thermally stable and recrystallization resistant with boundary particles impeding boundary migration. The bending of the boundaries around particles in Figure 18 for the I/M extrusion product indicates a boundary particle pinning mechanism. For these solution heat treated products, diffraction patterns along the extrusion direction, show the orientation difference between subgrains to be only a few degrees. In the direction perpendicular to the extrusion direction, diffraction patterns show a high frequency of significant orientation differences (large angle grain

boundaries) as well as some small orientation differences (subgrains).

1 3.5 Fractography

An investigation of the fracture surfaces of various I/M and P/M tensile and notch tensile specimens was conducted to see if there was any difference in the fracture mechanisms. Fractographs are shown only for the transverse tensile fracture surfaces as the appearance of the other specimens' fracture surfaces is identical to that which may be found elsewhere [49].

The fracture surface of longitudinal tensile specimens from both I/M and P/M extrusion products (5.54:1, 10:1, and 25:1) is transgranular. The fracture surfaces of the P/M products reveals a uniform dimple rupture fracture which corresponds to the fine, uniform constituent particle distribution. In contrast, the I/M products reveal a nonuniform dimple rupture fracture with some secondary cracking; large dimples resulting from large, cracked constituent particles, as well as flat, 50 μm wide areas with small dimples resulting from the chromium dispersoid are observed.

The longitudinal and transverse notch tensile fracture surfaces for both I/M extrusions and P/M products (10:1 and 25:1 extrusions and vacuum hot-pressed) are totally transgranular, dimple ruptured. The dimples of the P/M product's fracture surface are more uniform in size than those of the I/M product's surface.

The fracture surface of tensile specimens machined from the transverse direction of 10:1 extrusions, for both I/M and P/M products, reveals the stringer effect of the constituent particles, Figures 20 and 21. Both products show a predominantly transgranular, dimple rupture fracture, but the dimple structure of the P/M product is finer and more uniform. In addition, approximately 30 % of the I/M product's fracture surface has the appearance of possible slip plane or grain boundary fracture, Figure 21b. The surfaces appear smooth, but at high magnification fine, uniform dimples become evident, Figure 21c. These surfaces are approximately as wide as the grain width, but are

also on the order of the distance between stringers of large constituent particles. In contrast, the P/M product shows a considerably lower percent of these smooth appearing fracture surfaces. However, the width of these surfaces are also the same size as the larger grain widths of the P/M product, and are on the order of the distance between occasional stringing of the larger constituent particles. These flat surfaces also show a very fine, uniform dimple rupture fracture.

The fracture surface of the transverse tensile specimen from the 5.54:1 P/M extrusion product, Figure 22, does not show the uniform dimple size seen in Figure 20 for the 10:1 extrusion. Instead, the fracture surface ranges from large cracked particles to featureless walls. The extrusion direction and stringing of particles are easily identifiable. The lack of complete, uniform dimple rupture, as in Figure 20, indicates the 5.54:1 P/M extrusion contains zones of weakness. These zones are probably areas predominantly parallel to the extrusion direction where insufficient shear has resulted in unsound welding of the powder particles.

The absence of a predominant dimple rupture fracture in the 5.54:1 P/M extrusion product correlates with the lower ductility values found for this product when compared to the predominant dimple rupture fracture and higher ductility values of the 10:1 P/M extrusion product. These fractographic results further indicate that in order to develop acceptable transverse ductility in P/M extrusion products a minimum extrusion ratio of approximately 10:1 is required.

2. 2024

2.1 Processing

The 2024 P/M products were produced from powders of various average particle diameters, Table 12, all of which were vacuum-preheated prior to compaction. The main effort with the 2024 alloy was accomplished with the alloy E 82 μ m APD powder.

The results of various compaction techniques for the 2024 powders have been previously reported [1]. This investigation revealed that only uniaxial vacuum hot compaction (610 MPa at 763 K with a 10 minute dwell) produced sound P/M billets. Extrusion products were produced from the vacuum hot-pressed billets by direct extrusion, 10:1 and 25:1 extrusion ratios.

Since the manganese dispersoid particle's capability to retard recrystallization in the 2024 alloy is not as effective as the chromium dispersoid particle in the 7075 alloy [39], the selection of an extrusion-preheat temperature for the 2024 alloy was more critical. Several temperatures from 613 K to 753 K were evaluated for the P/M extrusion products. Highest strength and notch fatigue properties were developed in the P/M product with a 643 K extrusion-preheat. A 753 K extrusion-preheat temperature produced slightly lower mechanical properties.

Back reflection pinhole X-ray analysis was conducted on solution heat treated (766 K) P/M and I/M extrusion products. Based on this analysis, the texture of the P/M extrusion products fabricated with the 643 K and 753 K extrusion-preheat temperature is similar. Whereas no recrystallization is revealed in these X-ray pictures for the 753 K extrusion-preheat, the 643 K extrusion-preheat X-ray picture shows a slight amount of recrystallization even though this extrusion-preheat developed the best properties. Analysis of the back reflection pinhole X-ray pictures for the 613 K extrusion-preheat P/M product revealed considerable recrystallization but with some degree of retained texture. Analysis of the 673 K extrusion-preheat P/M product did not show any recrystallization.

The back reflection pinhole X-ray analysis of the I/M alloy C extrusion products manufactured with a 643 K extrusion-preheat showed a totally recrystallized structure. No strong recrystallization texture was observed in the 25:1 I/M extrusion product and a very slight recrystallization texture in the 10:1 I/M extrusion products was observed.

2.2 Mechanical Properties

Because of the good fracture toughness and fatigue behavior of I/M 2024 in the naturally aged condition, the P/M 2024 products were initially evaluated with the naturally aged T3510 precipitation heat treatment. The T3510 treatment yields the best fatigue properties [53, 54] for I/M products. Artificial aging and thermal mechanical treatments were subsequently evaluated in order to produce I/M and P/M products for fatigue testing at equivalent yield strength levels.

The 2024-T3510 P/M extrusion products show significant strength improvements in comparison to their I/M counterparts, Figure 23 and Table 13. The P/M extrusion from a 643 K extrusion-preheat has 20 % improvement (102 MPa) in tensile strength and 26 % improvement (99 MPa) in yield strength over the average values from alloy A, B and C I/M 25:1 extrusions. This strength improvement is accompanied by some loss of ductility and fracture toughness, as would be expected, but these reductions are not severe. In comparison to typical properties, Figure 23, the P/M extrusion product offers significant improvements except for fracture toughness. While the mechanical properties of the vacuum hot-pressed P/M product are not as good as the P/M extruded products' properties, they are essentially equivalent to those of the I/M extrusion products. Thus vacuum hot-pressing to near net shape or to forging preform shape may represent a useful processing technique for this alloy.

Mechanical properties from the control I/M alloy C extrusion product are in agreement with those of the commercial alloy A and B extrusion products. Therefore, comparisons made between P/M and I/M alloy C extrusion products fabricated with the same

processing parameters developed for P/M extrusion products, represent valid comparisons between P/M and I/M extrusion products in general.

2.2.1 Effect of Extrusion-Preheat Temperature

The effect of the 643 K and 753 K extrusion-preheat temperature on the mechanical properties of P/M extrusion products was investigated for various precipitation treatments. The 643 K extrusion-preheat yields strength properties which are consistently better than the 753 K extrusion-preheat, independent of precipitation heat treatment, Figure 24. This improvement is obtained without loss of ductility, and it is thought to result from the slightly smaller grain/subgrain size of the 643 K extrusion-preheat product.

2.2.2 Aging Response

The response of the P/M extrusion products to various aging treatments is also shown in Figure 24. The enhanced aging response produced by the T3510 treatment (cold-worked by stretching between SHT and RT age) in comparison to the T4 Treatment (without cold-work) is effective for both the P/M and I/M extrusion products. Of additional significance is the higher strength of the naturally aged T3510 P/M extrusion product manufactured with a 643 K extrusion-preheat as compared to the I/M extrusion product given the high strength, standard T851 thermal mechanical treatment, i.e. artificial aging following 1 to 3 % deformation. This strength improvement is obtained without any significant loss of ductility.

In order to investigate the P/M and I/M extrusion products' fatigue response at equal yield strength levels and with equivalent microstructures, it was necessary to employ artificial aging and thermal mechanical treatments. The tabulated mechanical properties in Tables 13 and 14 for natural aging show that it is impossible to obtain an I/M product via natural aging at strength levels equivalent to those of the P/M extrusion products. From published yield strength values it was determined that even if an

enhanced precipitation response T35X treatment were to be employed, the yield strength of the naturally aged I/M extrusion products would not equal those of the T351 P/M extrusion products. Consequently it was necessary to investigate the extrusion products' response to elevated temperature precipitation treatment (artificial aging), Tables 15 to 18.

With respect to the artificially aged T6 condition, the P/M extrusion products exhibited a mixed response with regard to strength properties when compared to those of the I/M extrusion products. However, the ductility properties of the P/M extrusion products are on the average slightly enhanced in comparison to those of the I/M extrusion products, Table 15. In the T6 condition, the P/M extrusion product manufactured with a 643 K extrusion-preheat exhibits a 2 % lower ultimate tensile strength and a 4.6 % higher yield strength in comparison to the respective properties of the I/M extrusion products. Whereas the P/M extrusion product manufactured with a 753 K extrusion-preheat had a 5.7 % lower ultimate tensile strength and a 0.9 % lower yield strength in comparison to the respective properties of the I/M extrusion products. Thus in general, the significant strength advantage of the P/M extrusion products over the I/M extrusion products which was developed via natural aging is not developed via artificial aging. For the 25:1 extrusion ratios, the average yield strength of the P/M extrusion products in the naturally aged T4 condition is 42 % higher than that of the I/M extrusion products (Table 14), whereas the average yield strength of the P/M extrusion products in the artificially aged T6 condition is essentially the same as that of the I/M extrusion products (Table 15). Since the yield strength of the I/M extrusion products in the T6 condition is 28 % improved over that of the T4 condition, artificial aging (T6) instead of natural aging, actually results in a strength degradation for the P/M extrusion products, Figure 24. No difference was found via hardness testing for the rate of artificial aging response between the P/M and I/M 2024 products. This latter finding is in agreement with that reported by Roberts [55]. Consequently, the degradation of the P/M product's strength with artificial aging is not due to overaging.

The aging response of products given a T8 thermal mechanical treatment (TMT) consisting of plastic deformation prior to artificial aging, was also investigated. The mechanical properties of P/M and I/M extrusion products subjected to several TMTs show that the strength parameters, and in general also the ductility parameters, of the P/M extrusion products remain slightly below the values determined for I/M extrusion products, given the same TMT, Tables 16 - 18 and Figure 24. For the T8510 treatment, Table 16, the P/M product manufactured with a 643 K extrusion-preheat and 25:1 extrusion ratio has a 1.5 % lower tensile strength and 3.5 % lower yield strength in comparison to the averages of the I/M alloy B and C extrusion products' properties. Similarly for the T8510 products manufactured with a 10:1 extrusion ratio, the P/M product has a 5 % lower tensile strength and a 11.2 % lower yield strength in comparison to the control I/M alloy C extrusion product. In addition, the ductility parameters for the P/M products for both extrusion ratios are lower than those of the I/M products: 24 % and 16 % lower for reduction in area and elongation at failure, respectively. Although the mechanism is not understood, it is apparent that when P/M 2024 extrusion products are subjected to the same artificial aging treatment as I/M extrusion products, the P/M products's mechanical properties are moderately lower than those of the I/M product.

Similar results to those discussed for the T8510 aging treatment were also found for a T8570 aging treatment, Table 18. In this case the TMT consisted of 7 - 8 % plastic deformation by stretching prior to elevated temperature aging. An accurate property comparison cannot be made for this treatment as the plastic deformation was determined to be nonuniform.

The tensile properties of I/M extrusion products given TMTs (Table 16 - 18) reveal that the enhanced precipitation response developed by such treatments is necessary to develop a yield strength in an I/M product which is equivalent to the yield strength of the P/M extrusion product given the simpler T3510 treatment (Table 13). However, over the range of TMTs investigated (up to 8 % plastic deformation prior to artificial aging) the ultimate tensile strength of the I/M extrusion products does not

reach that which can be obtained from the P/M extrusion products given the simpler naturally aged T3510 or T4 treatments.

In order to accomplish fatigue testing of the P/M and I/M extrusion products at an equivalent yield strength and for the same microstructure, P/M extrusion products require a separate TMT for each extrusion ratio. The I/M extrusion products were given a T8510 treatment. The P/M product manufactured with 25:1 extrusion ratio was given a T8540 TMT which consisted of 4 % plastic deformation followed by 11 h at 464 K. This TMT yields P/M 2024 extrusion products with equal strength and roughly equivalent ductility parameters compared to those of the 25:1 I/M 2024-T8510 extrusion product. The P/M extrusion product manufactured with a 10:1 extrusion ratio, for fatigue crack propagation testing, was also given a T8540 TMT but with only 8.5 h at 464 K. This TMT yields P/M 2024 extrusion products with equivalent strength but slightly lower ductility parameters compared to those of the 10:1 I/M 2024-T8510 extrusion product. This fatigue testing is currently being conducted.

2.2.3 Effect of Extrusion Ratio and Directional Properties

In the naturally aged condition, the strength properties of P/M extrusion products manufactured with a 10:1 extrusion ratio are somewhat reduced from those produced with a 25:1 extrusion ratio, with equivalent ductility values, Table 14. However, the 10:1 P/M extrusion products have strength properties which are an average 26.8 % (16.8 % UTS and 36.8 % YS) higher than those of 25:1 I/M extrusion products, and also have higher ductility parameters. The 10:1 P/M extrusion products exhibit an average 26.7 % increase in longitudinal and 11 % increase in transverse strength properties in comparison to those of 10:1 I/M extrusion products, with equivalent ductility in the longitudinal direction and enhanced ductility in the transverse direction. It is also interesting to note that the strength properties of the I/M extrusion product are slightly higher in the transverse direction than in the longitudinal direction.

2.2.4 Notch S-N Fatigue Behavior

The notch S-N fatigue behavior was characterized in a laboratory air environment with longitudinal specimens from 25:1 extrusions. The notch $K_t = 3$ specimens were subjected to constant amplitude axial loading. Results of this investigation show that the 2024-T3510 P/M extrusion product manufactured with a 643 K extrusion-preheat has a 140 MPa fatigue strength at 10^7 cycles, Figure 25. In comparison, a 105 MPa fatigue strength at 10^7 cycles was found for the control I/M extrusion product manufactured with the same 643 K extrusion-preheat, Figure 26. This 33 % improvement is presently being evaluated for statistical significance according to the method described by Maennig [27].

For comparison, the fatigue behavior of 2024-T3510 P/M and I/M extrusion products is shown in Figure 27. The S-N fatigue response for the control I/M extrusion product, alloy C, lies within the scatter band found for the alloy A and B commercial extrusion products in the HCF region and to the lower life side of the I/M scatter band in the LCF region. The P/M extrusion products exhibit an improved notch S-N fatigue response in the HCF region. The P/M extrusion processed with a 643 K extrusion-preheat has an improved notch HCF behavior in comparison to the P/M extrusion processed with a 753 K extrusion-preheat. However, the LCF behavior of both P/M extrusion products appears to yield a shorter life compared to the I/M alloy A and B extrusion products. These results are similar to the results found for the 7075 alloys.

Since the 2024-T3510 I/M and P/M extrusion products have significantly different strength properties, it was necessary to separate the strength difference from the fatigue results to see if the HCF improvement was solely a function of strength. Such a separation was made by normalizing the applied stress with the tensile strength of the material. The shape of the normalized curve, Figure 28, is quite similar to the S-N curve in Figure 27. In the HCF region the normalized S-N curve reveals that the improved fatigue responses of the P/M extrusion products is not solely dependent upon strength improvements. This is particularly clear for the 643 K extrusion-preheat product. The analysis

does indicate that the higher strength of the P/M products influences the notch S-N fatigue behavior. Normalization of the applied stress with the yield strength shows a similar trend. The only difference is found in the HCF region where the improvement shown by the P/M extrusion products, although evident, is not as large as that shown by tensile strength normalization.

In the LCF region the normalized S-N curve reveals the fatigue life of the P/M extrusion products is shorter than that of I/M extrusion products tested at the same percent of ultimate tensile strength. Normalization of the fatigue data exaggerates the flatness of the P/M fatigue response. From this analysis it appears that when the strain range increases and plasticity is required, the P/M products are not as fatigue resistant.

2.2.5 Effect of Powder Initial Average Particle Diameter (APD)

The mechanical properties of 2024 P/M extrusion products in both the longitudinal and transverse directions did not show any significant dependence on the powder's initial average particle diameter (APD) over the range 36 - 117 μm . The oxygen content of the P/M extruded product did show the expected increase, due to increased surface area, as the APD decreased, Table 1. However, no mechanical property trend with oxygen content was discovered.

Mechanical properties, with the exception of S-N fatigue, were evaluated in the naturally aged T4 condition to avoid variations which could have possibly been introduced by nonuniform deformation if the T35X condition had been examined. The notch S-N fatigue behavior was examined for the T351 heat treatment in order to maintain one naturally aged condition for the comparison of the various P/M and I/M extrusion products' fatigue responses. If slight variations in the yield strength were to exist from differences in the $1\frac{1}{2}\%$ stretch deformation, they were thought to not be significant in evaluating the notch fatigue behavior.

For longitudinal properties of 25:1 extrusion products, there was a slight decrease in strength as APD decreased. This varia-

tion was less than 2.5 % of the average strength value, Table 19. Variations in ductility parameters, fracture toughness indicators, oxygen content, or measured grain size did not correspond with these strength changes. Since no consistent interrelationship with these strength variations could be found, and since the strength variation was small, it was concluded that no significant variation of longitudinal strength with initial APD existed.

The transverse mechanical properties of 10:1 extrusion products were also investigated as a function of initial powder size since the transverse direction is much more sensitive to processing variations. Again no significant mechanical property trend could be established, Table 20. Whereas ductility parameters decreased as APD decreased (oxygen content increasing) there was no clear trend in the strength parameters or NTS/YS values.

Limited notch S-N fatigue testing was performed for the three APD P/M extrusion products with identical chemistry, i.e. APD's of 36, 82, and 117 μm . Results of these tests, Figures 29 - 31, indicated the notch fatigue behavior of extrusion products manufactured from the larger 117 μm APD could possibly provide a slight improvement in HCF response, Figure 29, over extrusion products manufactured from the smaller 36 and 82 μm APD powders. Additional investigations of 117 μm APD powder products were not conducted because of the following: (1) significant HCF improvements in the notch S-N fatigue behavior of the P/M product manufactured from 82 μm APD powder with a 643 K extrusion-preheat was found, (2) the microstructure of the 117 and 82 μm APD P/M products was similar with the exception that the 117 μm APD powder product's grain size was larger, and (3) the yield strength, which was shown to influence the notch S-N fatigue behavior for 2024 P/M extrusion products, Figure 28, was at least equivalent, if not better and with equal ductility, for the 82 μm APD P/M extrusion product tested in the T3510 condition.

2.3 Microstructure

2.3.1 Porosity

An examination for possible residual porosity in the 2024 P/M products was conducted as outlined in section 1.3.1. Results of this examination were similar to those for the 7075 P/M products: no definite residual porosity could be found. These results were as expected as density measurements of the 2024 P/M and I/M products [1] revealed 100 % dense P/M products.

2.3.2 Intermetallic (soluble and insoluble) Particles

Three different types of particles/precipitates form in the 2024 alloy. These particles are the:

- a. coarse intermetallic (constituent) particles ~ 0.1 to 30 μm which are formed during solidification, similar to that in the 7075 alloy.
- b. intermediate $\text{Al}_{20}\text{Cu}_2\text{Mn}$ precipitates (incoherent manganese dispersoid particles) ~ 0.03 to 0.5 μm which are formed by solid state precipitation during the homogenization treatment and, in the case of the P/M products, the amorphous oxide particles which also fit into the same size range.
- c. fine precipitates ~ 0.001 to 1 μm . These range from the coherent G.P. zones formed during room temperature natural aging, to the metastable partially coherent $\text{Al}_2\text{CuMg}'$ (S') phase formed during elevated temperature artificial aging, and finally to the relatively nonhardening incoherent Al_2CuMg (S) phase (probably the large grain boundary precipitate phase which can be 1 μm upon drastic overaging). The G.P. zones and S' precipitates are responsible for hardening.

2.3.2.1 Volume Percent Second Phase

The volume percent of the constituent particles (VPCP) for the 2024 aluminum alloy extrusion products was determined by the point count method outlined in section 1.3.2.1. The results of the VPCP determination, Table 21, show that for 2024 P/M products given a sufficient homogenization treatment, the VPCP can be significantly reduced below that of standard I/M 2024 products (alloy A) or specially processed 2124 alloy type products (alloy C). However, for the 2024 alloy reductions in VPCP accomplished by P/M processing are not as large as reductions that can be obtained by chemistry modification [39].

The VPCP results for P/M 2024 products (Table 21) show that the solidification rate experienced by the powder during air atomization was not capable of suppressing formation of the constituent particles. The high VPCP of the P/M product given a short time, low temperature homogenization treatment (Treatment B) demonstrates the requirement for a long time or high temperature homogenization treatment similar to Treatments A or C in order to reduce the VPCP. The P/M 2024 products do not show increased constituent particle solubility through elevated temperature homogenization (Treatment C), as the VPCP level resulting from the standard I/M homogenization treatment (Treatment A) is equivalent to the VPCP resulting from Treatment C, Table 21. Similar results have been reported for I/M 2024 and 2124 alloy products [19]. The VPCP of the P/M extrusion products given homogenization Treatment A or C is lower than the VPCP of the control I/M alloy C extrusion product given Treatment A, even though alloy C's chemistry was equivalent to that of the P/M products. Thus suggesting that some degree of suppression of constituent particle formation could take place.

The P/M products' refined dendritic structure, i.e. smaller dendritic cell size, is responsible for the refinement in the constituent particle size. Constituent particles in the P/M product given the standard 2024 I/M homogenization treatment (Treatment A) were one half of the size of constituent particles in the I/M control alloy C product, Table 21. In comparison to the

commercial product, alloy A, the P/M product's constituent particle size is almost one-third smaller.

Comparison of fracture toughness resistance between P/M and I/M 2024 extrusion products to determine the influence of VPCP was not possible because of yield strength and microstructural differences. Since both yield strength and the type of hardening precipitate influence fracture toughness, a direct comparison of the effect of VPCP on fracture toughness has not been possible because of the difference of the 2024 P/M and I/M products' aging responses. It is interesting to note, however, that for the T3510 aging treatment, the P/M extrusion product with a 6.5 VPCP exhibited an equivalent NTS/YS ratio (1.50, to that of the I/M product with a 3.3 VPCP. This result was found even though the P/M product had a 15 % higher yield strength, 424 MPa for the P/M extrusion product versus 369 MPa for the control I/M extrusion product which was also manufactured with a 643 K extrusion-preheat.

2.3.2.2 Particle Chemistry

Investigation of the P/M and I/M extrusion products' particles with EDAX did not reveal any significant differences in particle chemistry. The only difference found was that Mg_2Si type particles were observed in the I/M product but not in the P/M product. In general an effort is made during alloy production to balance the silicon content with that of iron in order to tie up the iron as $\alpha AlFeSi$. Thus iron is not allowed to drain copper from its hardening role through formation of Fe-Cu particles such as Cu_2FeAl_7 . However, the $\alpha AlFeSi$ constituent particles were not observed during the limited EDAX particle survey in either the I/M or P/M products, but the Al-Fe-Cu and Al-Mn-Fe-Cu particles were readily observed. It is possible that the strong aluminum intensity masked the silicon response, however, no indication of this was observed.

The lack of significant particle chemistry differences between the I/M and P/M extrusion products, as determined by EDAX analyses, is in agreement with the small differences in the

lattice parameters between these products, Table 21. These results further indicate that air atomizing of the 2024 alloy does not produce a supersaturated matrix or significantly suppress constituent particle formation in P/M extrusion products. Lebo and Grant [11] have reported that in extrusion products fabricated from splat quenched 2024 foils, the Al-Mn-Fe-Cu particles did not form. Similar results were found during the EDAX particle analysis of the P/M product given the short time, low temperature homogenization treatment (Treatment B, Table 21). This analysis showed many Al-Cu particles with very low intensity iron and manganese peaks and no clearly distinguishable Al-Mn-Fe-Cu particles. However, EDAX particle analysis of P/M extrusions given the standard I/M 2024 homogenization treatment (Treatment A, Table 21) or an elevated temperature homogenization treatment (Treatment C) revealed that the Al-Mn-Fe-Cu particles did subsequently form. Thus air atomization can initially suppress formation of Al-Mn-Fe-Cu particles, but since homogenization treatments of the A or C type are necessary to reduce VPCP and to optimize mechanical properties, the presence of the Al-Mn-Fe-Cu particles in the final P/M product can not be avoided.

2.3.3 Optical Microstructure

Examination of the optical microstructure of the P/M and I/I extrusion products manufactured with a 25:1 extrusion ratio revealed considerable differences. After the solution heat treatment the I/M extrusion product's microstructure is completely recrystallized, Figure 32. Whereas the degree of recrystallization in P/M extrusion product's microstructure after solution heat treatment is dependent upon processing variables, Figures 33 and 34.

For the P/M product, extrusion processing parameters were varied to yield P/M products with microstructures from completely recrystallized (Figure 33) to completely unrecrystallized. The grain structure of these P/M extrusions varies from $\bar{L} = 6.7$ to $63.5 \mu\text{m}$, Table 22, the latter grain size represents the completely recrystallized P/M extrusion product. It is of interest to note that the recrystallized P/M products' strength properties are

equivalent to those of the control I/M alloy C product, Table 23. However, the range of mechanical properties for the various P/M products given in Table 23 demonstrates that a strength-microstructure dependence exists for 2024-T3510. For the fine grain P/M products, which are either unrecrystallized or have a low degree of recrystallization the average strength increase is about 20 % over the recrystallized (coarse grain) P/M product of the same powder alloy. The strength-microstructure dependence for some of the P/M and I/M extrusion products given in Tables 22 and 23 are illustrated by graphing the relationship between yield strength and the reciprocal of the grain thickness G_L , Figure 35. Similar Hall-Petch relationships can be illustrated for the tensile strength, and as a function of the reciprocal of the square root of the mean grain intercept length, \bar{L} .

The strength-microstructure dependence was determined for the case of coherent G.P. zones, i.e. shearable hardening "precipitates", resulting from natural aging. A similar strength-microstructure relationship was found for the artificially aged P/M 2024 alloy products, although this relationship was not as extensively investigated for artificial aging as it was for natural aging. The effect of the different microstructures, developed through extrusion-preheat temperature variation, on the P/M extrusion products mechanical properties is independent of aging treatment, Figure 24. However, the strength-microstructure relationship between I/M and P/M extrusion products is not the same for artificial aging as it is for natural aging.

DISCUSSION

1. S-N Fatigue

1.1 7075

It is thought that a significant portion of the notch S-N fatigue improvements for the P/M products results from the refined size and more uniform distribution of the coarse constituent phase particles and the small grain size, both of which positively affect crack initiation resistance. For a fatigue resistant material Grosskreutz [56] has suggested that concentrations of plastic strain should be reduced by eliminating coarse intermetallic particles as well as other factors which promote inhomogeneous deformation. For the P/M products both of these conditions are at least partially fulfilled. The high solidification rate experienced by the powder particles eliminates the larger intermetallic particles by distributing the normally coarse constituent particles into a finer dispersion. As presented in the microstructure section, the mean constituent particle intercept length for the P/M product is 26 % smaller than the control I/M product. The small grain size of the P/M products serves to promote homogeneous deformation as the grain boundaries can impede cyclic slip motion. Thus two mechanisms are active in the P/M products which are not reflected in the strength parameters, Table 3, but which can significantly increase the applied stress required for crack nucleation.

The reduced scatter in the P/M product's response, and therefore a significantly higher stress level for a low probability of failure (i.e. $S_{10^7}^{P=10\%}$ or $S_{10^7}^{P=1\%}$) over the I/M product, is believed to be the result of the fine constituent particle size in the P/M product. Thus the probability of a large particle nucleating a crack due to strain incompatibility [25] in the area of the notch, is reduced in the P/M product.

The positive effects on S-N fatigue behavior of microstructural refinement of constituent particles due to P/M techniques may be overshadowed if P/M processing results in lower

ductility. If the P/M alloy's mechanical properties indicate reduced engineering ductility, the reduction in micro stress concentration in the area of a notch due to particle refinement, could very well be a secondary effect. Because the notch produces a region of strain controlled fatigue damage, material with lower macroscopic ductility could possibly show an exhaustion of cyclic ductility and therefore crack initiation at a lower number of cycles, or equivalently, at a lower applied stress for a given number of cycles. Unfortunately, the relationship between macroscopic ductility-microstructure and cyclic ductility is not understood. Examples of high strength aluminum P/M alloy products with low macroscopic ductility, improved smooth S-N fatigue response over I/M 7075, and notch S-N fatigue response equivalent to I/M 7075 exist in the literature [57].

The P/M and control I/M products investigated for this report have equivalent macroscopic strength and ductility parameters. Thus the possible early exhaustion of cyclic ductility is not a significant factor here. However, the influence of grain size on promoting homogeneous deformation has not been adequately characterized. In pursuit of this characterization goal, the fatigue response of the I/M alloy M(7475) extrusion product with constituent particle size equivalent to the alloy L 7075 P/M extrusion product, and grain size equivalent to the alloy H 7075 I/M extrusion product, will be investigated.

Additionally, the role of the finely dispersed oxide with regard to homogeneous deformation in the P/M extrusion products is not well understood. The powder particle's surface oxide layer is broken up during extrusion to about the same size as that of the dispersoid phase. It is therefore plausible that the oxide particles act in a manner similar to the dispersoid in promoting homogeneous slip deformation. However, in the 25:1 P/M extrusions the distribution of these oxide particles is much coarser than the fine distribution of the chromium E-phase dispersoid particles and is thought not to be a significant factor with regard to homogeneous deformation.

With regard to degraded LCF response, the limited I/M and P/M

data for the $K_t = 3$ behavior at a load of 200 MPa, Figures 3 and 4, together with the flatness of the P/M response in the $10^4 - 10^5$ cycles region, are indications of a poorer LCF response for the P/M product. In addition, preliminary indications from the ongoing smooth S-N fatigue investigation confirm this behavior. In order to quantify the LCF behavior of P/M products, it is suggested that constant strain amplitude fatigue testing be performed. In this manner the cyclic plastic strain, or fatigue damage, at a given stress level may be more adequately defined. Alternately, to determine if this observation can significantly impact service life, spectrum loading which incorporates the stress levels from the LCF region might be expected to show the importance of the LCF degradation and the HCF improvement.

LCF degradation has also been reported for high purity I/M alloy products. Kaufman [16] has presented smooth S-N fatigue data which shows that higher purity I/M alloy products have lower mid-life ($10^4 - 10^6$ cycles) fatigue strengths than conventional I/M products with higher iron and silicon contents. It is not understood whether the LCF degradation is a result of a decrease in the crack initiation or propagation resistance. In the LCF range, the larger constituent particles found in the high iron and silicon products may contribute to the capability to resist concentrated large scale slip. These constituent particles decrease the crack initiation resistance in the HCF range by increasing the strain concentration, but they may homogenize the large strain concentrations that occur in the LCF region and inhibit crack nucleation which would result from early slip band decohesion. Concerning propagation, Staley [58] has proposed a mechanism for variable amplitude loading where the constituent particles may improve the resistance to fatigue crack propagation. Cracks which nucleate at particle matrix interfaces from a high stress intensity overload, divide the stress intensity over many secondary crack sites and decrease the effective stress intensity at the main crack tip. Application of this mechanism to the constant load amplitude LCF region may also be applicable as the stress intensity at the crack tip is also increasing due to the reduced cross section. However, the increase in stress intensity resulting from crack growth in constant load amplitude

testing is significantly smaller than the increase resulting from an overload. The initiation mechanism rather than the propagation mechanism therefore is a more plausible explanation of the LCF degradation in higher purity alloy.

1.2 2024

For the same reasons discussed concerning the improved notch HCF fatigue response of 7075, the notch HCF fatigue improvement of the P/M 2024 extrusion product is also thought to be a result of improved fatigue crack initiation resistance. These factors include reduction in microstrain concentrations via more homogeneous slip deformation and elimination of the large constituent particles. The reduction in slip length, and therefore the reduction in stress concentration by reducing the number of dislocations in a pileup, results from a smaller grain size. The elimination of coarse particles through refinement of the constituent phases results from the rapid solidification of the powder. It is thought that the reduction in microstrain concentration resulting from the reduction in average constituent particle size is the main factor leading to the improved fatigue crack nucleation resistance of the normalized P/M fatigue data.

In addition to the above mentioned factors, the degree of recrystallization and its influence on the fatigue behavior must also be considered for the 2024 extrusion products. As discussed under processing section 2.1, the P/M extrusion product manufactured with a 643 K extrusion-preheat has a partially recrystallized microstructure after the solution heat treatment. Using the point count method described by Hilliard [59], the amount of recrystallization is estimated to be 2 %. The recrystallized grains are predominantly small nuclei located next to the grain boundaries. The P/M extrusion product manufactured with a 753 K extrusion-preheat is unrecrystallized. The 643 K P/M product also has a smaller grain size ($\bar{L} = 6.7 \mu\text{m}$) than the 753 K product ($\bar{L} = 8.6 \mu\text{m}$).

In terms of fatigue strength, unrecrystallized structure as well as nonshearable particles and grain boundaries increase fatigue

crack nucleation resistance by promoting homogeneous deformation. These three microstructure properties therefore must be to some degree redundant in their ability to reduce slip length. For the 2024 alloy the findings of Lütjering et al. [60] show the incoherent manganese dispersoid particle (nonshearable) is essential to developing homogeneous slip and good fatigue behavior. Also Lütjering et al. [61] have shown that reduction in grain size is effective in increasing the fatigue crack nucleation resistance for a 7XXX high strength aluminum alloy containing shearable particles. The influence of grain size on crack initiation has also been confirmed by others [62, 63]. Both the nonshearable particle and grain boundary mechanisms are active in the P/M products. The degree to which an unrecrystallized structure must be relied upon to promote homogeneous slip deformation is therefore reduced. This dependence can be expected to be further reduced as the grain and/or subgrain boundary spacing approaches the mean intercept length between dispersoid particles.

The low amount of recrystallization found in the P/M extrusion product manufactured with a 643 K extrusion-preheat is apparently not sufficient to affect the degree of homogeneous slip deformation. Apparently, the smaller grain size of this product was sufficient to override any deleterious effects resulting from the low degree of recrystallization and to yield an improved notch HCF response in comparison to the P/M extrusion product manufactured with a 753 K extrusion-preheat.

With regard to LCF degradation, the effect of purity (VPCP and particle size) on the I/M and P/M extrusion products can be seen in Figure 27. The higher purity P/M (alloy E) and I/M (alloy C) extrusion products have a shorter LCF life than the commercial purity I/M (alloys A and B) extrusion products. From the limited LCF data for these high purity P/M (Figure 25) and I/M (Figure 26) extrusion products, there appears to be no significant LCF behavior differences. Thus LCF strength appears to be dependent on alloy chemistry and not manufacturing methods.

2. Monotonic Properties

2.1 7075

The yield strengths of the I/M and P/M 25:1 extrusion products investigated do not show a clear dependence on grain size over the range investigated, even though the grain size of the P/M product is a factor of 4 smaller. The yield strengths of these products are summarized from Table 3 and presented below with the various grain sizes for comparison.

7X75-T6510 extrusion product	0.2% YS [MPa]	grain size	
		\bar{L}	G_{\perp}
		[μm]	
P/M 7075	627	7.5	5.0
I/M 7075	622	28.2	21.8
I/M 7475	618	28.5	17.2

This result agrees with previously published studies where the tensile properties of high strength aluminum alloys have been shown to have a low dependence on grain size [51, 64].

Waldman et al. [51] have shown grain sizes from 15 to 112 μm to have only a minor effect on the yield strength of 7075-T6 plate products. Their measurements were obtained from products with as-recrystallized grains and as-recrystallized plus 40 % hot rolled (800 K) microstructures. Lütjering et al. [61] have found no dependence of yield strength on grain size for a X-7075 alloy (without Cr) for two grain sizes, 30 μm and 220 μm .

This low dependence of yield strength on the grain size in 7075 has been explained by the joint effect of the chromium dispersoid and the partially coherent η' intermediate precipitate particles [51]. These particles reduce slip length and promote homogeneous slip within each grain, thereby reducing the influence of the grain boundary. The X-7075 alloy examined by Lütjering et al. [61] did not contain dispersoid particles, and was aged 24 h at 373 K to produce hardening by shearable, coherent GP zones. Their material showed intense slip bands and yet did not show an

effect of grain size on yield strength. Thus absence of a grain size-yield strength relationship is not dependent upon the homogeneity of deformation. Both Waldman et al. [51] and Lütjering et al. [61] have reported increased fracture ductility with decreasing grain size. Based on a TEM microstructure study of titanium alloys, Gysler and Lütjering [65] have also found that slip deformation becomes more homogeneous as grain size decreases. Thus while decreasing the grain size has a small or no effect on the yield strength, it can homogenize slip deformation and improve the tensile fracture properties. Decreasing the grain size reduces the slip length, thereby reducing stress concentration and delaying crack nucleation. While the dispersoid and hardening particles tend to mask the role of the grain boundaries, the grain boundaries can be expected to play a more significant role in homogenizing slip deformation as the grain size approaches the order of magnitude of the dispersoid spacing.

Abson [66] has extrapolated the data of Waldman et al. [51] based on a Hall-Petch relationship with a grain size exponent of $-1/2$ to a grain size of one micron. His data would suggest yield strengths between 480 and 525 MPa for the grain sizes produced in the current investigation. Although this extrapolation shows grain sizes on the order of 3 μm or less would have a significant effect on yield strength, it cannot account for the high yield strengths found in the current investigation.

The strength properties for both the 25:1 I/M and P/M 7075-T6510 extrusion products, Table 3, show a 40 - 50 MPa increase over published values for similar I/M extrusion products. Gurney et al. [22] and Roberts [67] for extruded I/M 7075-T6 and Anderson and Hurst [68] for extruded I/M 7075-T6 and T6510 did not find yield strength improvements due to increasing extrusion ratios beyond 580 MPa. Tests in the author's laboratory did not find any consistent difference in strength between T6 or T6510 treatments; this finding is in agreement with published values [68]. Additionally, the strength properties for the 10:1 extrusion products, Table 2, are higher than the maximum strength properties reported by Gurney et al., Roberts, or Anderson and Hurst. Consequently, the strength properties of the I/M and P/M extrusion

products may represent an upper strength limit for optimum processed 7075 extrusions, as discussed by Kaufman [16] for property variations in commercial products.

One possible explanation for the enhanced strength properties of the P/M and I/M extrusion products is the effect of the substructure. If substructure strengthening is the responsible mechanism for the additional improvement of the yield strength in the P/M and I/M extrusion products investigated, then one would not expect to find any measurable difference in yield strength among the P/M and I/M products since their subgrain sizes are very similar, Table 10.

Jacobson et al. [69] have reported significant tensile and yield strength improvements due to the effect of substructure in 7075-T6 extrusion products (8.5:1 extrusion ratio). They found a 110 MPa difference in both yield and tensile strength based on substructure and texture differences, when the degradation in precipitation response caused by substructure is avoided through a low temperature incubation period between the solution heat treatment quench and the elevated temperature artificial aging step [70, 71]. A similar 3 to 5 day incubation period at room temperature was also employed in the current investigation. Therefore, when considered together with grain size and texture strengthening, subgrain strengthening may account for the high levels of yield strength reported in Table 3.

2.2 2024

The 2024 P/M extrusion products exhibit a microstructure-strength relationship. For the unrecrystallized, naturally aged extrusion product, the strength increases as the controlling grain size width parameter (G_{\perp}) decreases below approximately 8 μm . The P/M extrusion products which exhibited this grain size dependence contained a well defined, recovered substructure where individual dislocations in the subgrain boundary could not be resolved by the TEM. The substructure by itself does not provide the increased strength. Tensile specimens from unrecrystallized material containing similar recovered substructure and a grain width

of 12 μm , have strength properties equivalent to the large grain, recrystallized P/M and I/M products. The substructure of the small grain size products, $G_1 \approx 8 \mu\text{m}$, may enhance the grain size effect, but for grain sizes larger than 8 μm , the strength properties of microstructures with 50 % recrystallization or greater are equivalent to those of unrecrystallized microstructures which have a well defined substructure.

The strength properties of the large grain P/M products are equivalent to those of the I/M extrusion product, even though significant grain size differences exist. It follows that as the mean free boundary to boundary distance increases, the degree to which nonshearable manganese dispersoid particles become the governing factor in determining the slip length, and therefore the strength parameters, also increases [60, 72]. For the recrystallized P/M extrusion products, the mean free distance between boundaries is two orders of magnitude greater than the mean free distance between the dispersoid particles. Consequently, the recrystallized P/M extrusion products as well as the large grain, recrystallized I/M extrusion products do not show a strength-grain size relationship. On the other hand as the mean free spacing between the grain boundaries approaches the dispersoid spacing, even though still an order of magnitude larger, boundaries exert an influence on the slip length and therefore on the strength parameters.

The smallest grain size determined for the P/M products was equivalent to the large dendritic cell spacing of the powder. Thus providing independent evidence to the hypothesis reported by Dean and Anderson [72] that dendritic cell spacing could pose a lower limit to the attainable grain size.

Artificial aging affects the grain size-strength relationship. The degree to which the grain size affects the strength properties is reduced as the hardening precipitate's resistance to shearing increases. In the naturally aged condition shearing of the GP zones leads to inhomogeneous, planar slip. In this case the boundaries and dispersoid particles interact with dislocations to limit the planar slip length. The semi-coherent

artificial age hardening precipitate, S', has a greater resistance to shear than the GP zones. Consequently, the degree to which deformation takes place by particle looping increases as the degree of artificial aging increases. The looping of precipitate particles results in a more homogeneous slip deformation. The degree to which the material's yield strength is dependent upon grain size is thereby reduced as artificial aging decreases the role of the boundaries in determining the slip length. Consequently, the effectiveness of the strength-grain size dependence found in the naturally aged (T3X and T4) products is reduced for the artificially aged (T6 and T8X) 2024 extrusion products. Figure 24 and Tables 13 - 16 exhibit this relationship for the P/M extrusion products fabricated with 643 K and 753 K extrusion-preheat temperatures.

In addition to the reduction of the influence of grain size on yield strength caused by the precipitate morphology change, artificial aging of the fine grain P/M products causes an overall reduction in the strength properties compared to those in the naturally aged condition. Taken together, the artificially aged P/M extrusion products shown in Figure 24 have lower strength values than the P/M extrusion products in the naturally aged condition and the I/M extrusion product in the artificially aged condition. This strength reduction results from a reduction in the volume fraction of strengthening precipitates as solute diffuses to the grain and subgrain boundaries. At these boundaries the nonhomogeneous solute concentration results in the formation of nonhardening grain/subgrain boundary precipitates, a precipitate free zone (PFZ), as well as a region between the PFZ and fully hardened matrix which has a possible different precipitate density, size, and chemistry. Based on solute diffusion rates, the maximum calculated width across the grain boundary of a region of possible solute reduction is 1 μm . Transmission microscopy reveals that both the 2024-T851 P/M and I/M products have grain boundary precipitates and a PFZ width of approximately 0.2 μm . The subgrain boundaries of the artificially aged P/M products also affect the precipitate structure. Depending on the orientation difference across the subgrain boundary, either coarse S' precipitates, which grew into the interior of

each subgrain occur, or boundary precipitates in the middle of a PFZ form. Not all subgrain boundaries have a PFZ; for those boundaries which have a PFZ, the width varies up to 0.2 μm . No direct evidence was observed of a region of different precipitate size or density between the PFZ and fully hardened matrix, although some small region must exist. Therefore, the strength reduction predominantly results from the reduction of the volume fraction of strengthening precipitates in a region approximately as wide as the PFZ.

The reduced precipitate volume fraction could be predicted to show an important effect on the macroscopic yield strength only when the grain boundary surface area per unit volume becomes very large. Using the quantitative metallographic techniques discussed by Underwood and Starke [42] the grain boundary surface area of the P/M extrusion products is 30 times larger than the grain boundary surface area of the I/M extrusion product. Since the PFZ width is approximately 0.2 μm for the 2024-T851 P/M and I/M alloys, the volume of the PFZ in the P/M products is approximately 30 times larger than that in the I/M products. When the product's strength is derived by the law of mixtures from the strength of the PFZ and the precipitation hardened matrix, the degree to which this PFZ volume change affects the strength properties may be visualized. If the strength of the PFZ is taken as the yield strength of the material in the annealed condition (103 MPa), and the strength of the precipitation hardened matrix is assumed as the average yield strength of I/M products from Table 16 (462 MPa), the calculated P/M product's yield strength would be 430 MPa. This value compares favorably with the average 437 MPa yield strength for the P/M extrusion products in the T851 condition, Table 16. Disregarding the effect of grain size strengthening in the artificially aged condition, this approximation provides an explanation as to why it is necessary to thermally mechanically treat the P/M products in order to obtain the same yield strength in P/M and I/M extrusion products.

The difference in the stress-strain behavior between the 2024-T851 I/M and P/M extrusion products provides additional evidence

that the increase in PFZ volume is responsible for the reduction in strength. The initiation of microplasticity occurs between 305 and 312 MPa for the I/M products and between 215 and 255 MPa for the P/M products. The consistent early departure from proportional stress-strain behavior for the P/M products therefore provides strong evidence that microplasticity and strain hardening is occurring in the PFZ.

The strengthening mechanism in the artificially aged extrusion products is therefore not an additive effect of grain size and precipitation hardening as was the case for natural aging, Figure 24.

CONCLUSIONS

1. Uniaxial vacuum hot-compaction of prealloyed, air atomized 7075 aluminum alloy powder can provide strength properties equivalent to I/M 7075 products with acceptable ductility. These vacuum hot compacted products did not show any porosity and exhibit improved notch fatigue behavior compared to I/M 7075.
2. The constituent phase particles in P/M 7075 are refined compared to the size and distribution of the particles in I/M 7075. The volume percent of the constituent particles in the P/M product is slightly lower than the corresponding I/M product with the same chemistry. Rapid solidification during atomization does not suppress the formation of constituent particles in the final P/M product which was subjected to standard, short time low temperature, and short time high temperature homogenization treatments. A significant amount of the constituent phases in the P/M products is soluble. The volume percent of the constituent phase can be significantly reduced in 7075 P/M products by high temperature homogenization.
3. The grain size of the 7075 P/M extrusion product manufactured from 88 μm APD powder is an order of magnitude smaller than the grain size of commercial I/M 7075 extrusions. Special processing of I/M 7075 extrusion products yields grain sizes which are 4 to 5 times larger than the grain size of P/M products, but whose strength properties are equivalent to the high strength P/M extrusion product.
4. Extrusion ratios on the order of 10:1 or greater are required to impart good transverse ductility to the 7075 P/M extrusion products, although good longitudinal and transverse strength properties and longitudinal ductility properties are developed for 5.54:1 extrusion ratios.

5. No significant difference in the longitudinal strength properties between 7075 P/M and specially processed I/M extrusion products are developed, although the strength anisotropy in the P/M extrusion products is significantly less than in the respective I/M product.
6. The notch fatigue behavior in a laboratory environment of the 7075 P/M extrusion products is significantly improved in comparison to that of the 7075 I/M product. Characterization of the P/M 7075 microstructure indicates that this improvement results from favorable alteration of microstructure parameters which are known to affect the fatigue crack nucleation resistance.
7. Similar to the results of P/M 7075, the mechanical properties of vacuum hot compacted 2024 aluminum alloy powder are equivalent to typical I/M 2024 mechanical properties.
8. The volume percent of the constituent phase in the P/M 2024 extrusion product is reduced compared to that of the I/M 2024 extrusion product. Unlike the response to variations in the homogenization treatment found for the P/M 7075, the VPCP of the P/M 2024 can not be significantly reduced by high temperature homogenization treatments. Short time homogenization of the P/M 2024 products is insufficient to reduce the VPCP level to typical values for I/M 2024 products.
9. Variation of the initial powder size produces slight variations in the 2024 P/M extrusion product's grain size. P/M products made from powder whose APD was varied over the range 36 μm to 117 μm did not show any significant mechanical property effect for P/M products in the naturally aged condition.
10. The extrusion-preheat temperature affects the grain size and significantly affects the strength and notch S-N fatigue properties of the 2024 P/M extrusion products. An extrusion-preheat temperature of 643 K was found to yield the smallest grain size and the best mechanical properties.

11. The 2024 aluminum alloy when hardened by coherent G.P. zones shows a strength - grain size correlation. A weaker correlation exists in the artificially aged condition where hardening is the result of partially coherent S'precipitates.
12. In the naturally aged condition the P/M 2024 extrusion products show a combined grain size and G.P. zone hardening effect. The P/M product in the naturally aged condition therefore exhibits a significant improvement in strength without any loss of ductility in comparison to I/M 2024 products. In the artificially aged condition the fine grain 2024 P/M extrusion products exhibit a slightly lower strength than that of the 2024 I/M extrusion products.
13. The notch S-N fatigue behavior in a laboratory air environment of the naturally aged 2024 P/M extrusion products is significantly improved in comparison to that of naturally aged 2024 I/M extrusion products. The greatest portion of this improvement results from the strength increase. Characterization of the microstructure indicates that the additional improvement results from favorable alteration of microstructure parameters which are known to affect fatigue crack initiation resistance.

Appendix A

Solution Heat Treatment Study for P/M 7075

As a supplementary mechanical property investigation, the effect of solution heat treatment temperature on the strength and ductility (longitudinal and transverse) of extrusion products was investigated. The aim of this investigation was to determine if an evacuation-preheat temperature higher than the 743 K solution heat treatment temperature would adversely affect mechanical properties; incipient melting of nonequilibrium phases was the main concern [23].

The results of this investigation, Table 6, show that from a strength and ductility standpoint, no general detrimental ductility effects or significantly enhanced strengthening response can be obtained by this treatment. For tensile specimens from the longitudinal direction, there is a slight reduction in ductility and a slight increase in yield strength as the solution heat treatment temperature increases. This ductility reduction, which should not present problems as significant ductility remains, is probably the result of the grain structure coarsening due to the long elevated temperature exposure. For tensile specimens from the critical transverse direction which were solution heat treated at 793 K, the yield stress shows a 5.4 % decrease while the ductility parameters show a slight increase.

Metallographically these property changes correlate with: a coarsening of the hot-worked grain morphology (mean subgrain intercept length increased from $\bar{\lambda} = 2.1 \mu\text{m}$ to $\bar{\lambda} = 3.8 \mu\text{m}$), a significant reduction in the volume percent coarse intermetallic particles (VPCP decreased from 2.3 vol.% to 1.7 vol.%), as well as no evidence of incipient melting in the grain boundaries as observed by optical metallography up to 1000 x.

Therefore, outgassing of the powder compacts at 793 K offers the potential for extruded products with improved fracture toughness due to VPCP reduction without significantly affecting the subsequently extruded P/M product's ductility.

With regard to the chromium E-phase dispersoid, no detrimental effect on static or dynamic properties [19, 24, 25] should occur as excessive coarsening of the dispersoid phase does not take place. A TEM examination of a 7075 P/M extrusion product which was solutionized at 788 K for 65 h did reveal possible coarsening; however, the maximum size of the dispersoid particles observed (0.3 μm) was within the normal size range reported for the particles (0.5 - 0.05 μm). Haarr [26] reports that preheating 7075 powder at 805 K and above, noticeably coarsens the chromium dispersoid. He also reported that after 12 h at 755 K coarsening had appeared.

FUTURE RESEARCH EFFORT

1. effect of short time preheat-treatment on P/M 7075 when evacuated to control hydrogen partial pressure, also evaluation of same but employing a 793 K evacuation temperature
2. notch ($K_t = 3$) and smooth fatigue of 2024 P/M alloy E and I/M alloy C extrusions at equivalent yield strengths (T8 temper)
3. smooth fatigue response of 7075-T6510 alloys H and L (if da/dn results don't show significant differences)
4. FCG studies of 10:1 extrusions and unidirectional hot pressed specimens: 2024 P/M alloy E, T-351, and T-854 for comparison with alloy C at an equivalent yield stress level in T-852 temper; 7075-T6510 P/M alloy L and I/M alloys H and M, as well as hot pressed alloy L (T6) [tests in progress].
5. further characterization of microstructure (optical, TEM, SEM)
6. texture investigation of extrusions and hot pressed products

REFERENCES

- [1] Voss, D.P. Development of Improved High Strength Aluminum Powder Metallurgy Products.
EOARD-TR-78-3, 31 May 1978. (AD AO62981).
- [2]a.Jäniche, H. Kaltpreßschweißen von Aluminiumpulver durch Strangpressen.
Doktor-Ingenieur Dissertation, Technical University of Berlin: 1975, D 83.
- b.Grosch, J.
Jäniche, H. Kaltpreßschweißen von Aluminiumpulver durch Strangpressen.
Aluminium, Vol. 50, No. 5 (1974) pp. 343-349. (Translation w/o figures: "Cold Pressure Welding of Aluminum by Extrusion". Aluminium - Supplement in English, pp. 34-48.
- c.Grosch, J.
Jäniche, H. Cold Extrusion of Aluminum Powders.
Presented at 5th International P/M Conference, Chicago, June 27, 1976, and published in Modern Developments in Powder Metallurgy. Vol. 10, pp. 325-346.
- [3] Lyle, J.P., Jr. Properties of High Density Aluminum P/M Products.
Cebulak, W.S.
Buchovecky, K.E. Progress in Powder Metallurgy - 1972 National P/M Conference Proceedings, April 17-19, Vol. 28, pp. 93-114, Bufford, A.S. (Ed.). New York: Metal Powder Industries Federation, 1972.
- [4]a.Lyle, J.P., Jr. Properties of High-Strength Aluminum P/M Products.
Cebulak, W.S. Presented at "The Third Air Force Metal Working Conference, Western Metal and Tool Exposition", March 13-16, 1972. Los Angeles, CA
- b.Lyle, J.P., Jr. Properties of High Strength Aluminum P/M Products.
Cebulak, W.S. Metals Engineering Quarterly, Vol. 14, No. 1 (February 1974) pp. 52-63.
- [5] Cebulak, W.S. Program to Develop High Strength Aluminum Powder Metallurgy Products - Phase III - Scale Up A.
Truax, D.J. Contract No. DAAA 25-70-CO358, Sept 29, 1972.

- [6] a.Cebulak, W.S.
Johnson, E.W.
Markus H. High Strength Aluminum Powder Metallurgy Mill Products.
Presented at "P/M Ordnance" Seminar, April 19-20, 1976, Dover, N.J. Proceedings published by Metal Powder Industries Federation, Princeton, N.J. pp. 119-137; also International Journal of Powder Metallurgy, Vol. 12, No. 4 (April 1976) pp. 299-310.
- b.Cebulak, W.S.
Johnson, E.W.
Markus, H. High Strength Aluminum P/M Products.
Metals Engineering Quarterly, Vol. 16, No. 6 (November 1976) p. 37.
- [7] Cebulak W.S. Program to develop High-Strength Aluminum Powder Metallurgy Mill Products - Phase IVB - Scale Up to 1545 kg (3400 lb) Billet.
Contract No. DAAA 25-72-C-0593. Final Report, FA-TR-76067 April 25, 1977, (AD O39 862).
- [8] Otto, W.L., Jr. Metallurgical Factors Controlling Structure in High Strength Aluminum P/M Products.
AFML-TR-76-60, Contract No. F 33615-74-C-5077, May 1976.
- [9] Fatigue Resistant Al P/M Alloy Development.
USAF/AFML Contract No. F 33615-77-C-5174, in Progress.
- [10] a.Rafalin, M.
Koczak, M.J.
Lawley, A. Fatigue of High-Strength Aluminum Alloy P/M Forgings.
Thermo-Mechanical Processing of Aluminum Alloys, AIME, in press. (Paper presented at Fall AIME Meeting, St. Louis, Missouri, Oct 1978.
- b.Koczak, M.J.
Lawley, A. A Fundamental Study of Fatigue in Powder Metallurgy Aluminum Alloys.
Annual Technical Report, AFOSR Grant 77-3247, Oct 1978.
- [11] Lebo, M.
Grant, N.J. Structure and Properties of a Splat Cooled 2024 Aluminum Alloy.
Metallurgical Transactions, Vol. 5, No. 7 (July 1974) pp. 1547-1555.
- [12] Sankaran, K.K. Structure and Properties of Splat Quenched 2024 Type Al Alloys Containing Li.
Ph.D.Thesis, MIT, Cambridge, Mass. 1978.

- [13] Hunter, M.S.
Fricke, W.G. Metallographic Aspects of Fatigue Behavior of Aluminum.
Proceedings ASTM, Vol. 54, 1954, p. 717-736
- [14] Schijve, J. Significance of Fatigue Cracks in Micro-Range and Macro-Range, Fatigue Crack Propagation.
ASTM STP No. 415, 1967, p. 415-459.
- [15] Reimann, W.H.
Brisbane, A.W. Improved Fracture Resistance of 7075 Through Thermomechanical Processing.
Engineering Fracture Mechanics, Vol. 5, 1973, pp. 67-78.
- [16] Kaufman, J.G. Design of Aluminum Alloys for High Toughness and High Fatigue Strength.
Specialists Meeting on Alloy Design for Fatigue and Fracture Resistance, AGARD-CP-185, 13-19 April 1975, p. 2-1 to 2-24.
- [17] Hunter, M.S.
Fricke, W.G., Jr. Cracking of Notch Fatigue Specimens.
Proceedings ASTM, Vol. 57, 1957, p. 643-654.
- [18] Danilkin, V.A.
et al. Effect of Degassing Atmosphere on Mechanical Properties of Granulated Aluminum Alloy Semi-Finished Products.
Poroshkovaya Metallurgiya No. 8, 1978, p. 97-101, (in Russian).
- [19] Rosenfield, A.R.
Price, C.W.
Martin, C.J.
Thompson, D.S.
Zinkham, R.E. The Relation Between Precipitate Microstructure and Mechanical Properties in Aluminum Alloys.
AFML-TR-74-129, Part I, December 1974.
- [20] Munz, D.
Eschweiler, J. Kerbzugversuche an verschiedenen Aluminiumlegierungen zur näherungsweisen Bestimmung der Rißzähigkeit. (Notch Tensile Tests on Various Aluminum Alloys for the Approximate Determination of Fracture Toughness).
Institut für Werkstoff-Forschung der DFVLR, 5000 Köln 90, W.-Germany, IB 354-79/1979.

- [21] Hyatt, M.V. New Aluminum Aircraft Alloys for the 1980's. Proceedings of International Symposium on Aluminum Alloys in the Aircraft Industries, Torino, Italy, October 1-2, 1976.
- [22] Gurney, F.J.
Abson, D.J.
De Pierre, V. The Influence of Extrusion-Consolidation Variables on the Integrity and Strength of the Product from Prealloyed 7075 Aluminum Powder.
Powder Metallurgy, Vol. 17, No. 33 (1974) pp. 46-69.
- [23] Sperry, P.R. Discussion of Solution Kinetics of a Cast and Wrought High Strength Aluminum Alloy and 'Influence of Ingot Structure and Processing on Mechanical Properties and Fracture of a high Strength Wrought Aluminum Alloy'.
Metallurgical Transactions, Vol. 1, May 1970, p. 1465.
- [24] Hunsicker, H.Y. Metallurgical Structure Control, Key to Fracture Resistant Strong Aluminum Alloys. Presented at National Conference on Controlled Metallurgical Structures, New York University, January 13-14, 1975.
- [25] Staley, J.T. Microstructure and Toughness of High-Strength Aluminum Alloys.
Properties Related to Fracture Toughness ASTM STP 605, 1976, pp. 71-96.
- [26] Haarr, A.P. Development of Aluminum-Base Alloys. Second Annual Progress Report, Report No. 7-63-AP 59-s, October 30, 1963 (AD 423398).
- [27] Maennig, W. Statistical Planning and Evaluation of Fatigue Tests.
International Journal of Fracture, Vol. 11, No. 1, February 1975, pp. 123-129.
- [28] Kaufman, J.G.
Schilling, F.E.
Nordmark, G.E.
Lifka, B.W.
Coursen, J.W. Fracture Toughness, Fatigue and Corrosion Characteristics of X7080-T7E41 and 7178-T651 Plate and 7075-T6510, 7075-T73510, X7080-T7E42, and 7178-T6510 Extruded Shapes.
AFML-TR-69-255, November 1969, (AD 864895).

- [29] Barker, R.S.
Sutton, J.G.
(Editor -
Van Horn, K.R.) Stress Relieving and Stress Control.
Aluminum - Fabrication and Finishing,
Vol. III, Chapter 10, p. 355. ASM,
Metals Park, Ohio, 1967.
- [30] Sanders, R.E.
Starke, E.A., Jr. The Effect of Intermediate Thermomechanical
Treatments on the Fatigue Properties of a
7050 Aluminum Alloy.
Metallurgical Transactions, Vol. 9A, No. 8,
August 1978, pp. 1087-1100
- [31] Lin, F.S.
Starke, E.A., Jr. The Effect of Copper Content and Degree
of Recrystallization on the Fatigue
Resistance of 7XXX-Type Aluminum Alloys.
Ph.D.Thesis at Georgia Institute of Tech-
nology 1978 (Accepted for publication in
Material Science and Engineering).
- [32] Lyle, J.P., Jr.
Cebulak, W.S. Fabrication of High Strength Aluminum
Products from Powder.
Proceedings of 18th Sagamore Army Materials
Research Conference, Powder Metallurgy
for High Strength Applications, Syracuse
University Press, 1972, pp. 231-254.
- [33] Lyle, J.P., Jr.
Cebulak, W.S. Powder Metallurgy Approach for Control of
Microstructure and Properties in High
Strength Aluminum Alloys.
Metallurgical Transactions, Vol. 6A,
April 1975, pp. 685-699.
- [34] Otto, W.L., Jr. Metallurgical Factors Controlling Struc-
ture in High Strength Aluminum P/M Pro-
ducts.
AFML-TR-76-60, May 1976 (AD A030606).
- [35] Determining Volume Fraction by Systematic
Manual Point Count.
ASTM Standards, Part 11, Designation:
E 562-76.

- [36] Andrews, C.W. Volume Fraction Determination in Cast Superalloys and Directionally Solidified Eutectic Alloys by a New Manual Point Count Practice.
Journal of Testing and Evaluation, Vol. 6, No. 1, 1978, pp. 20-28.
- [37] El-Soudani, S.M. Influence of Inclusion Content on Fatigue Crack Propagation in Aluminum Alloys.
Pelloux, R.M.
Metallurgical Transactions, Vol. 4, No. 2, February 1973, pp. 519-531.
- [38] Mulherin, J.H. Influence of Nonequilibrium Second-Phase Particles Formed During Solidification upon the Mechanical Behavior of an Aluminum Alloy.
Rosenthal, H.
Metallurgical Transactions, Vol. 2, No. 2, 1971, pp. 427-432.
- [39] Thompson, D.S. Metallurgical Factors Affecting High Strength Aluminum Alloy Production.
Metallurgical Transactions, Vol. 6A, April 1975, pp. 671-683.
- [40] Hunsicker, H.Y. Tear Resistant Sheet and Plate and Method for Producing.
Staley, J.T.
U.S. Patent 3,791,880, Feb 12, 1974.
- [41] Abson, D.J. Microstructure and Mechanical Properties of Product from Extrusion Consolidated Gurney, F.J. 7075 Al prealloyed Powder.
De Pierre, V.
AFML-TR-76-194, November 1976 (AD A037188).
- [42] Underwood, E.E. Quantitative Stereological Methods for Analyzing Important Microstructural Features in Fatigue of Metals and Alloys.
Starke, E.A., Jr.
Proceeding of ASTM Symposium on Fatigue Mechanics, Kansas City, Mo., May 22-24, 1978.
- [43] Van Horn, K.R. X-Ray and Electron Diffraction.
(Editor)
Aluminum - Properties, Physical Metallurgy and Phase Diagrams, Vol. I, ASM Metals Park, Ohio, 1967, p. 400.

- [44] Durand, J.P.H.A.
Pelloux, R.M
Grant, N.J. Properties of Splat Quenched 7075 Aluminum Type Alloys.
Materials Science and Engineering, Vol. 23, 1976, pp. 247-256.
- [45] Mondolfo, L.F. Aluminum Alloys: Structure and Properties.
Butterworths, London-Boston, 1976, pp. 282-289.
- [46] Quist, W.E.
Hyatt, M.V. The Effect of Chemical Composition on the Fracture Properties of Al-Zn-Mg-Cu Alloys.
Proceedings American Institute of Aeronautics and Astronautics American Society of Mechanical Engineers, Seventh Structures and Materials Conference, Cocoa Beach, Florida, April 1966, pp. 228-242.
- [47] Quist, W.E.
Hyatt, M.V.
Anderson, W.E. Discussion to Microstructure and Toughness of High Strength Aluminum Alloys.
Properties Related to Fracture Toughness, ASTM STP 605, 1976, pp. 96-103.
- [48] Hunsicker, H.Y.
(Editor -
Van Horn, K.R.) The Metallurgy of Heat Treatment.
Aluminum - Properties, Physical Metallurgy and Phase Diagrams, Vol. I, Chapter 5, p. 125, ASM, Metals Park, Ohio, 1967.
- [49] Bhandarkar, M.D.
Lisagor, W.B. Metallurgical Characterization of the Fracture of Several High Strength Aluminum Alloys.
NASA Technical Paper - 1086, December 1977.
- [50] Hilliard, J.E. Estimating Grain Size by the Intercept Method.
Metals Progress, Vol. 85, May 1964, pp. 99-100.
- [51] Waldman, J.
Sulinski, H.
Markus, H. The Effect of Ingot Processing Treatments on the Grain Size and Properties of Al Alloy 7075.
Metallurgical Transactions, Vol. 5, No. 3, (March), 1974, pp. 573-584.

- [52] Ziegler, G. Structural and Morphological Investigations of Ceramic Powders and Compacts.
Powder Metallurgy International, Vol. 10, No. 2, 1979.
- [53] Nock, J.A., Jr. Properties of Commercial Wrought Alloys.
 (Editor - Aluminum Properties, Physical Metallurgy and Phase Diagrams, Vol. I, Chapter 9,
 Van Horn, K.R.) p. 303, ASM, Metals Park, Ohio, 1967.
- [54] Broek, D. The Effect of Precipitate Size on Crack
 Bowles, C.Q. Propagation and Fracture of an Al-Cu-Mg Alloy.
Journal of the Institute of Metals, Vol. 99, August 1971, pp. 255-257.
- [55] Roberts, S.G. Research Study for Development of Aluminum Base Alloys by Powder Metallurgy Techniques.
Summary Project Report No. MS PR 61-69, November 15, 1961, (AD 287852).
- [56] Grosskreutz, J.C. Fatigue Mechanisms and the Development of Fatigue-Resistant Materials.
AFML-TR-70-55, May 1970.
- [57] Lyle, J.P., Jr. Properties of High Strength Aluminum P/M Products.
 Cebulak, W.S. Metals Engineering Quarterly, Vol. 14, No. 1, February 1974, pp. 52-63.
- [58] Staley, J.T. How Microstructure Affects Fatigue and Fracture of Aluminum Alloys.
Presented at International Symposium on Fracture Mechanics, George Washington University, Washington, DC, September 11-13, 1978.
- [59] Hilliard, J.E. Applications of Quantitative Metallography in Recrystallization Studies.
Recrystallization, Grain Growth, and Textures, Chapter 7, p. 267, ASM, Metals Park, Ohio 1966.

- [60] Lütjering, G.
Döker, H.
Munz, D. Microstructure and Fatigue Behavior of Al-Alloys.
Proceedings Third International Conference on Strength of Metals and Alloys, Vol. 1, 1973, pp. 427-431.
- [61] Lütjering, G.
Hamajima, T.
Gysler, A. Influence of Grain Size on the Fracture of Aluminum Alloys.
Fracture 1977, Proceedings of the Fourth International Conference on Fracture, Vol. 2, Waterloo, Canada, June 19-24, 1977, pp. 7-16.
- [62] Sanders, R.E., Jr.
Starke, E.A., Jr. The Effect of Grain Refinement on the Low Cycle Fatigue Behavior of an Aluminum-Zinc-Magnesium-(Zirconium) Alloy.
Materials Science and Engineering, Vol. 28, 1977, pp. 53-68.
- [63] Gysler, A.
Terlinde, G.
Lütjering, G. Influence of Grain Size on the Ductility of Titanium Alloys.
Proceedings 3rd International Conference on Titanium, Moscow, USSR, May 1976, (to be published ASM/Pergamon Press).
- [64] Lütjering, G.
Gysler, A. Fatigue and Fracture Aluminum Alloys.
Proceedings First International Symposium on Aluminum, Puerto Madryn, Argentina, 1978, (ASM).
- [65] Gysler, A.
Lütjering, G. Unpublished TEM microstructure study.
- [66] Abson, D.J. Grain Boundary and Sub-Boundary Strengthening in Aluminum at Room Temperature.
Metal Processing Operations.
AFML-TR-72-142, Vol. I, July 1974.
- [67] Roberts, S.G. An Exploratory Investigation of Pre-alloyed Powders of Aluminum.
Powder Metallurgy, New York: Interscience Publishers (W. Leszinski, Ed.), 1961, p. 799-818.

- [68] Anderson, C.R.
Hurst, A.L.
(Editor -
Van Horn, K.R.) Extrusion.
Aluminum-Fabrication and Finishing,
Vol. III, Chapter 3, ASM Metals Park,
Ohio, 1967, p. 109.
- [69] Jacobson, L.A.
Pierce, C.M.
Cook, M.M. Microstructure of Powder and Convention-
ally Processed 7075 Aluminum Alloy.
AFML-TR-71-240, December 1971. (AD 744845).
- [70] Holl, H.A. Effects of a Sub-Grain Structure on
Precipitation-Hardening in a Aluminum-
Zinc-Magnesium-Chromium Alloy.
Journal of the Institute of Metals,
Vol. 93, 1964-65, pp. 364-365.
- [71] Holl, H.A. The Influence of a Subgrain Structure on
Precipitation Hardening and Nucleation of
Precipitates in a Al-Zn-Mg Alloy.
Metal Science Journal, Vol. 1, 1967,
pp. 111-118.
- [72] Dean, W.A.
Anderson, W.A.
(Editors -
Burke, J.J. and
Weiss, V.) Effects of Grain Size in Aluminum Alloys.
Ultrafine-Grain Metals - Proceedings of
16th Sagamore Army Materials Research
Conference, August 19-22, 1969, pp. 373-
375.

Acknowledgements

This work has been partially funded by USAF/EOARD-London under AFOSR Grant # 77-3440.

Portions of the investigation carried out under this Grant have been presented by D. Voss according to the below list:

1. Processing Study:

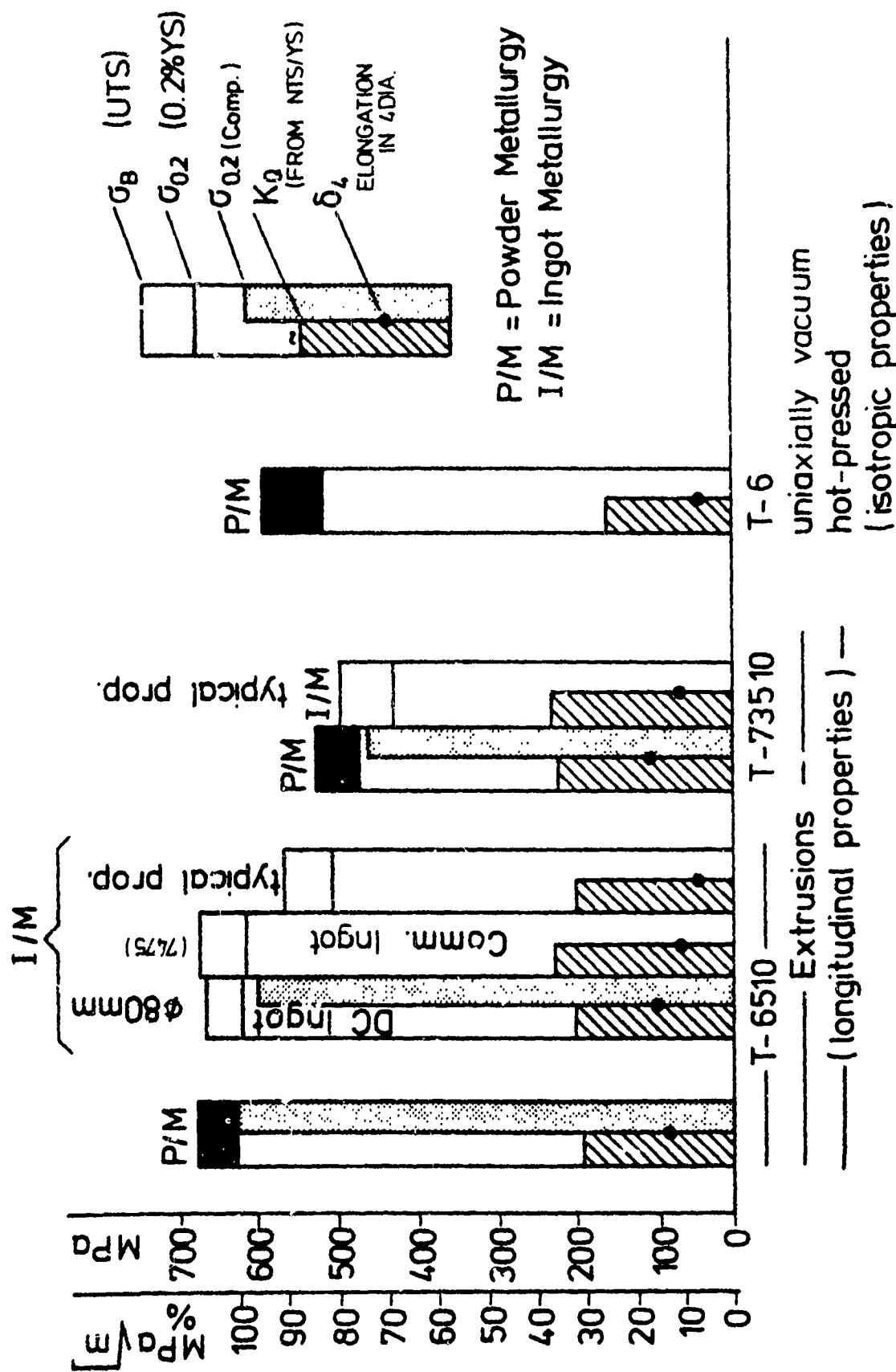
"High Strength Aluminum P/M"

at P/M 78 SEMP5 5th European Symposium on Powder Metallurgy,
Stockholm, 4 June 1978.

2. Fatigue Properties:

"Fatigue and Fracture Mechanics of a Powder Metallurgically
Produced Al Alloy"

at Schwingfestigkeit und Bruch bei Betriebsbeanspruchung,
Werkstoff-Kolloquium, Cologne, 29 November 1978.



7075

Figure 1 Mechanical properties [ultimate tensile strength (UTS), 0.2% yield (0.2% YS), 0.2% compressive yield (0.2% CYS), candidate plane strain fracture toughness (K_Q), and elongation (δ_4)] of 7X75 type aluminum alloys [P/M alloy L, I/M alloy H (ϕ 80 mm ingot) and M (7475 commercial ingot)]. Extrusions are 25:1 with 643 K extrusion-preheat. Uniaxial, vacuum hot-pressing was at 733 K. Typical values are after Hyatt [21].

STRENGTH ANISOTROPY OF 7075-T6 I/M AND P/M 25:1 EXTRUSION PRODUCTS

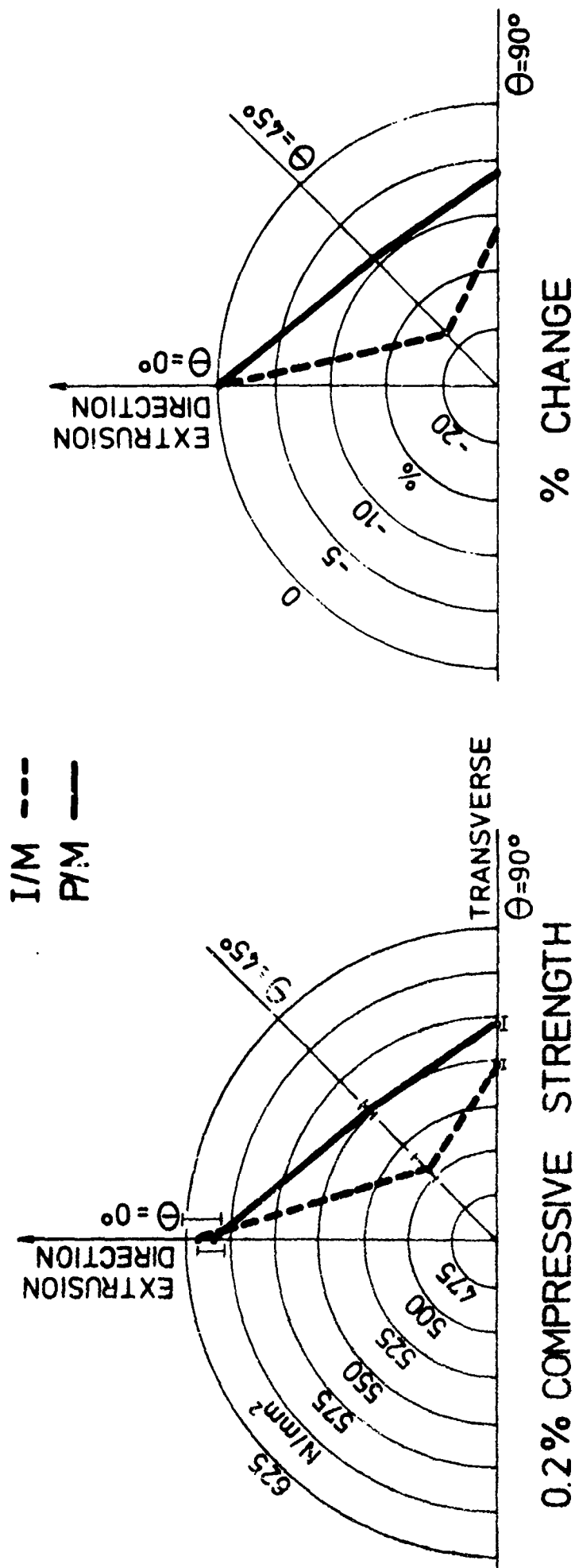


Figure 2 Indication of strength variation and mechanical property anisotropy for 7075-T6 P/M and I/M extrusion products. Extrusions were fabricated with a 25:1 extrusion ratio and a 643 K extrusion-preheat.

P/M 7075-T6510		25:1 Direct Extrusion
Powder	APD 88 μm	643 K Extrusion-Preheat
Grain Size	$\bar{L}=7.5\mu\text{m}$	LONGITUDINAL
ρ	$= 2.81 \cdot 10^3 \text{ kg} \cdot \text{m}^{-3}$	AMSLER (resonance)
UTS	679 MPa	axial stress
02YS	627 "	$f = 100 \text{ Hz}$
NTS	782 "	$R = 0.1$
R.A.	14.5 %	$K_t = 3$
δ_4	126 %	Lab Air

o-- did not fail

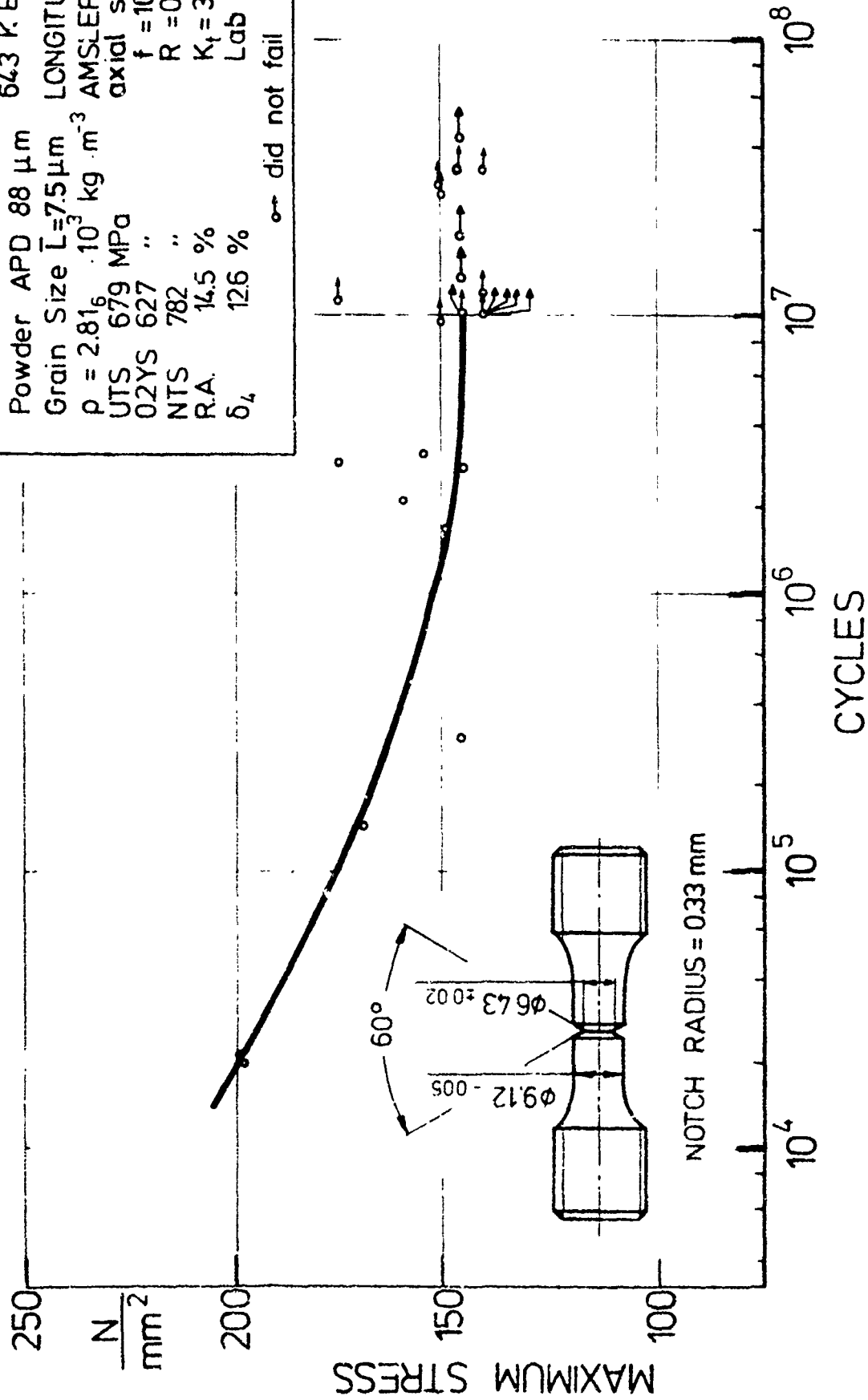
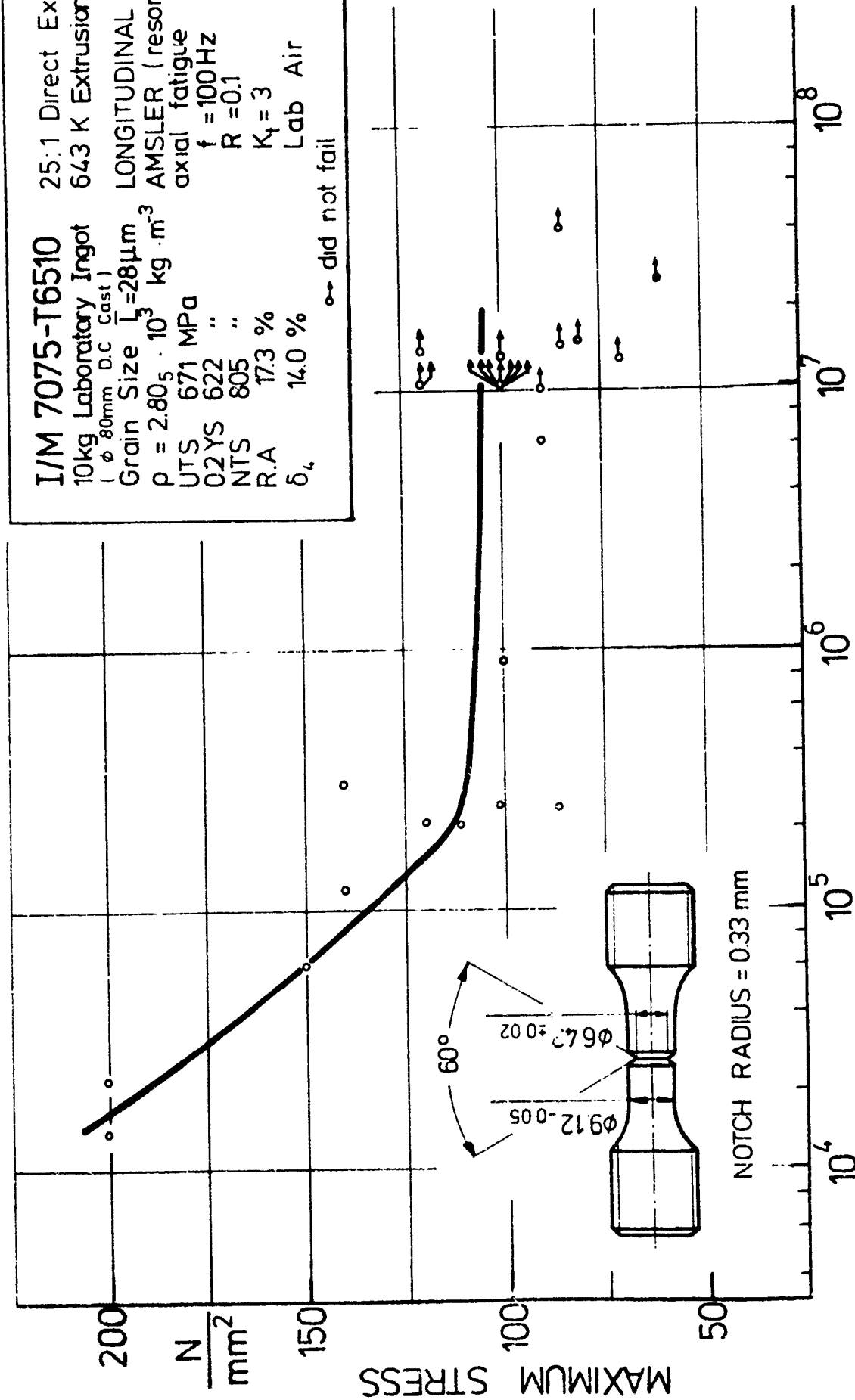


Figure 3 Notch $K_t = 3$ constant load amplitude axial fatigue response of P/M 7075-T6510 extrusions which were produced with identical chemical composition to control I/M 7075 extrusions.

I/M 7075-T6510		25:1 Direct Extrusion
10kg Laboratory Ingot		643 K Extrusion-Preheat
(ϕ 80mm D.C Cast)		
Grain Size $L_3=28\mu\text{m}$		LONGITUDINAL
$\rho = 2.805 \cdot 10^{-3} \text{ kg} \cdot \text{m}^{-3}$		AMSLER (resonance)
UTS 671 MPa		axial fatigue
02YS 622 "		$f = 100\text{Hz}$
NTS 805 "		$R = 0.1$
R.A 173 %		$K_t = 3$
δ_4 14.0 %		Lab Air
		$\circ \rightarrow$ did not fail



CYCLES

Figure 4 Notch $K_t = 3$ constant load amplitude axial fatigue response of control I/M 7075-T6510 extrusions which were produced with identical chemical composition to P/M 7075 extrusions.

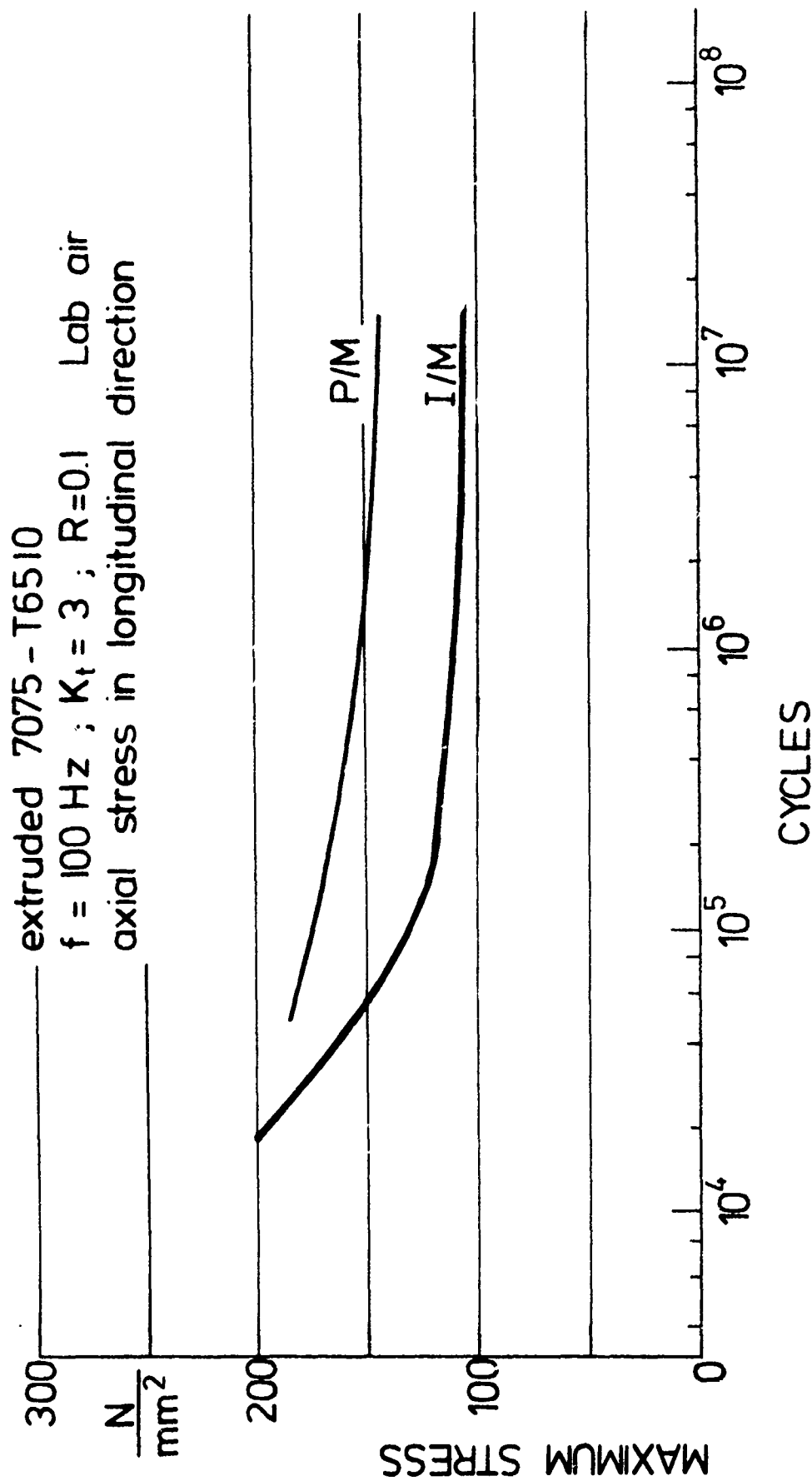


Figure 5 Notch $K_t = 3$ constant load amplitude axial fatigue response of P/M and control I/M 7075-T6510 extrusion products produced and tested under identical conditions - 25:1 extrusion ratio with 643 K extrusion-preheat.

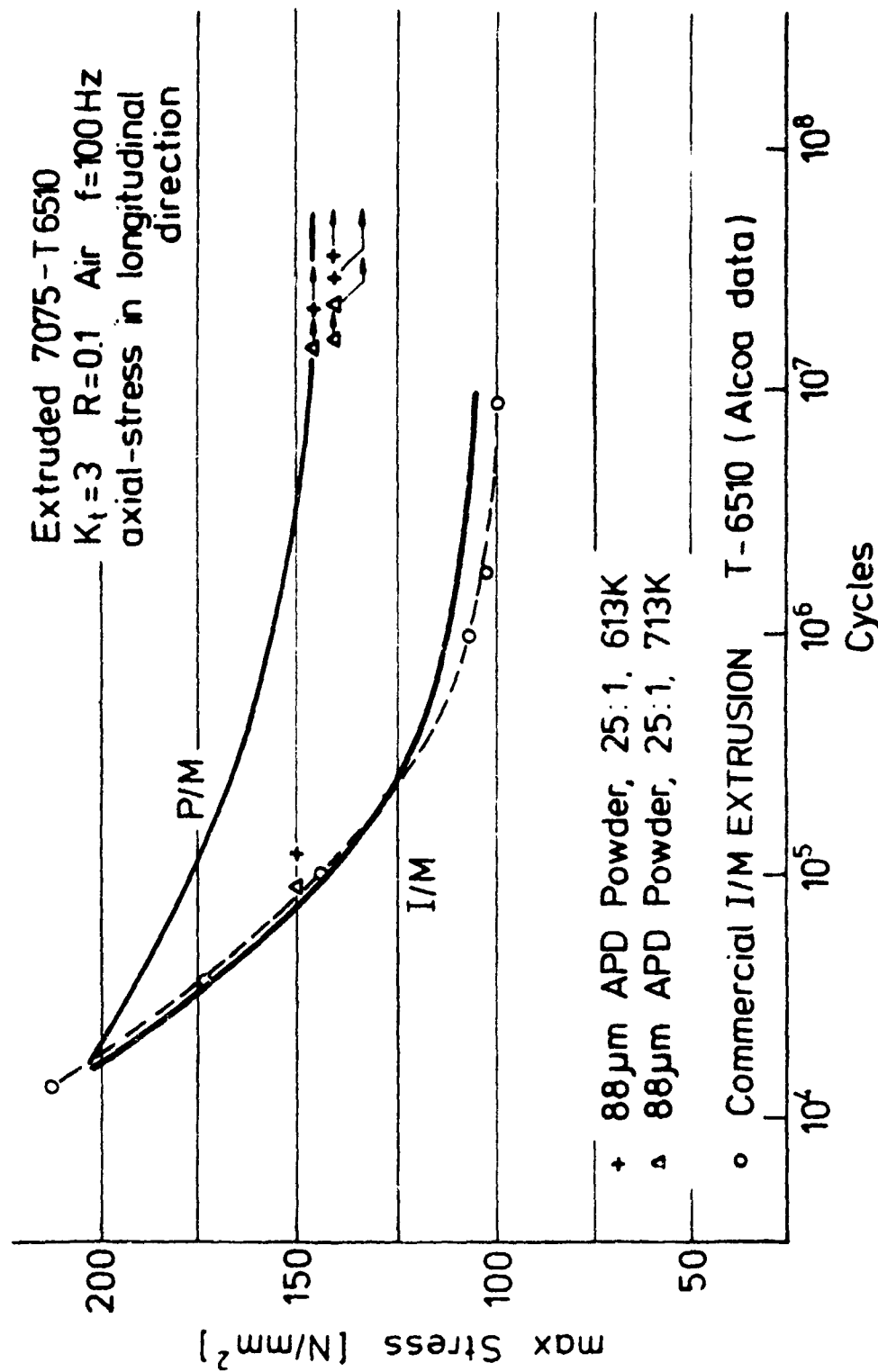


Figure 6 Notch $K_t = 3$ constant load amplitude axial fatigue response of P/M and I/M 7075-T6510 extrusions. The P/M and control I/M products (solid lines) were produced as 25:1 extrusions with a 643 K extrusion-preheat, the additional P/M products were also 25:1 extrusions but with 613 K and 713 K extrusion-preheats. The commercial I/M extrusion is after Kaufman reference [28].

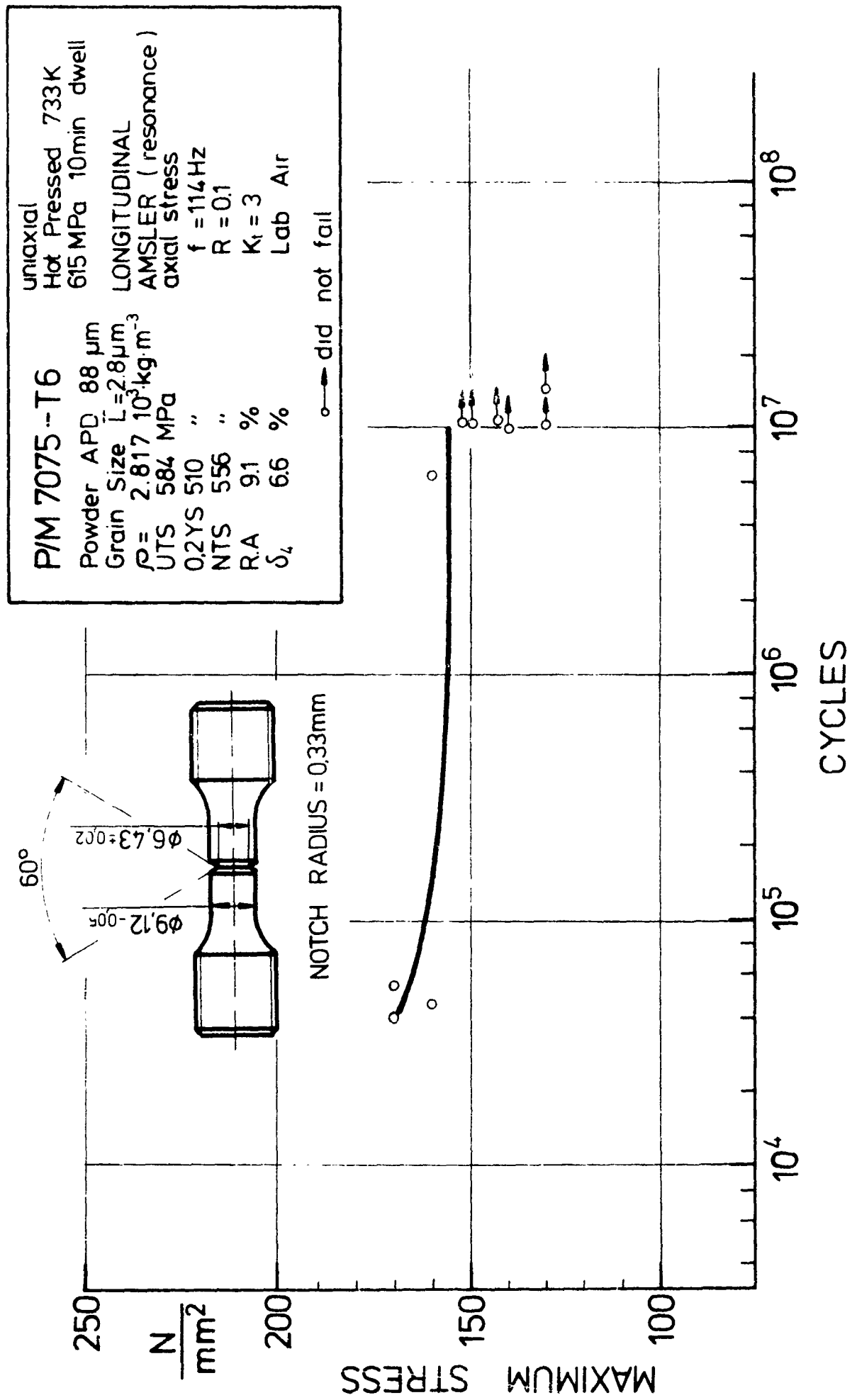


Figure 7 Notch $K_t = 3$ constant load amplitude axial fatigue response of vacuum hot-pressed P/M 7075-T6.



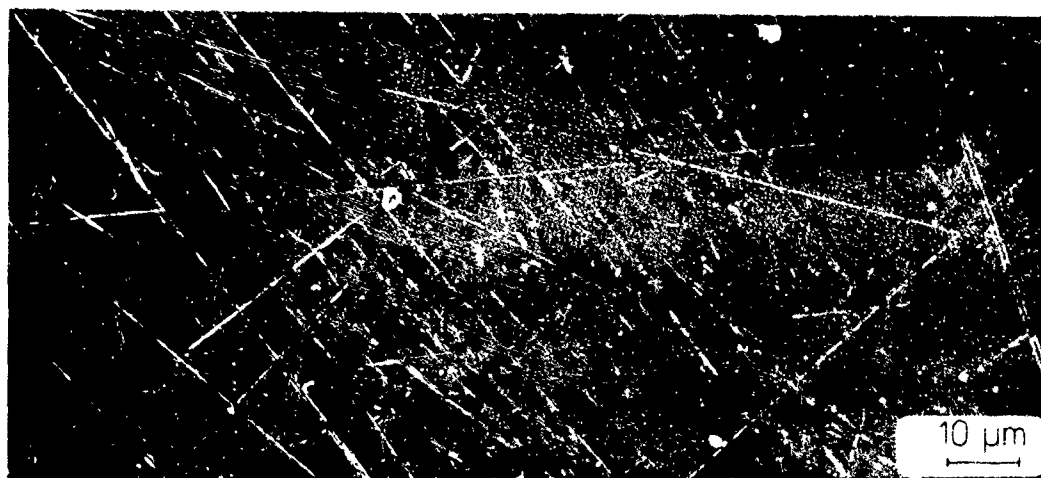
(a)



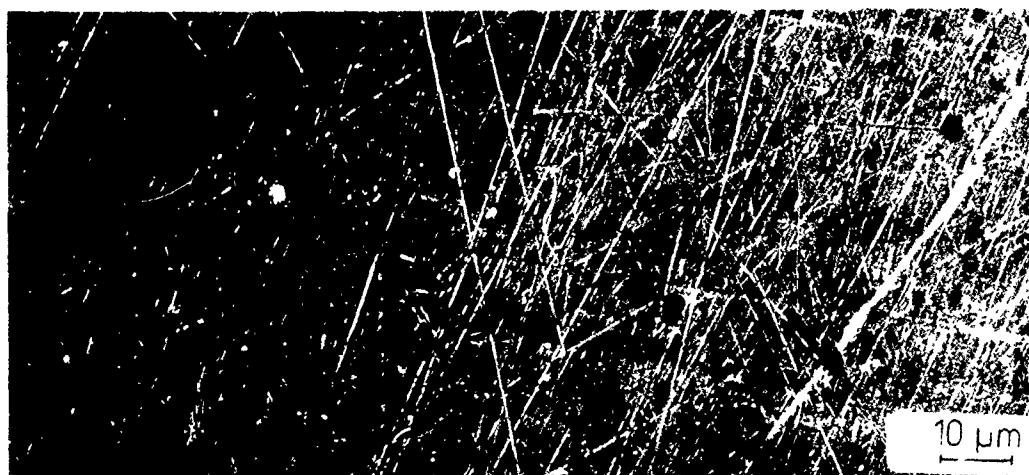
(b)

Figure 8 Back-reflection pinhole X-ray patterns for 7075 (a) I/M and (b) P/M 25:1 extrusion products with 643 K extrusion-preheat. Diffraction pattern of (422).

(a)



(b)



(c)

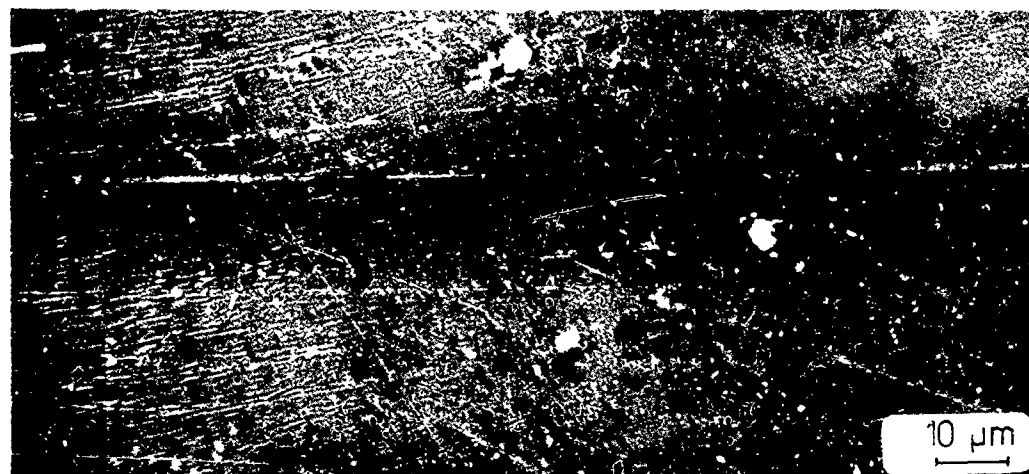


Figure 9 Optical micrographs under polarized light of solution heat treated, lightly polished and unetched surface of: (a) vacuum hot-pressed 88 μm APD 7075 powder (also representative of hot isostatic pressed surface from the same powder), (b) 25:1 P/M 7075-T651 extrusion, (c) 25:1 I/M 7075-T651 extrusion (alloy H).

(a)

10 μ m

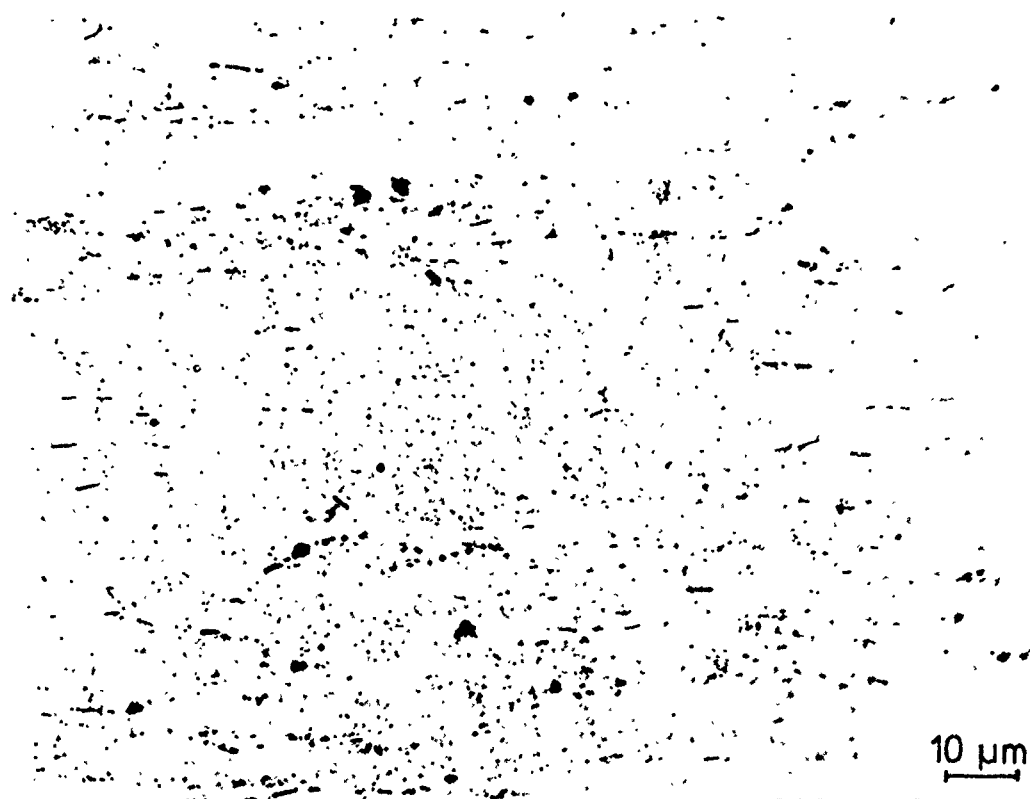
(b)

10 μ m

(c)

10 μ m

Figure 10 Optical micrographs of lightly polished and unetched surfaces shown in Figure 9, under unpolarized light: (a) vacuum hot-pressed 7075 powder, (b) 25:1 P/M 7075-T651 extrusion, (c) 25:1 I/M 7075-T651 extrusion (alloy H).



(a)

Figure 11 Representative optical micrographs of lightly etched 7X75 aluminum alloy 10:1 extrusions. (a) 7075 P/M alloy L [homogenization Treatment A], (b) 7075 I/M alloy H [homogenization Treatment A], (c) 7075 P/M alloy L [short time homogenization Treatment B], (d) 7075 P/M alloy L [high temperature homogenization Treatment C], and (e) 7475 I/M alloy M [commercially processed] . Homogenization treatments and VPCP are given in Table 7. Etchant: $2\frac{1}{2}$ ml HF (40 %) - 5 ml H_2SO_4 - 92.5 ml H_2O at RT for 4 seconds.

(b)

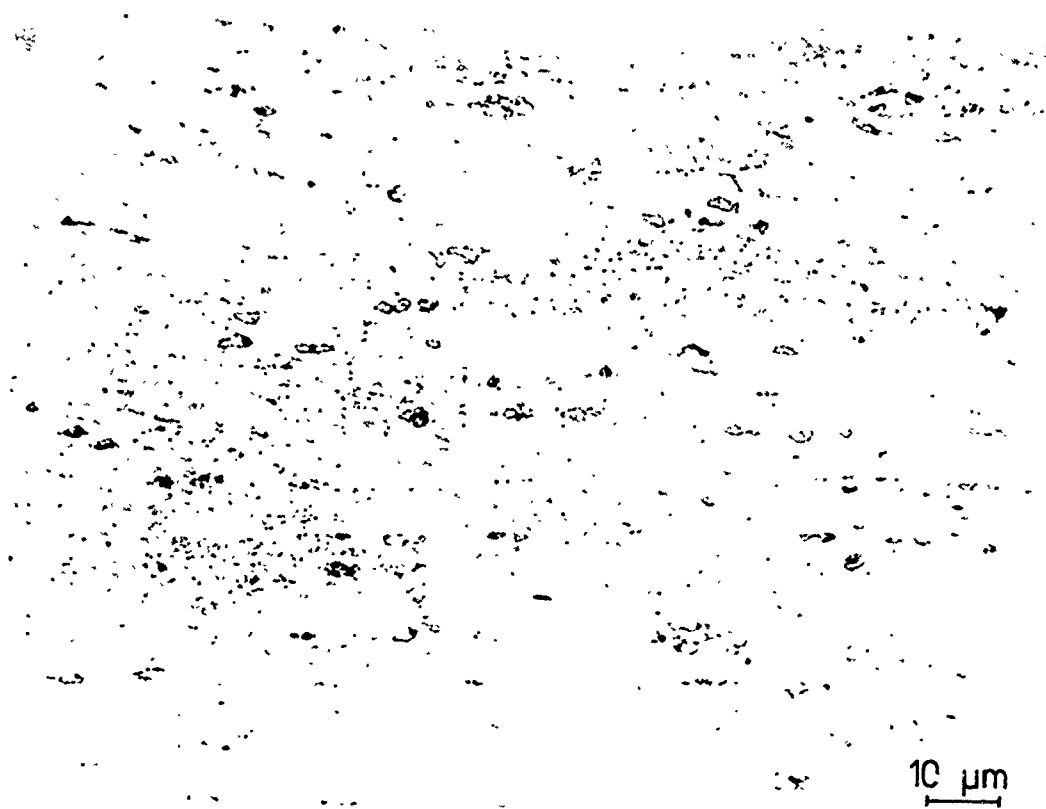
10 μ m

(c)

10 μ m

Figure 11 Continued.

(d)



(e)

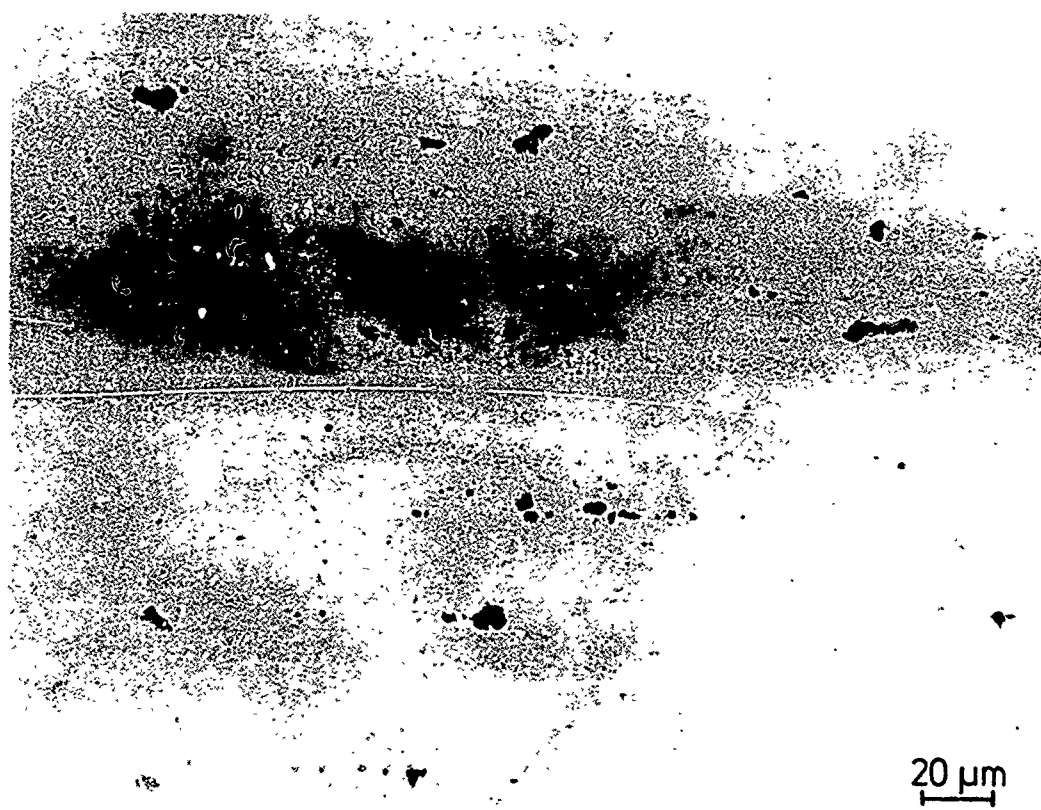
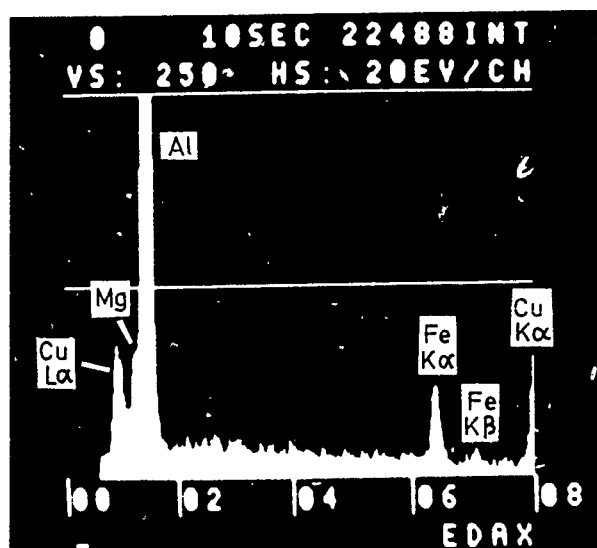
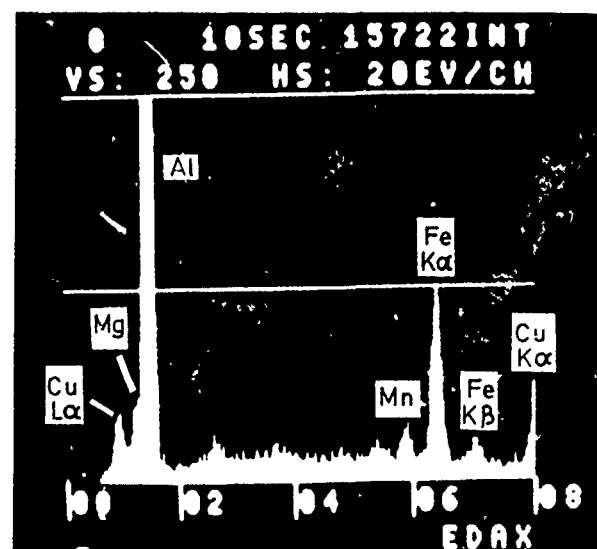


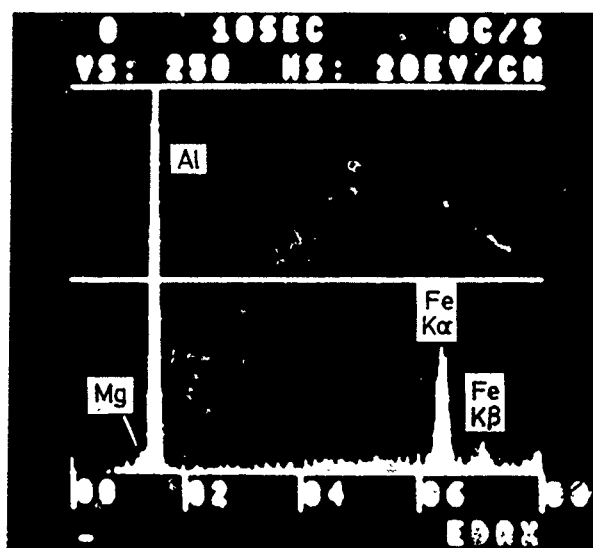
Figure 11 Continued.



(a)



(b)



(c)

Figure 12 EDAX patterns of intensity vs the element's characteristic energy level for representative iron containing Al-Fe-Cu second phase particles in 7X75-T6510 extrusions. (a) P/M 7075 [identical to I/M-homogenizing treatment A], (b) I/M 7475 (c) P/M 7075 [treatment C].



(a)

→
extrusion direction

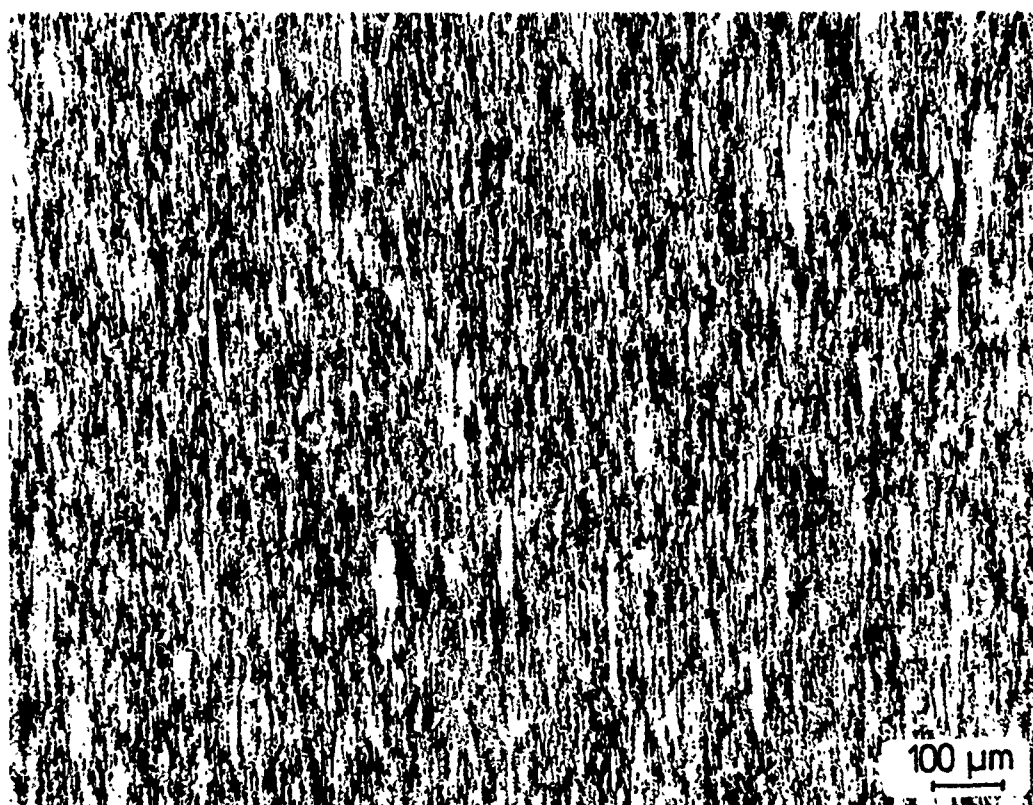
Figure 13 Representative optical micrographs of 7075-T6510 P/M 25:1 Direct Extrusions, with 643 K extrusion-preheat, parallel to extrusion direction.

(a) grain structure: Barker's etchant

(b) " " : 10 ml HF-5 ml HNO₃-90 ml H₂O
(diluted)

(c) substructure : 0.5 ml HF (conc)-15.5 ml HNO₃-
84 ml H₂O-3 g CrO₃.

(b)



(c)

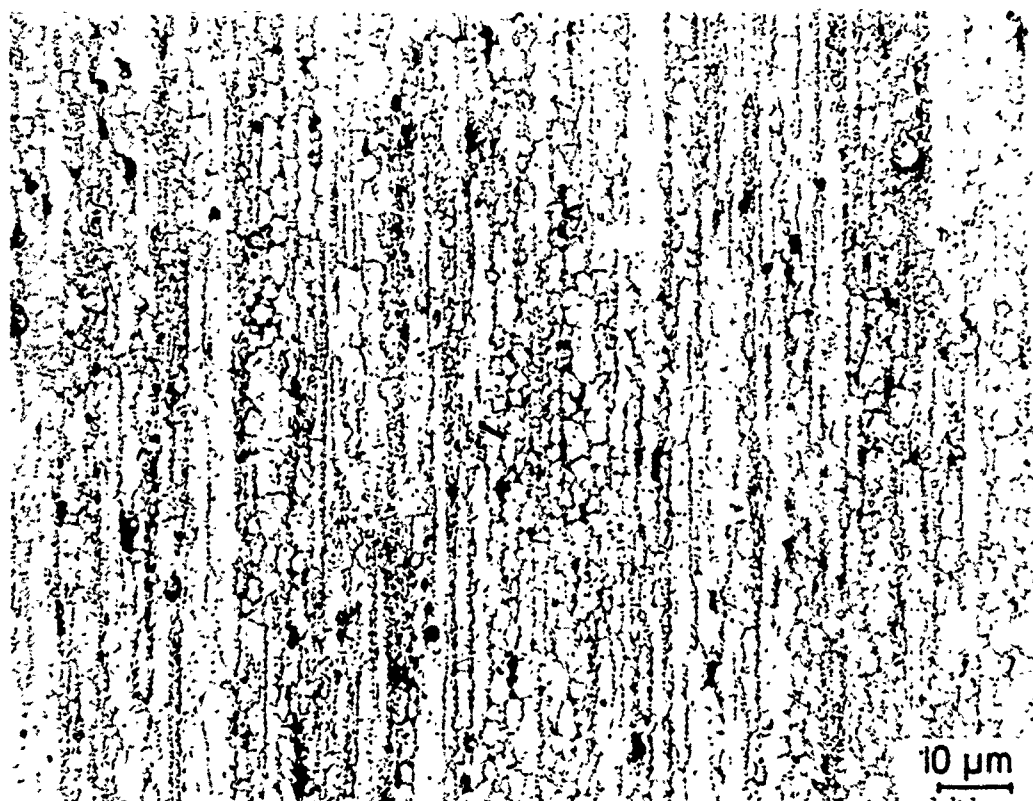
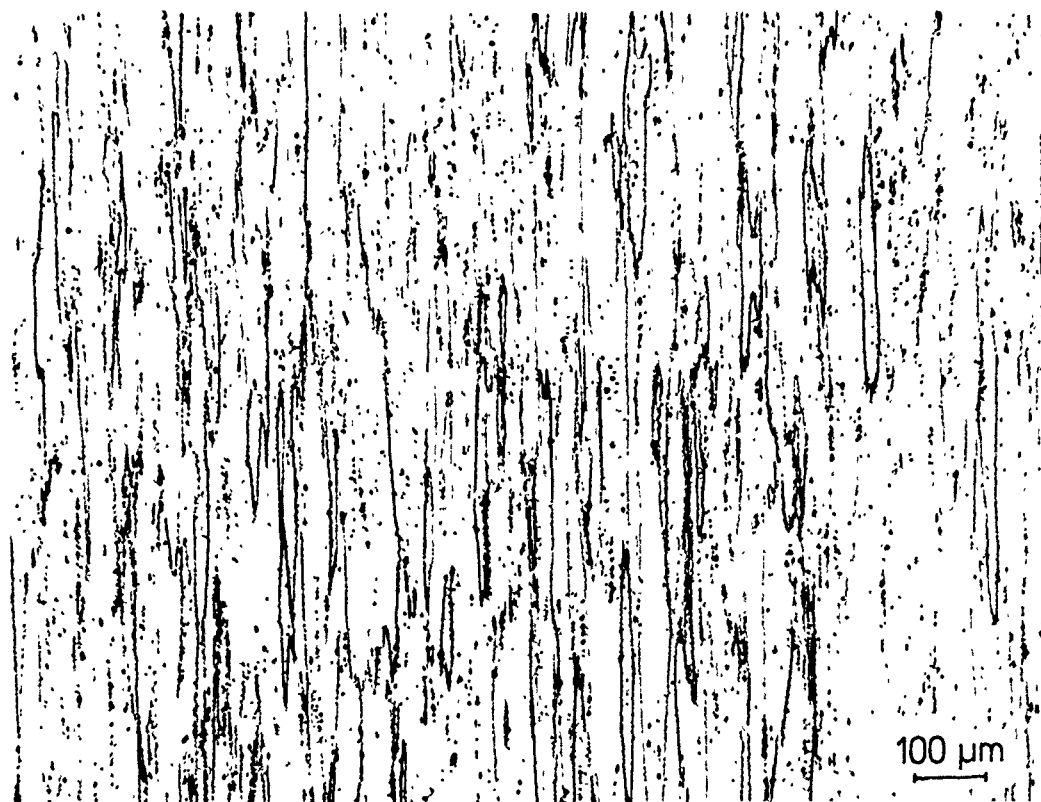


Figure 13 Continued

(a)



(b)

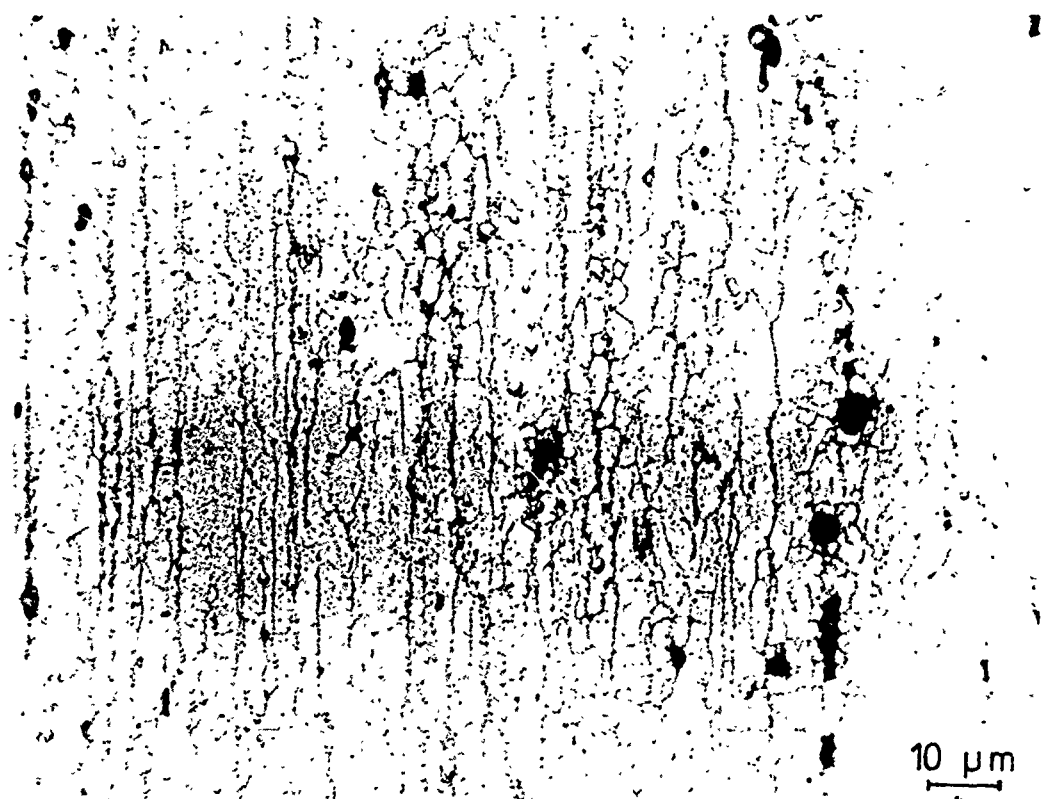
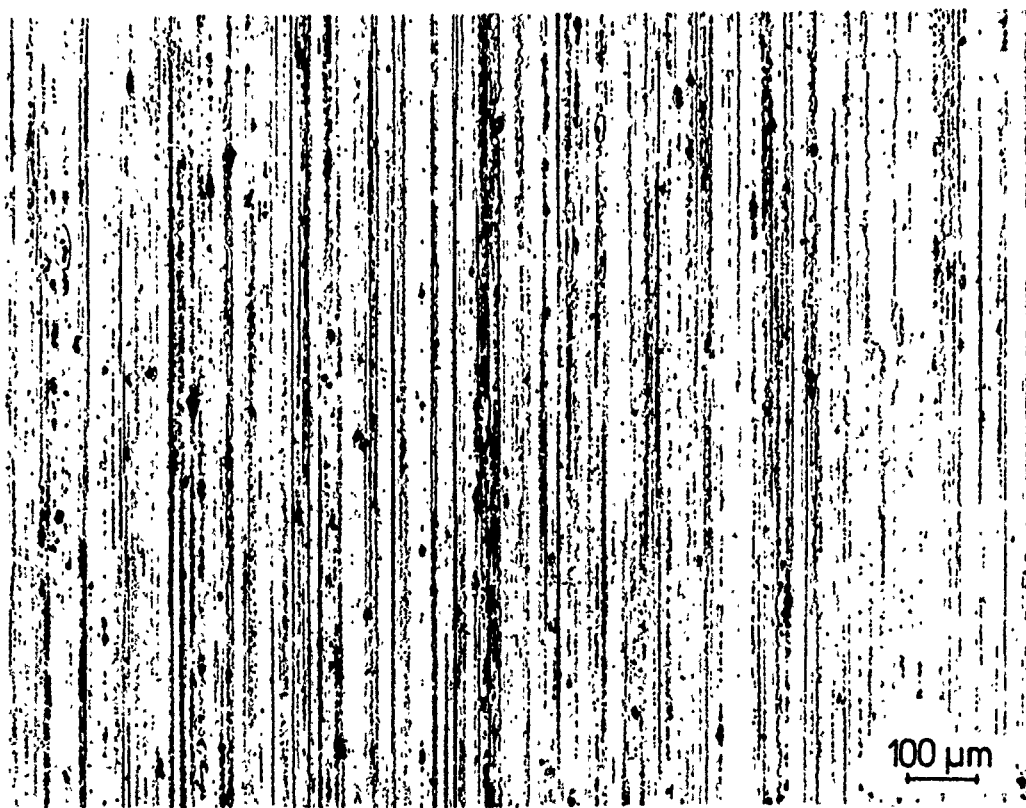


Figure 14 Representative optical micrograph of 7075-T6510 I/M 25:1 Direct Extrusions, with 643 K extrusion-preheat, parallel to extrusion direction.

(a) grain structure (b) substructure

(a)



(b)

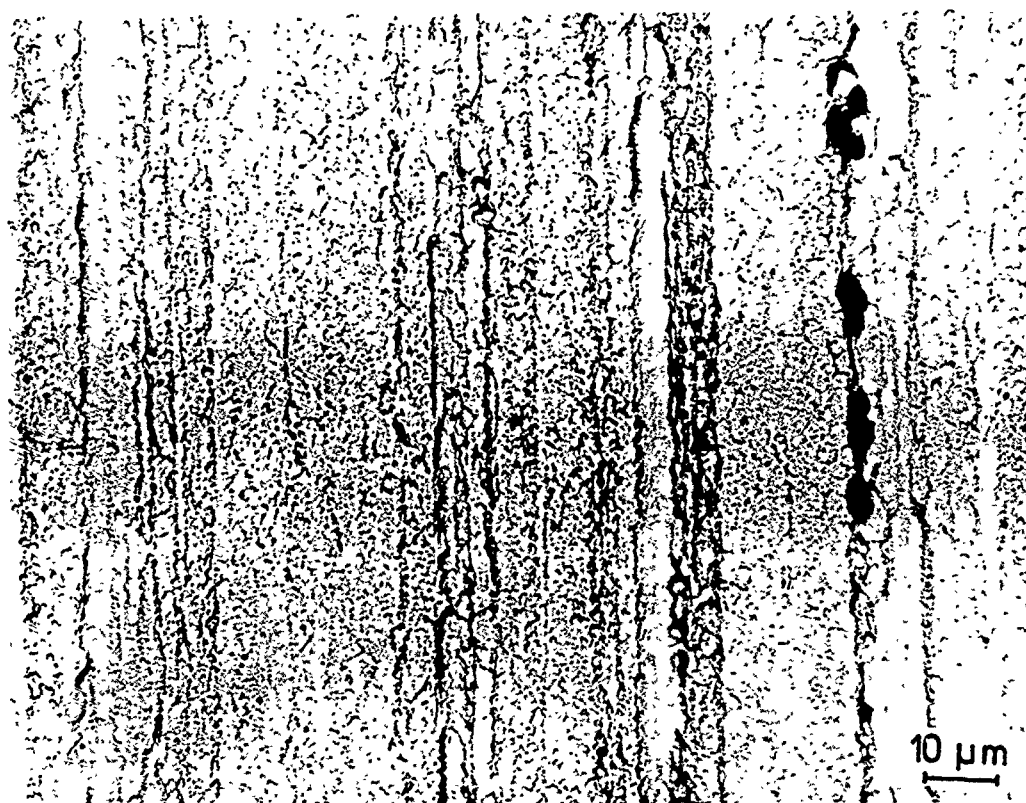
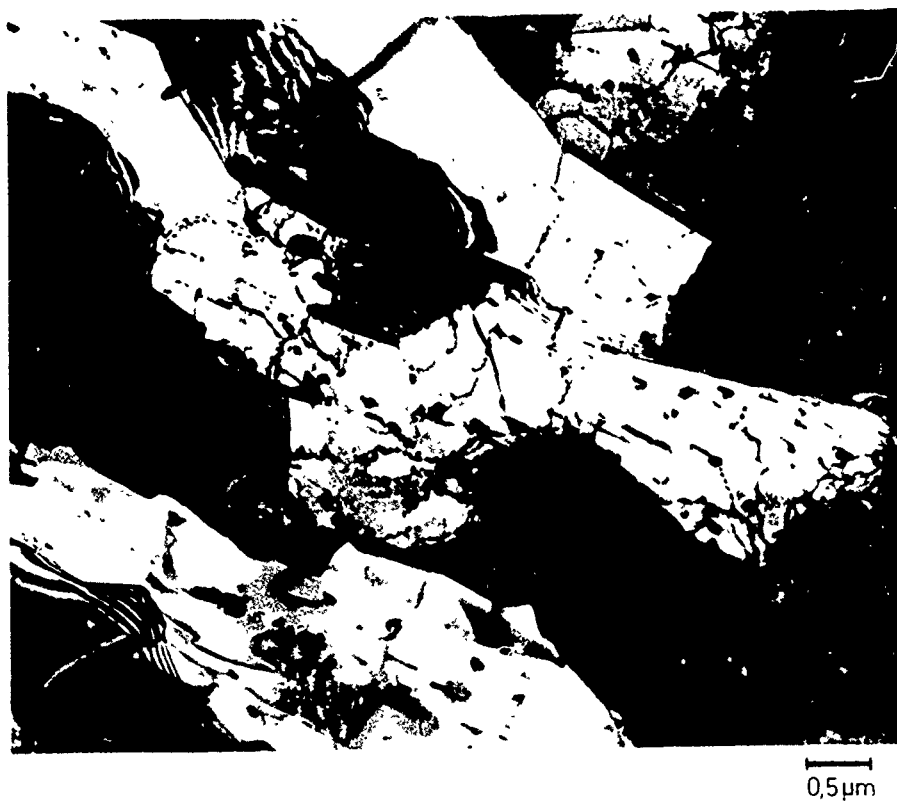


Figure 15 Representative optical micrograph of 7475-T6510 I/M 25:1 Direct Extrusions, with 643 K extrusion-preheat, parallel to extrusion direction.

(a) grain structure (b) substructure

(a)



(b)

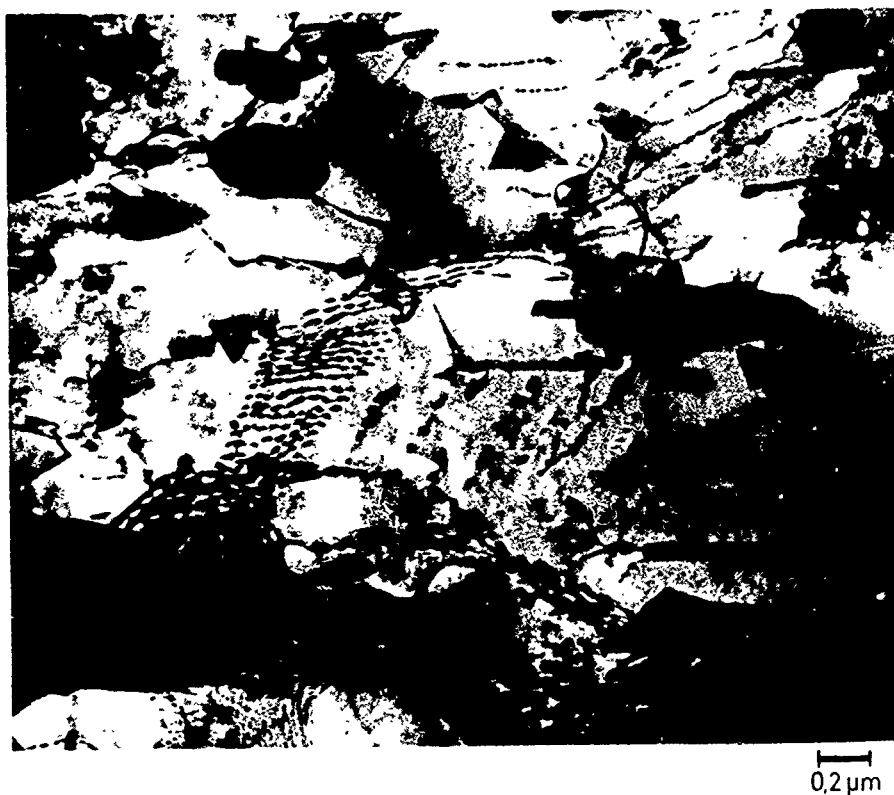


Figure 16 Transmission electron micrographs of an as-extruded 7075 I/M 25:1 extrusion produced with a 643 K extrusion-preheat. TEM specimens were taken parallel to the extrusion direction.

(a)



(b)



Figure 17 Transmission electron micrographs of an as-extruded 7075 P/M 25:1 extrusion produced with a 643 K extrusion-preheat. TEM specimens were taken parallel to the extrusion direction.

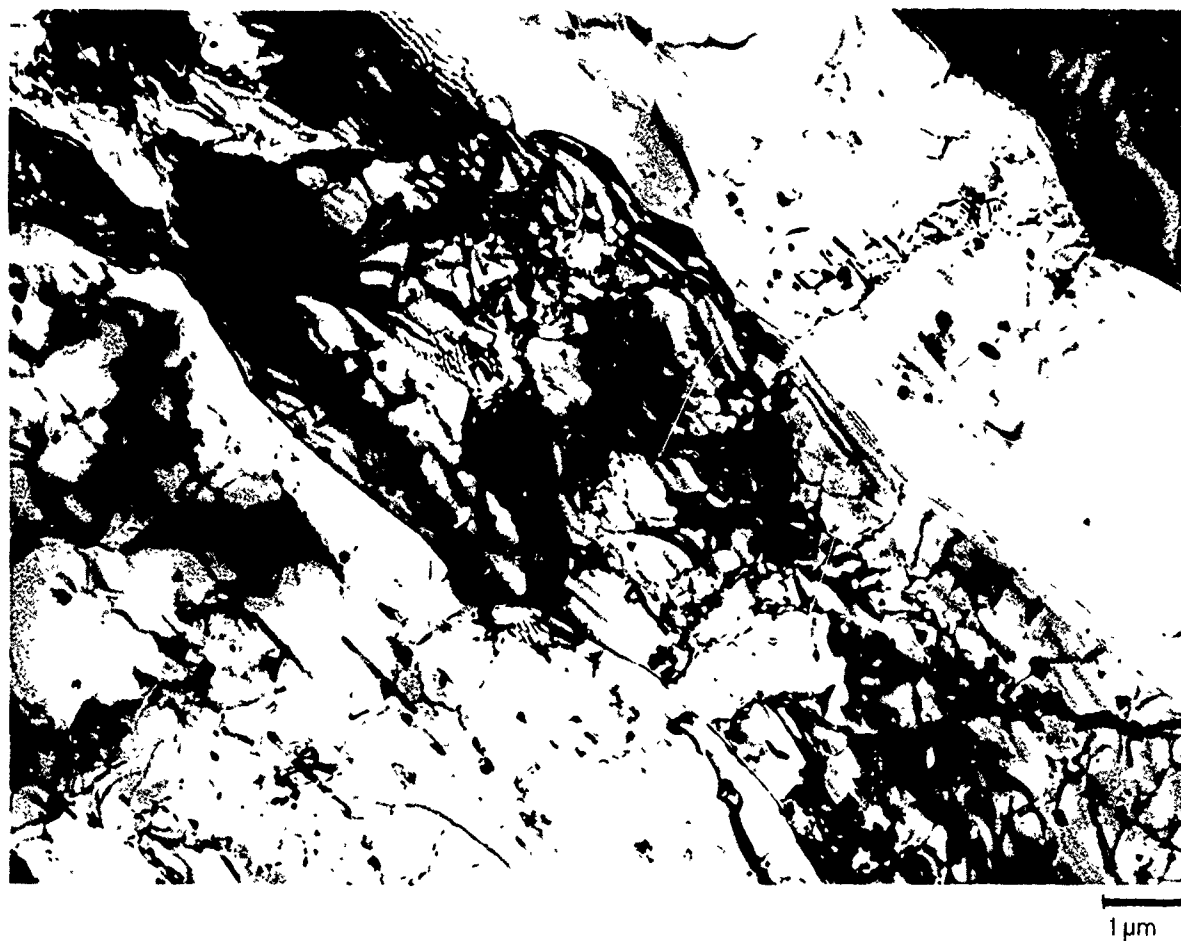


Figure 18 Transmission electron micrograph of a solution heat treated 7075 I/M 25:1 extrusion produced with a 643 K extrusion-preheat. The TEM specimen was taken parallel to the extrusion direction.



Figure 19 Transmission electron micrograph of a solution heat treated 7075 P/M 25:1 extrusion produced with a 643 K extrusion-preheat. The TEM specimen was taken parallel to the extrusion direction.

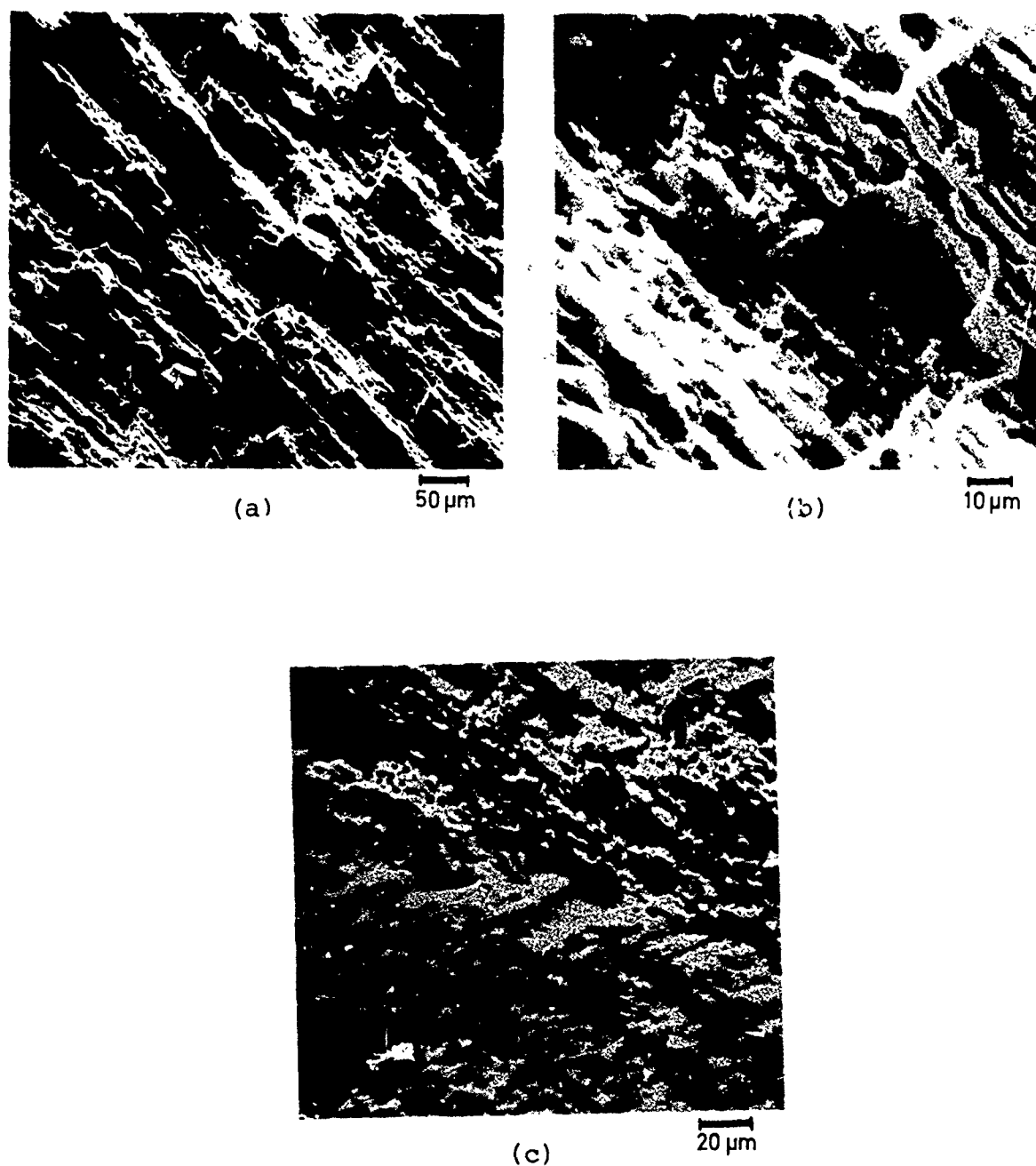
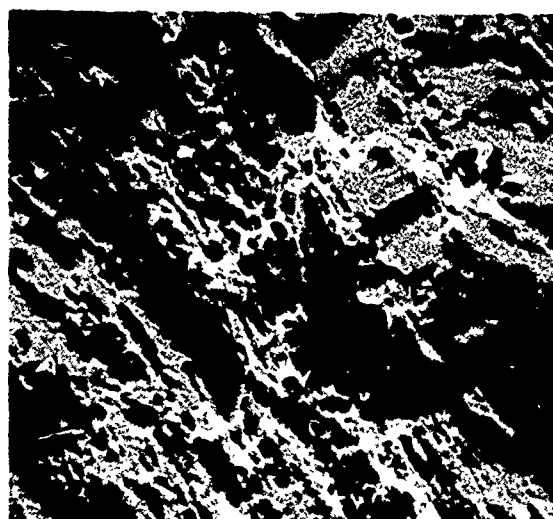
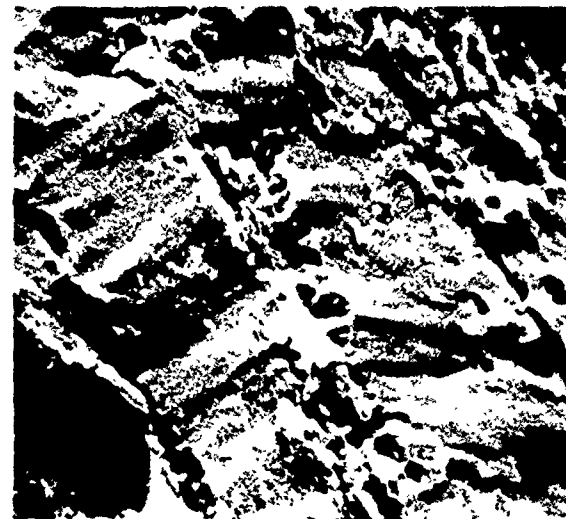


Figure 20 Scanning electron fractographs of a tensile fracture surface. The tensile specimen was machined from the transverse direction of a 10:1 P/M 7075-T6 extrusion produced with a 643 K extrusion-preheat. The fracture surface was 60° to the transverse direction (specimen axis). Fractograph (b) is a higher magnification of the center of (a). The dimple spacing on the flat fracture surface in the middle of (c) is approximately 1 μm.



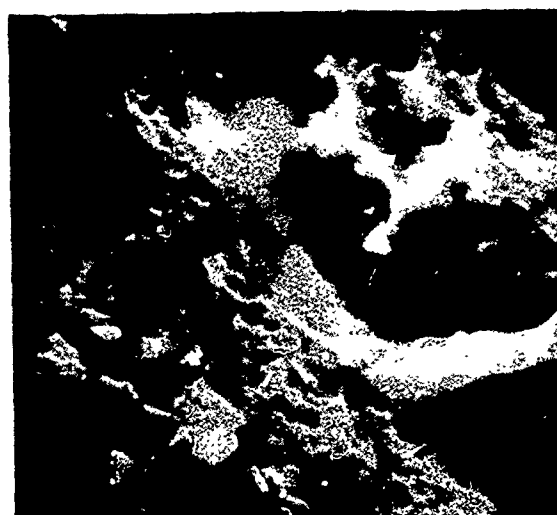
(a)

20 μm



(b)

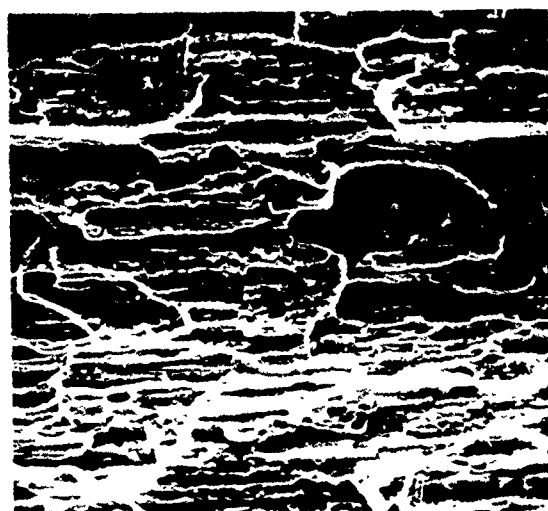
10 μm



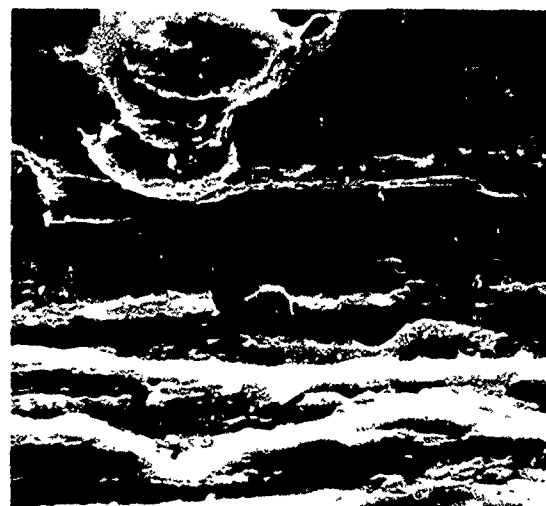
(c)

2 μm

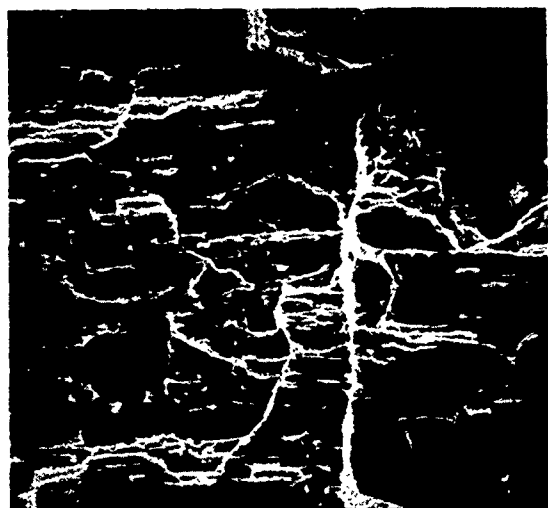
Figure 21 Scanning electron fractographs of a tensile fracture surface. The tensile specimen was machined from the transverse direction of a 10:1 I/M 7075-T6 extrusion produced with a 643 K extrusion-preheat. The fracture surface was 35° to the transverse direction (specimen axis). Fractograph (b) is a higher magnification of the upper right corner of (a), and (c) is a higher magnification of the center of (b).



(a) 20 μm



(b) 5 μm



(c) 20 μm



(d) 5 μm

Figure 22 Scanning electron fractographs of a tensile fracture surface. The tensile specimen was machined from the transverse direction of a 5.54:1 P/M 7075-T6 extrusion produced with a 643 K extrusion-preheat. The fracture surface was 90° to the transverse direction (specimen axis). Fractograph (d) is a higher magnification of the cracked particle shown on the right side of (c).

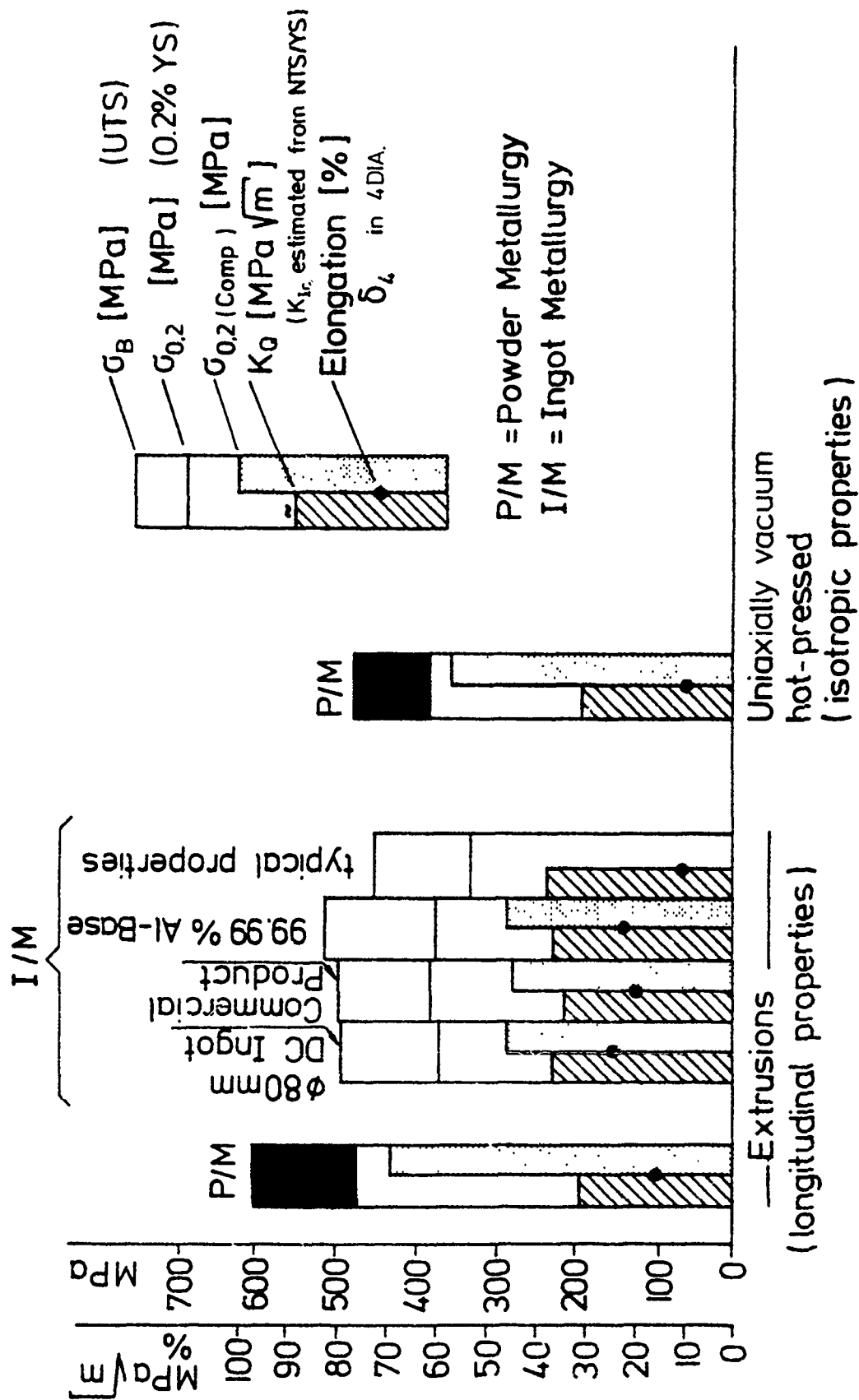


Figure 23 Mechanical properties [ultimate tensile strength (UTS), 0.2% yield (0.2% YS), 0.2% compressive yield (0.2% CYS), candidate plane strain fracture toughness (K_Q), and elongation (δ_4)] of 2024 type aluminum alloys [P/M alloy E, I/M alloys: C (ϕ 80 mm ingot), B and A (commercial products)]. Except for the commercial products, extrusions are 25:1 with 643 K extrusion-preheat. Uniaxial, vacuum hot-pressing was at 753 K. Typical values are after Hyatt [21].

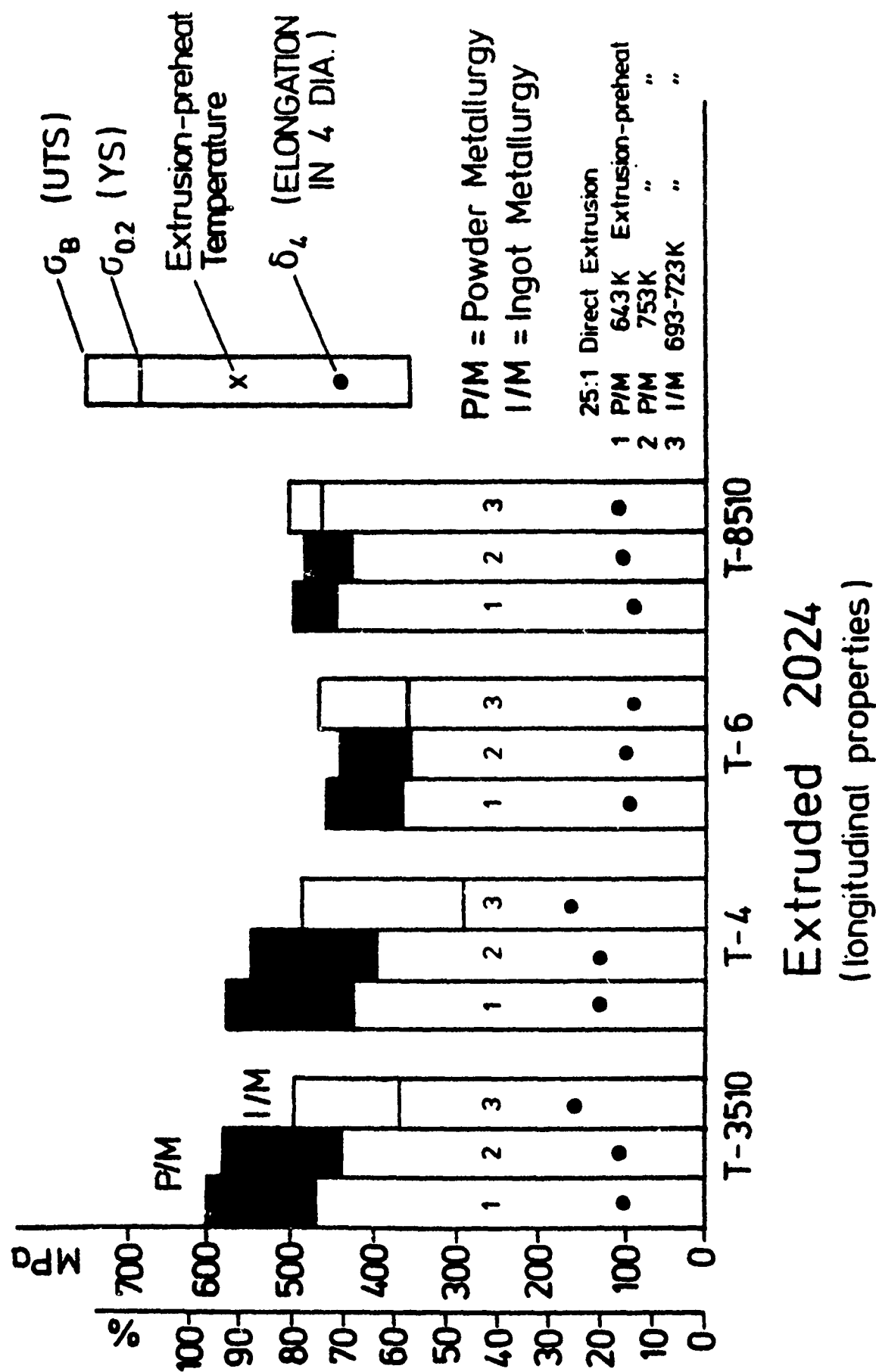


Figure 24 Aging response of P/M and I/M 2024 extrusion products and effect of extrusion-preheat temperature on aging response of the P/M extrusion products.

P/M 2024-T3510		25:1 Direct Extrusion
Powder	APD 82 μm	64.3K Extrusion-Preheat axial stress
Grain Size	$\bar{L}=6.7\mu\text{m}$	LONGITUDINAL
UTS	587 MPa	AMSLER (resonance)
0.2YS	460 "	$f = 100\text{ Hz}$
NTS	667 "	$R = 0.1$
R.A.	18 %	$K_t = 3$
δ_c	15 %	Lab Air

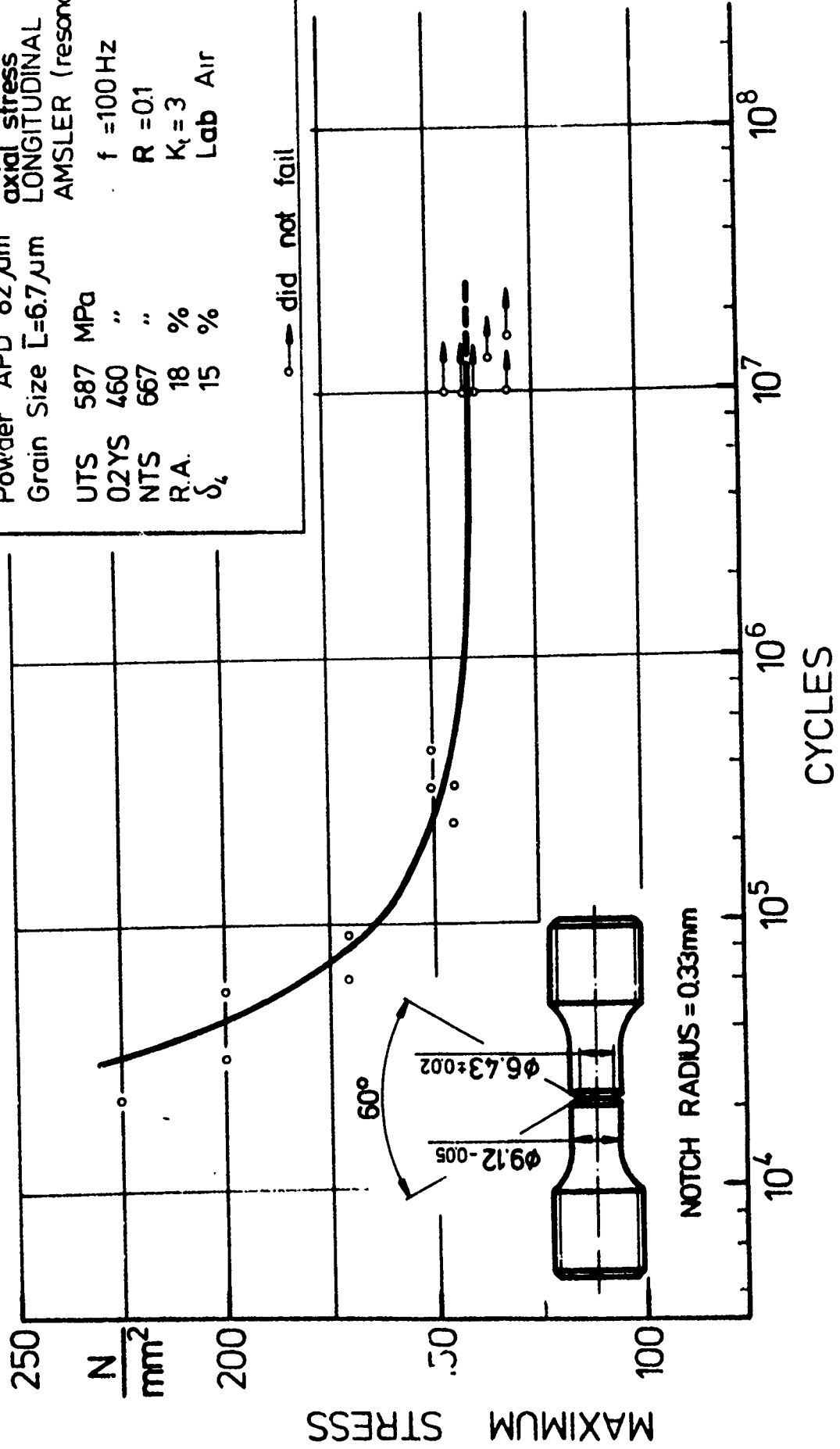
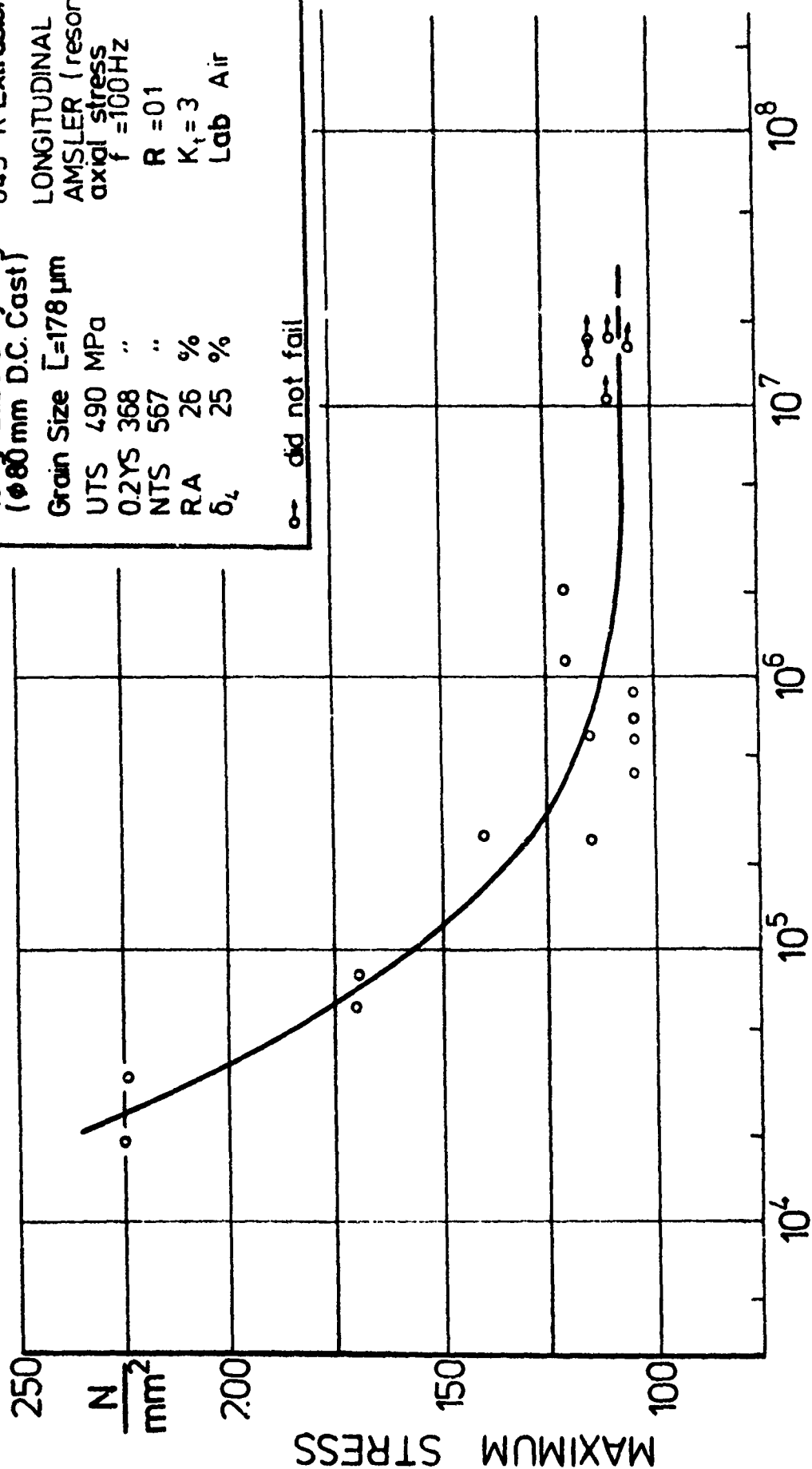


Figure 25 Notch $K_t = 3$ constant load amplitude axial fatigue response of P/M 2024-T3510 extrusions which were produced with identical chemical composition to control I/M 2024 extrusions.



I/M 2024-T3510 25.1 Direct Extrusion
 10 kg Laboratory Ingot 64.3 K Extrusion-Preheat
 (Ø80 mm D.C. Cast) LONGITUDINAL
 Grain Size $\bar{L}=178 \mu\text{m}$ AMSLER (resonance)
 UTS 490 MPa axial stress
 0.2YS 368 " $f = 100\text{Hz}$
 NTS 567 " $R = 0.1$
 RA 26 % $K_t = 3$
 δ_L 25 % Lab Air

o- did not fail

Figure 26 Notch $K_t = 3$ constant load amplitude axial fatigue response of control I/M 2024-T3510 Alloy C extrusions which were produced with identical chemical composition to P/M 2024 extrusions.

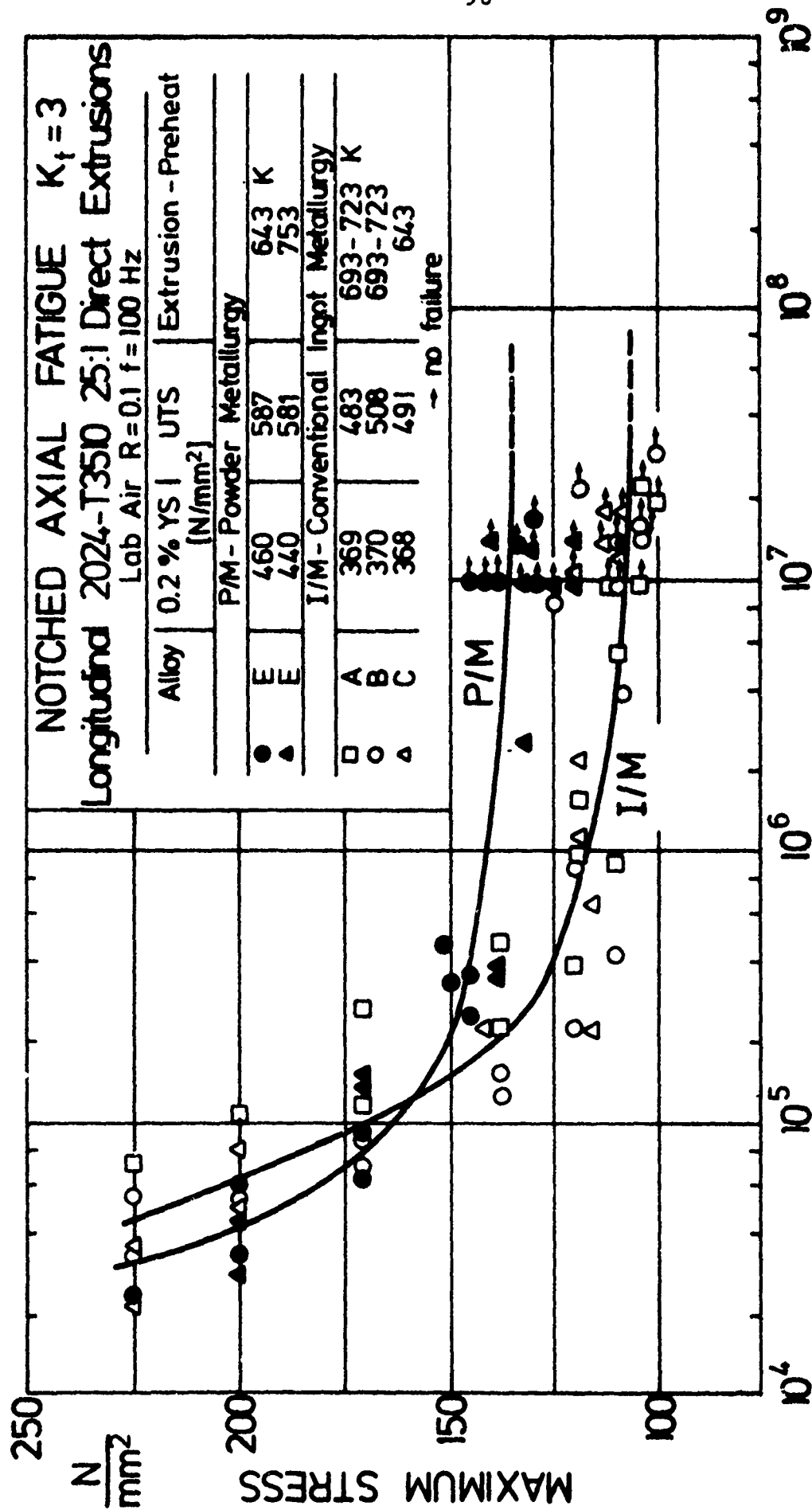


Figure 27 Notch $K_t = 3$ constant load amplitude axial fatigue response of P/M and I/M 2024-T3510 extrusion products. Curves shown represent "best fit" to the data.

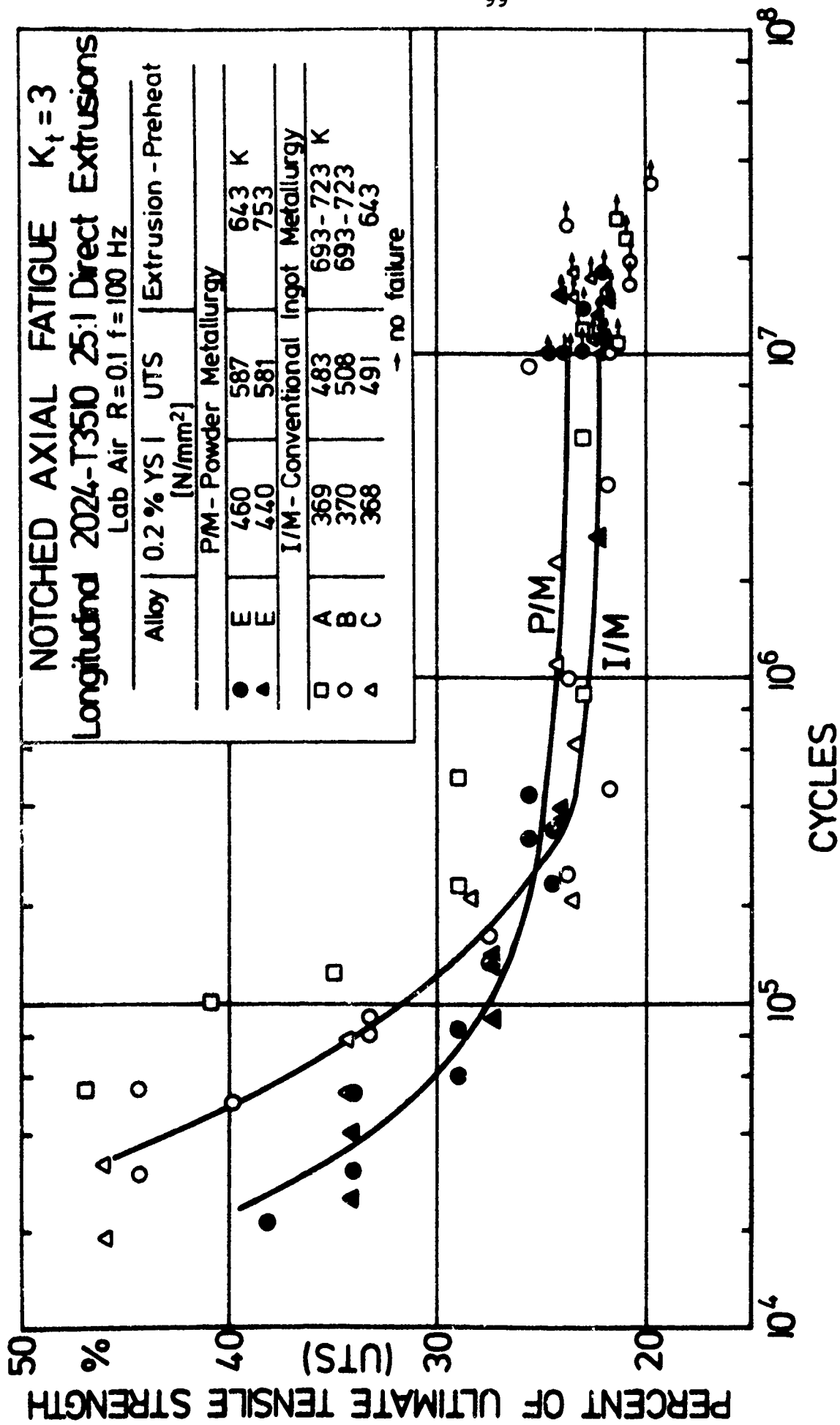


Figure 28 Normalized notch $K_t = 3$ constant load amplitude axial fatigue response of P/M and I/M 2024-T3510 extrusion products. Applied maximum stress has been normalized with the respective ultimate tensile strength. Curves represent "best fit" to the data.

P/M 2024-T3510
 25:1 Direct Extrusion
 753 K Extrusion-Preheat
 Powder APD 117 μm
 Grain Size: $G_L=79\mu\text{m}$
 LONGITUDINAL
 AMSLER (resonance)
 axial stress
 $f=100\text{Hz}$
 UTS 582 MPa
 0.2YS 428 " "
 NTS 565 " "
 R.A. 21.8 %
 δ_L 16.1 %
 $Q = 2.796 \cdot 10^3 \text{ kg m}^3$
 R = 0.1
 $K_t = 3$
 Lab Air
 did not fail

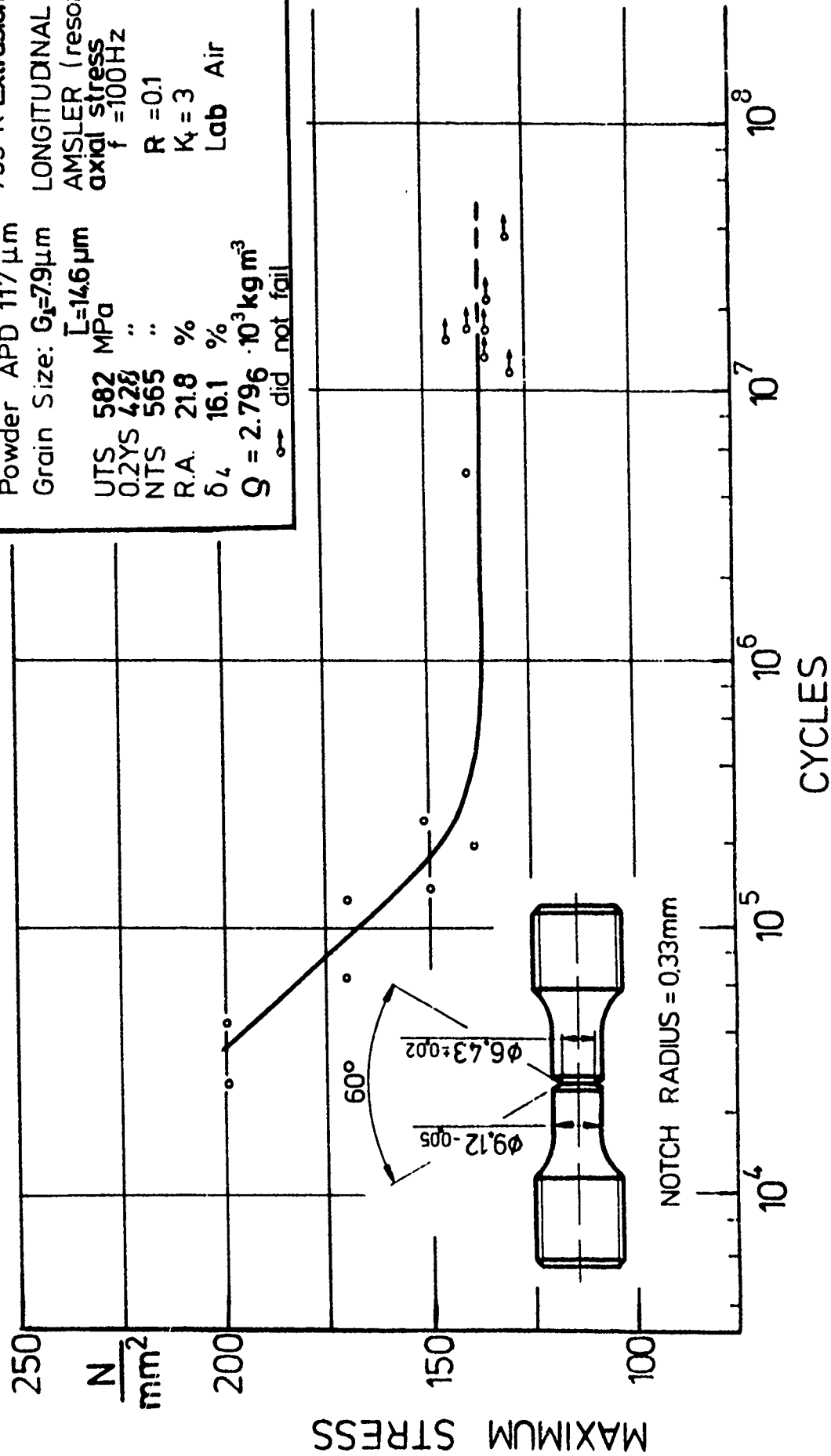


Figure 29 Notch $K_t = 3$ constant load amplitude axial fatigue response of a P/M 2024-T3510 extrusion product manufactured from powder with a 117 μm APD and with a 753 K extrusion-preheat.

P/M 2024-T3510 25:1 Direct Extrusion
 753K Extrusion-Preheat
 Powder APD 82 μm
 Grain Size: $G_L=60\mu\text{m}$
 $L=86\mu\text{m}$
 UTS 581 MPa
 0.2YS 440 " $R=0.1$
 NTS 611 " $K_t=3$
 R.A. 22 % Lab Air
 δ_L 16.2 %
 $Q = 2.793 \cdot 10^3 \text{ kg m}^{-3}$

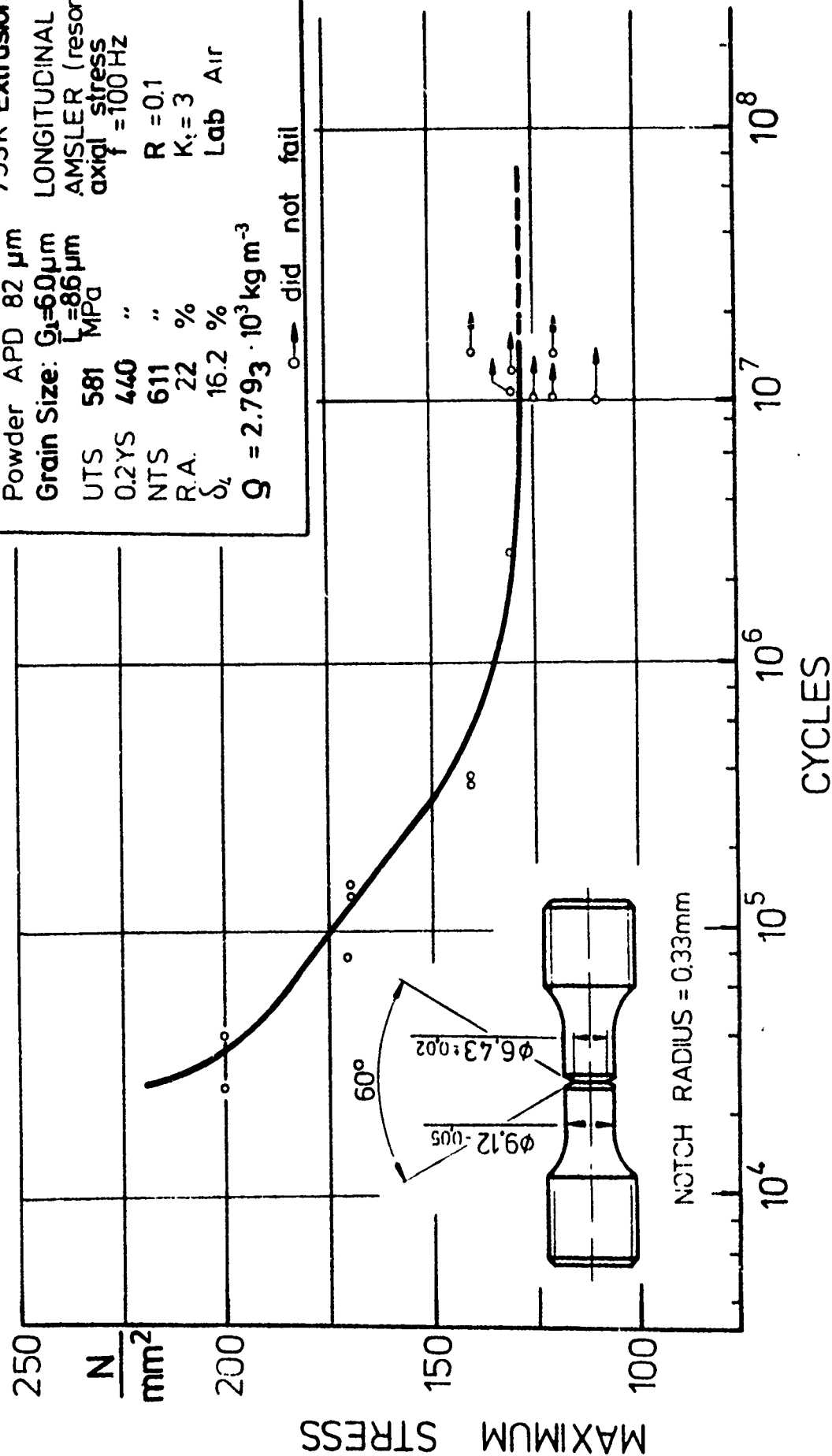


Figure 30 Notch $K_t = 3$ constant load amplitude axial fatigue response of a P/M 2024-T3510 extrusion product manufactured from powder with a 82 μm APD and with a 753 K extrusion-preheat.

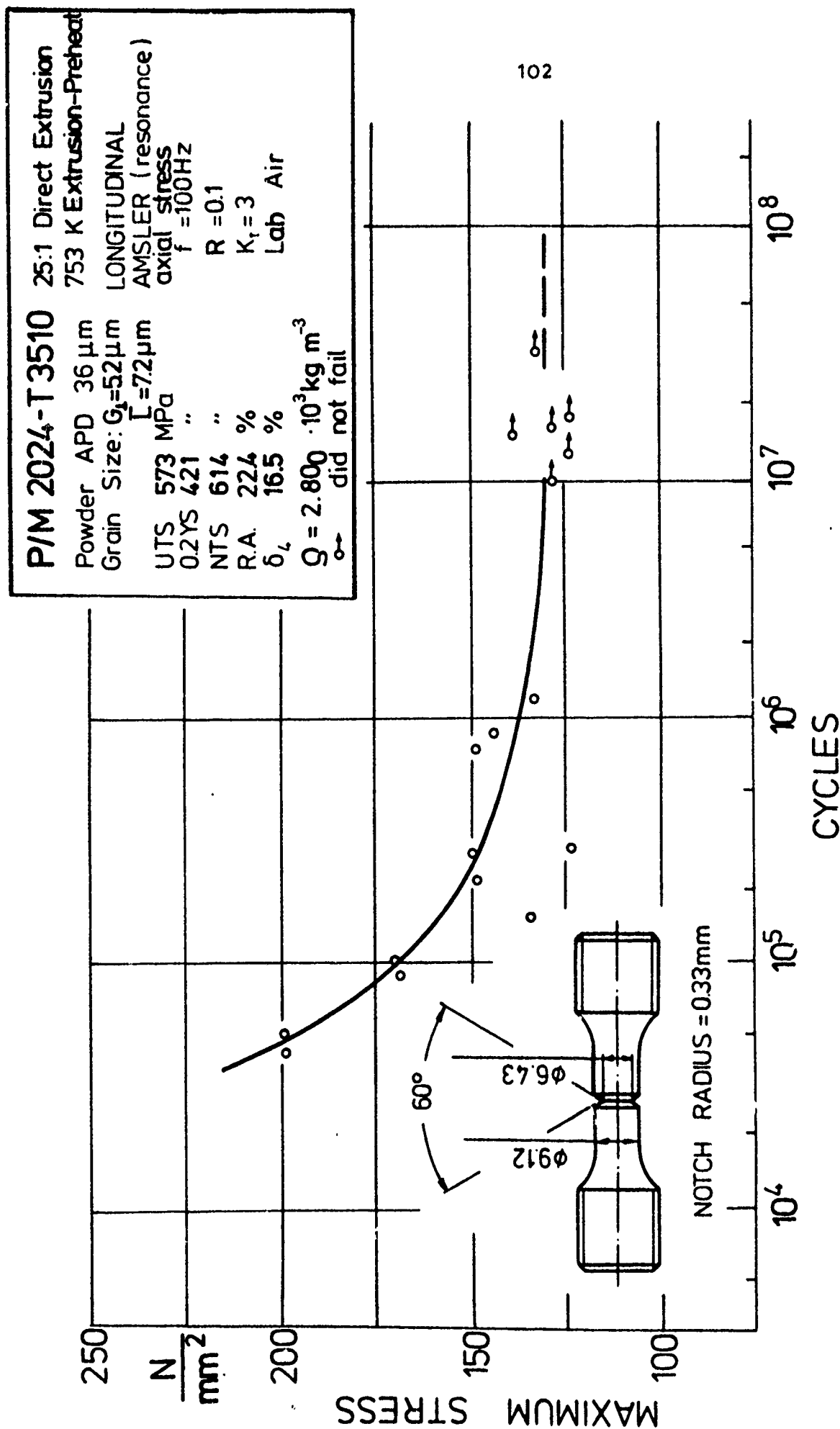
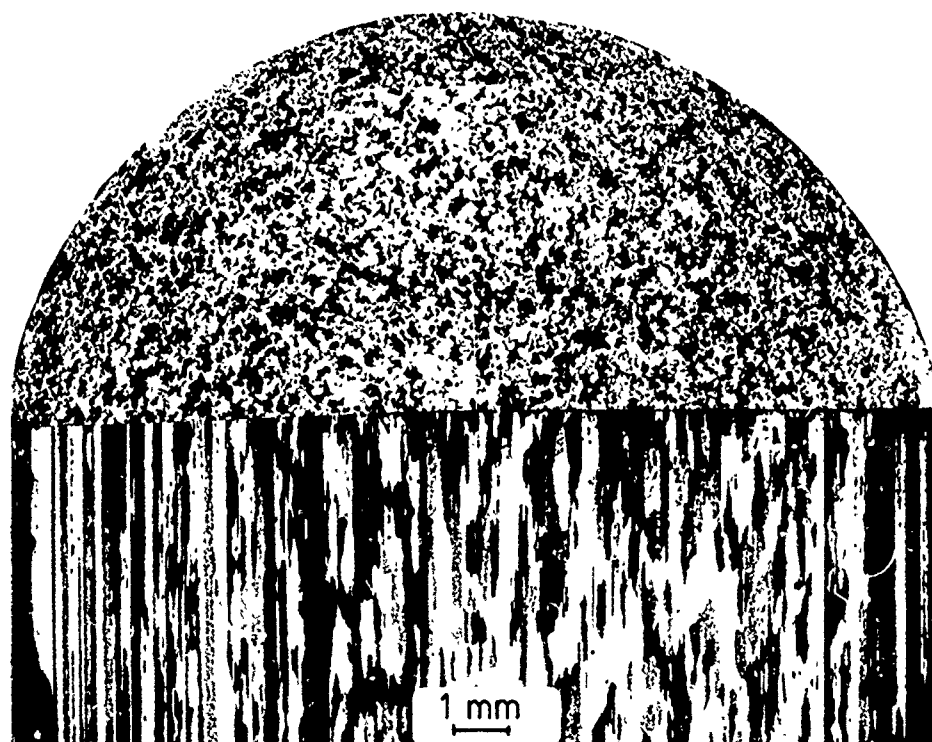


Figure 31 Notch $K_t = 3$ constant load amplitude axial fatigue response of a P/M 2024-T3510 extrusion product manufactured from powder with a 36 μm APD and with a 753 K extrusion-preheat.

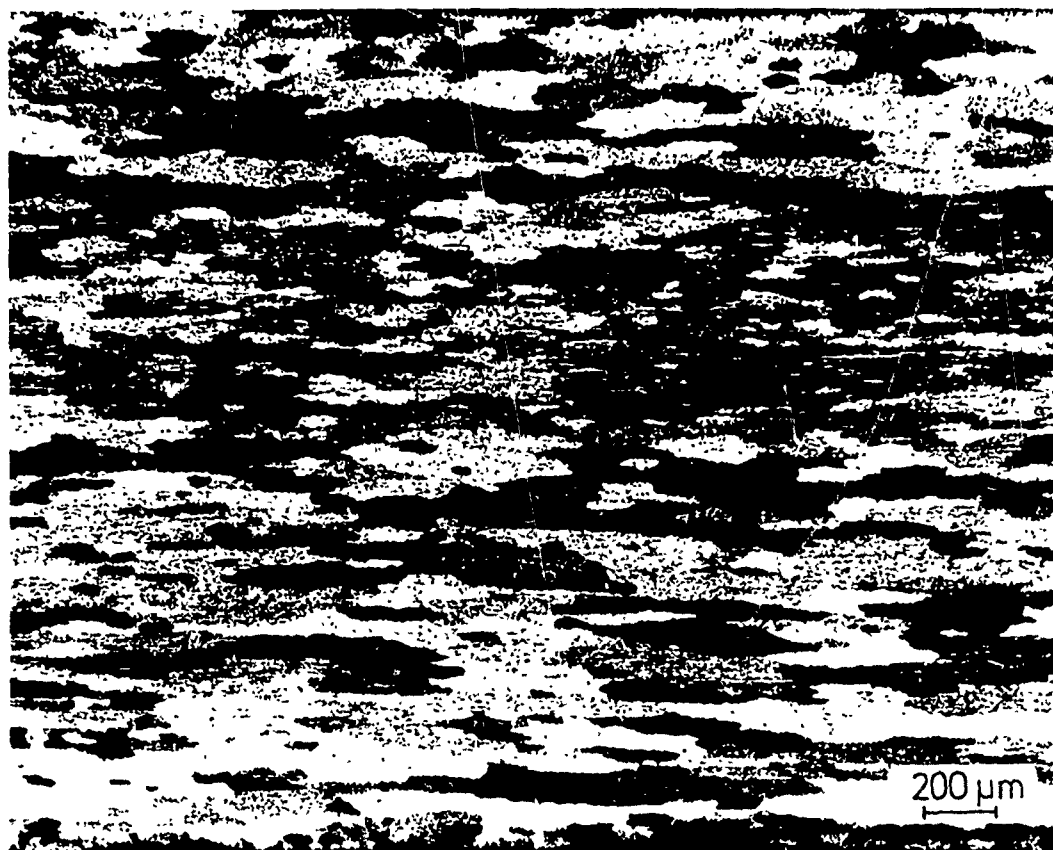
(a)



b)



Figure 32 Representative optical micrographs of the grain structure of 2024-T3510 I/M 25:1 direct extrusions etched with 10 ml HF - 5 ml HNO_3 - 90 ml H_2O : (a) alloy A (commercial product) parallel and perpendicular to the extrusion direction, also typical of alloy B (b) control alloy C (643 K extrusion-preheat) parallel to the extrusion direction.



extrusion direction

Figure 33 Representative optical micrograph of the grain structure of a 2024-T3510 P/M 26.1:1 direct extrusion, perpendicular to the extrusion direction in the web section of the extruded channel (depth: 40 mm x width: 25 mm x thickness: web 2 mm, flange 2.5 mm). etchant: 10 ml HF - 5 ml HNO₃ - 90 ml H₂O.

(a)



(b)



Figure 34 Representative optical micrographs of the grain structure of 2024-T3510 P/M 25:1 direct extrusions, with a 643 K extrusion-preheat, parallel to extrusion direction.
(a) Barker's etchant, (b) electrolytically polished, and etched with 10 ml HF - 5 ml HNO₃ - 90 ml H₂O (diluted).

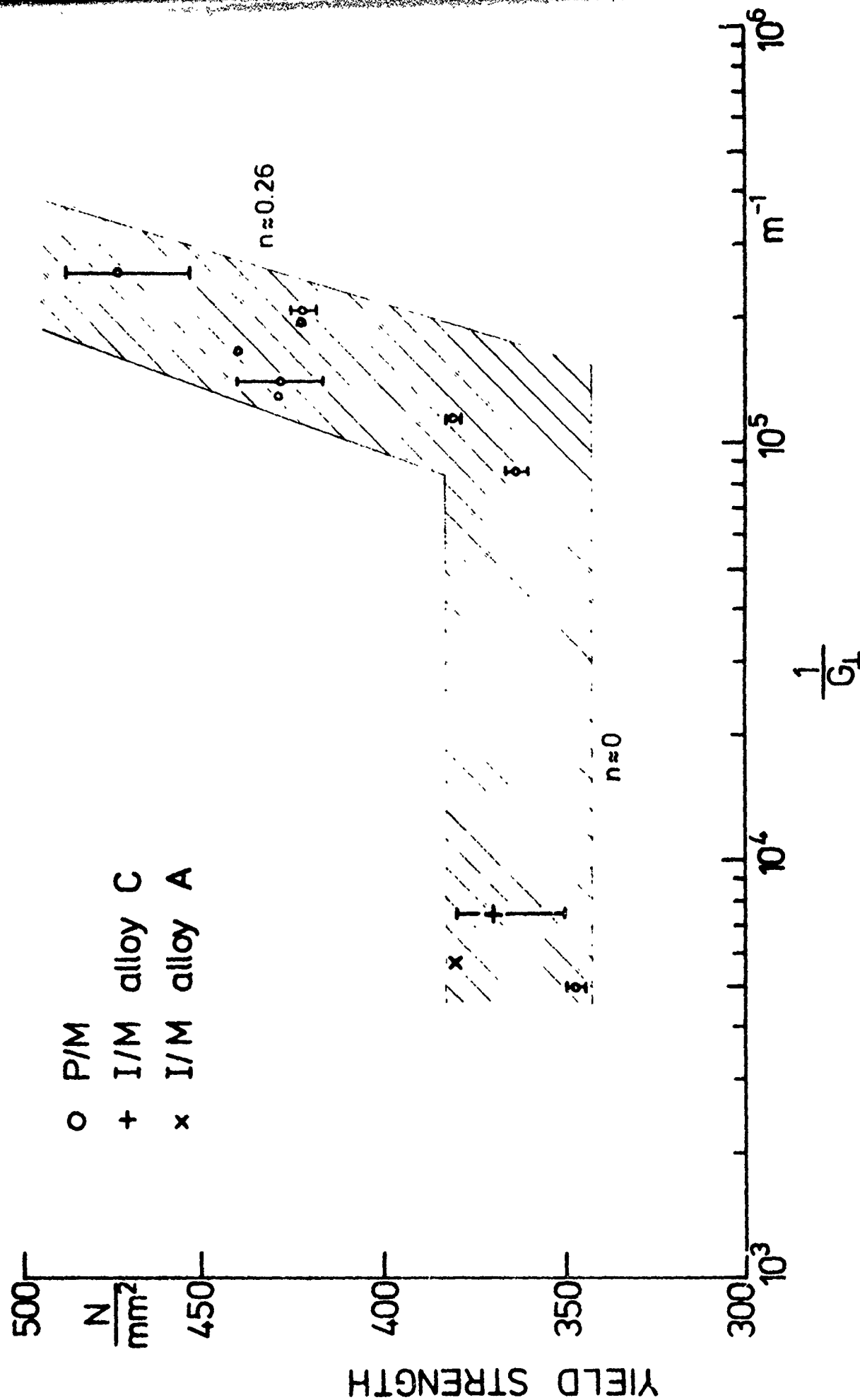


Figure 35 Longitudinal yield strength of 2024-T3510 extrusion products as a function of the reciprocal of the long transverse grain width.

alloy designation	fabrication condition	composition weight percent [%]										(balance Al)		
		Cu	Mg	Zn	Mn	Cr	Ti	Ni	Fe	Si	O ¹ .	O ² .	H ³ .	
2024 - A	I/M - Commercial Extrusion	4.80	1.58	N.D.	0.81	N.D.	N.D.	N.D.	0.34	0.27	N.D.	N.D.	0.23	
2024 - B	I/M - high purity base 99.99% Commercial Extrusion	4.10	1.50	N.D.	0.89	N.D.	N.D.	N.D.	0.25	0.20	N.D.	N.D.	N.D.	
2024 - C	I/M - 10 kg D.C.Cast Laboratory Ingot (Fe&Si content levels similar to powder)	4.42	1.50	<0.01	0.66	N.D.	0.01	N.D.	0.15	0.07	N.D.	20.4 PPM	0.22	
2024 - D	P/M APD 117 µm	4.45	1.37	0.01	0.64	N.D.	<0.01	N.D.	0.12	0.05	0.134	0.273	N.D.	
2024 - E	P/M " 82 µm	4.45	1.37	0.01	0.64	N.D.	<0.01	N.D.	0.12	0.05	0.195*	0.316	0.22	
2024 - F	P/M " 44 µm	4.46	1.51	0.02	0.73	N.D.	0.03	0.01	0.27	0.10	N.D.	0.566	N.D.	
2024 - G	P/M " 36 µm	4.45	1.37	0.01	0.64	N.D.	<0.01	N.D.	0.12	0.05	0.012	0.343	N.D.	
7075 - H	I/M - 10 kg D.C.Cast Laboratory Ingot (Fe&Si content levels similar to powders)	1.72	2.68	5.67	0.02	0.19	0.01	N.D.	0.16	0.07	N.D.	15.6 PPM	0.31	
7075 - L	P/M APD 88 µm	1.66	2.67	5.83	N.D.	0.20	0.04	N.D.	0.12	0.07	0.054	0.282	0.28	
7475 - M	I/M Commercial ingot	1.56	2.60	5.43	0.07	0.22	0.02	N.D.	0.05	0.02	N.D.	N.D.<0.20		

Notes: N.D. - not determined

* - 0.54 % in the as isostatic compacted condition, determined by standard wet analysis, prior to degassing

1. - determined by photon activation analysis
2. - " " neutron
3. - ml H₂/100 grams of the alloy at STP
- + - sieve fractionated from alloy E at 63 µm

Table 1. Chemical Analysis of powder and ingot materials as determined from the wrought aluminum products. (I/M - ingot metallurgically produced, P/M - powder metallurgically produced)

alloy	Processing Parameters		Mechanical Properties					
	charge	extrusion ratio	UTS	0.2% YS	0.2% CYS	R.A.	e	NTS
				[MPa]			[%]	[MPa]
longitudinal								
(P/M) L 7075	52	5.54:1 (81.9%)	659.0 661.4	604.5 608.5	- -	9.7 15.9	9.2 12.5	773.6 771.0
	32	10:1 (90%)	654.3 636.9 652.0 644.8	595.5 567.8 601.5 592.3	- - - -	10.8 10.5 12.8 16.8	13.1 11.9 13.2 12.1	756.9 794.8 - -
(I/M) H 7075	55	10:1	657.0 653.0	601.6 585.0	- -	12.2 15.3	7.5 11.9	777.7 802.2
	56	10:1	650.9 612.1 683.7	587.3 574.5 603.0	- - -	16.4 15.9 15.3	14.4 20.0 19.3	822.5 795.7 -
transverse								
(P/M) L 7075	52	5.54:1	580.1 574.4 582.7	514.6 515.4 517.6	- - -	5.5 4.1 4.6	5.6 3.8 5.6	- - -
	32	10:1	613.5 607.3	545.1 540.6	- -	15.0 22.8	12.5 16.3	635.2 601.9
(I/M) H 7075	55	10:1	592.0 589.9	524.5 524.0	- -	20.9 21.8	15.6 14.4	756.7 734.6
	56	10:1	585.3 588.8	513.5 517.1	- -	25.5 22.4	18.8 19.4	799.4 774.3

*NTS/YS for 10:1 extrusions was measured with sub ASTM specimens which in some cases showed excessive yielding.

Table 2: Mechanical properties of 7X75-T6 extrusions with 643 K extrusion-preheat.

alloy	Processing Parameters		Mechanical Properties					
	charge	extrusion ratio	UTS	O.2% YS [MPa]	R.A. [%]	e	NTS [MPa]	NTS/YS
(I/M) H 7075	45	25:1 (96 %)	670.1 671.4	622.6 621.7	13.8 20.8	12.5 15.4	803.6 806.3	1.29 1.30
(P/M) L 7075	38	25:1	682.4 675.3	629.4 625.1	11.4 17.6	10.4 14.8	782.8 781.8	1.25 1.25
(I/M) M 7475	57	25:1	661.3 685.7	604.2 631.4	10.2 14.7	10.0 12.5	812.8 836.7	1.32 1.35

Table 3: Longitudinal mechanical properties of 7X75-T6510 extrusions with 643 K extrusion-preheat.

Processing Parameters				Mechanical Properties				
alloy (Charge No.)	preheat temperature [K]	pressure [MPa]	dwelt time [minutes]	UTS [MPa]	O.2% YS [MPa]	R.A. [%]	e	NTS [MPa]
								NTS/YS
isotropic								
7075-T6 (31B)	733	610	10	584.4 583.7	509.4 511.4	8.7 9.5	7.1 6.1	561.8 551.1
longitudinal								
2024-T351 (27)	753	610	10	471.2 473.1	377.1 377.1	14.7 15.4	11.4 11.7	526.8 503.0
transverse								
				475.9 477.4	373.0 375.6	14.5 14.2	12.5 10.0	538.4 526.4
								1.44 1.41

Table 4: Mechanical properties (isotropic) of vacuum hot-pressed 7075-T6 and 2024-T351 products produced from air atomized, prealloyed powder. Powder parameters: 7075 88 μm APD with 26 $\%$ - 325 mesh, and 2024 82 μm APD with 28 $\%$ - 325 mesh (44 μm).

alloy	Processing Parameters		angle from extrusion direction	Mechanical Properties		
	extrusion- preheat temperature [K]	reduction in area [%]		0.2% CYS [MPa]	average 0.2% CYS [MPa]	strength deviation from longitudinal - 0° [%]
(P/M) L 7075	643	96	0° (longitudinal)	608.7	609.4	-
				603.4		
				616.0		
			45°	555.8	552.9	- 9.3
				553.6 549.4		
(I/M) H 7075	643	96	90° (transverse)	571.3	571.3	- 6.3
				575.6		
				567.0		
			0°	605.9	618.4	-
				626.5 623.9		
(I/M) M 7475	643	96	45°	511.3	504.6	-18.4
				499.2		
				503.2		
			90°	546.0	548.6	-11.3
				550.4 549.4		
(I/M) M 7475	643	96	0°	605	606.5	-
				608		

Table 5: Effect of direction on the 0.2 % compressive yield stress of 7X75-T6 extrusions.

P/M 7075-T6 Extrusion (1) Solution Heat Treatment (2) (SHT) Study

SHT (K)	longitudinal				Mechanical Properties				transverse (3)			
	UTS [MPa]	O.2%YS	R.A. [%]	e (4D)	UTS [MPa]	O.2%YS	R.A. [%]	e (4D)	UTS [MPa]	O.2%YS	R.A. [%]	e (4D)
743	673	616	18.7	12.5	-	-	-	-	-	-	-	-
	667	612	17.5	12.5	-	-	-	-	-	-	-	-
743 (3)	654	596	10.8	13.1	614	545	15.0	13.1	614	545	15.0	13.1
	637	568	10.5	11.9	607	540	22.8	11.9	607	540	22.8	11.9
753	675	624	9.1	7.9	-	-	-	-	-	-	-	-
	672	620	8.4	8.3	-	-	-	-	-	-	-	-
763	672	622	10.1	7.5	-	-	-	-	-	-	-	-
	680	626	11.1	10.0	-	-	-	-	-	-	-	-
773	671	626	15.2	14.6	-	-	-	-	-	-	-	-
783	679	629	8.6	9.2	-	-	-	-	-	-	-	-
	676	624	10.7	7.5	-	-	-	-	-	-	-	-
783 (4)	680	627	10.8	10.8	-	-	-	-	-	-	-	-
	676	623	13.7	10.4	-	-	-	-	-	-	-	-
793	679	633	9.5	8.3	612	515	25.3	12.5	612	515	25.3	12.5
	674	627	16.1	8.8	574	485	25.4	17.5	574	485	25.4	17.5

..... Ingot Properties

743	670	623	13.8	12.5	-	-	-	-
	671	622	20.8	15.4	-	-	-	-
743 (3)	657	602	12.2	7.5	592	525	20.9	15.6
	653	585	15.3	11.9	590	524	21.8	14.4

(1) 25:1 extrusions with 673 K extrusion-preheat except as noted

(2) 1h 743 K (salt) plus 5 K/hr thereafter until referenced SHT, plus 1h at SHT

(3) 10:1 extrusions with 643 K extrusion-preheat

(4) placed in salt pot and held for 1h at 778 K, plus 1h at 783 K

Table 6 Influence of elevated solution heat treatment temperature on the mechanical properties of 7075-T6 extrusions.

Product Form
7075-T6

Density
 $\times 10^3$
[kg m⁻³]

Remarks

I/M alloy H

2.80₅

P/M 25:1 extrusion

2.81₆

P/M vacuum hot-pressed

2.81₇

P/M hot isostatic pressed
(HIPped)

2.80₂

P/M vacuum hot impact
compacted

2.79₇

- low ductility

From a tensile specimen which failed during machining, an elongated pore on both halves of the fracture surface was revealed.

Table 7: Density measurements of 7075 P/M and I/M products. (7075 powder: 88 μ m APD with 26 & -325 mesh (44 μ m)).

Density measurements were made by the Archimedeian Principle in a constant temperature water bath. Each value represents a minimum of at least two measurements with the uncertainty shown by subscripting the last decimal digit.

7X75 Aluminum Alloy Extrusions

charge	alloy	\bar{L}_p^1 [μm]	VPCP ² . [vol. %]	lattice constant [10^{-10}m]	time [h]	temperature [K]	homogenization treatment ^{3,4} .
32	P/M 7075	0.406	2.3 ± 0.44	4.0545	TREATMENT A: 16 h at 733 K followed by 24 h at 743 K (Standard I/M 7075 homogenization treatment)		
55	I/M 7075	0.541	2.4 ± 0.88	4.0559			
56	I/M 7475	0.400	0.4 ± 0.22	-			
66	P/M 7075	0.364	2.3 ± 0.33	4.0557	TREATMENT B: (short time homogenization) 7.6 h at 743 K during outgassing of green compact		
67	P/M 7075	0.4425	1.7 ± 0.22	4.0548	TREATMENT C: (high temperature homogenization) 3 h at 743 K plus 3.7 h at 793 K with 1 h heating rate between the two temperatures, during outgassing of green compact		

Note: 1. mean particle intercept length after [42].
 2. VPCP values based on a 95 % confidence limit, after [35].
 3. all times plus 1 h solution heat treatment at 743 K after extrusion.
 4. for P/M products, the homogenization treatment was accomplished during outgassing of the green compact.

Table 8 Quantitative metallographic characterization of the coarse intermetallic (soluble and insoluble) particles for P/M and I/M 7X75 aluminum alloy 10:1 extrusion products.

Alloy	VPSP [%]	NTS/YS	Extrusion Ratio	Property Direction
P/M 7075-T6510	2.77	1.25	25:1	longitudinal
I/M 7075-T6510	2.4	1.30		
I/M 7475-T6510	0.4	1.34		
P/M 7075-T6	2.77	1.14	10:1	transverse
I/M 7075-T6	2.4	1.42		
I/M 7475-T6	0.4	1.53		
P/M 7075-T6	2.77	1.34	10:1	longitudinal
I/M 7075-T6	2.4	1.33		
I/M 7475-T6	0.4	1.38		

Table 9: Influence of relative amount of volume percent second phase (VPSP) on fracture toughness, as measured by notch tensile strength to yield strength ratio (NTS/YS) for various 7X75 aluminum alloy extrusion products.

Alloy	Grain Structure			Substructure			Remarks
	\bar{L} [μm]	G_{\perp} [μm]	G_{\parallel}/G_{\perp}	$\bar{\lambda}$ [μm]	g_{\perp} [μm]	g_{\parallel}/g_{\perp}	
P/M 7075	7.5	5.0	8	2.1	1.5	1.9	extrusion-preheat 643 K
I/M 7075	28.2	21.8	10.9	3.3	2.8	1.5	" "
I/M 7475	28.5	17.2	>13.6	2.7	6.4	1.2	" "
P/M 7075 SHT at 793 K	-	5.4	-	3.8	3.2	3.6	" with solution heat treatment at 793 K and 5 K/h heat up from 743 K
P/M 7075	11.9	6.2	6.5	2.6	1.8	2.1	extrusion-preheat 713 K

\bar{L} - mean grain intercept length (indication of mean grain size independent of grain shape or orientation)

G_{\perp} - average grain thickness measured perpendicular to extrusion direction

G_{\parallel}/G_{\perp} - grain size aspect ratio

α - shape parameter or degree of orientation, indicating percent of grain boundary surface area oriented parallel to the extrusion direction

$\bar{\lambda}$ - mean subgrain intercept length

g - subgrain property

Table 10 Quantitative metallographic values for the grain morphology of 7X75-T6510 aluminum alloy 25:1 extrusion products.

Effect of Compact ⁽¹⁾ -preheat Processing on Strength/Ductility of P/M 7075-T6 10:1 Extrusions

Compact Preheat		Mechanical Properties					
Temp. [K]	Environment	longitudinal			transverse		
		UTS	O.2%YS [MPa]	e(in 4D) [%]	UTS	O.2%YS [MPa]	e(in 4D) [%]
648	Vacuum	654	596	13.1	614	545	12.5
		637	568	11.9	607	541	16.3
655	Argon (10 CFH)	613	551	10.0	544	479	8.0
		614	552	10.5	543	480	8.0
		Ingot Properties					
		607	552	10.0	517	448	5.0
		657	601	7.5	592	525	15.6
		653	585	11.9	590	524	14.4

(1) 80-85 % dense compacts

Table 11 Influence of evacuation-preheat environment.

Alloy	APD [μm]	- 325 mesh fraction [%]
D*	117	3
E	82	28
F	44	50
G*	36	66

*separated by screening from alloy E at 0.063 μm .

Table 12: Characterization of 2024 alloy powders investigated for this report. Chemical analysis is given in Table 1.

Charge No.	Processing Parameters		Longitudinal Mechanical Properties					
	Extrusion- preheat	Extrusion Ratio	UTS [MPa]	0.2%YS	R.A. [%]	e	NTS [MPa]	NTS/YS
2024-T3510 (1 $\frac{1}{2}$ % tensile deformation plus 7-10 days room temperature age)								
P/M 40	643	25:1	587	461	17.2	15.6	-	-
P/M 41	643	25:1	598 576	467 453	16.9 19.9	15.0 16.3	-	-
P/M 15	643	25:1	618 620	486 488	20.0 22.1	15.0 16.3	668 610	1.37 1.39
P/M 22	753	25:1	581 582	440 440	22.1 22.2	15.8 16.7	610 612	1.39 1.39
I/M Alloy A	693-723	25:1	494 490	378 377	28.0 27.8	20.8 20.0	547 542	1.45 1.44
I/M Alloy B	693-723	25:1	522 519	378 376	41.0 41.0	23.3 25.8	572 576	1.52 1.53
I/M Control Alloy C 44			491 491	377 361	26.9 25.6	24.6 25.2	566 568	1.53 1.54
61	643	25:1	489 488	349 349	23.4 32.1	21.3 22.8	-	-
P/M 48B	643	10:1	553 531	438 412	12.0 16.6	13.1 15.6	-	-

Table 13 Natural aging response of P/M and I/M 2024-T3510 aluminum alloy extrusion products manufactured with various extrusion-preheat temperatures and extrusion ratios. P/M extrusion products were made from alloy E powder.

Charge No.	Processing Parameters		Mechanical Properties					
	Extrusion-preheat	Extrusion Ratio	UTS [MPa]	O.2%YS [MPa]	R.A. [%]	e	NTS [MPa]	NTS/YS
2024-T4 (7-10 days room temperature age)								
longitudinal properties								
P/M 41	643	25:1	576 573	421 419	18.3 19.0	18.1 19.4	-	-
P/M 16	753	25:1	561 554 554	393 391 395	21.1 34.2 25.6	20.0 20.8 17.9	-	- 1.54
P/M 22	753	25:1	561	401	17.7	16.7	603	1.50
I/M Alloy B	693-723	25:1	482 484	282 288	42.2 41.3	25.4 27.5	-	-
P/M 49	643	10:1	553 569	374 406	19.1 17.5	21.9 16.9	726 619	1.86 1.59
I/M-Control Alloy C 54	643	10:1	461 469 476	299 282 294	19.1 24.7 21.7	21.9 23.1 20.6	544 562	1.86 1.93
transverse properties								
P/M 49	643	10:1	507 505	356 353	23.7 28.4	23.1 23.8	619 617	1.75 1.74
I/M-Control Alloy C 54	643	10:1	475 478 470 490	311 303 301 305	15.7 13.9 17.7 15.4	20.0 21.3 19.4 18.1	583 588	1.91 1.93

Table 14 Natural aging response of P/M and I/M 2024-T4 extrusions manufactured with various extrusion-preheat temperatures and extrusion ratios. P/M extrusion products were made from alloy E powder.

Charge NO.	Processing Parameters		Longitudinal Mechanical Properties			
	Extrusion- preheat [K]	Extrusion Ratio	UTS [MPa]	O.2%YS [MPa]	R.A. [%]	e
			2024-T6 (12 h 464 K)			
P/M 41	643	25:1	476 480	379 383	41.5 38.2	11.3 12.9
P/M 16	753	25:1	467 472	363 368	37.2 43.5	15.0 15.4
			438 462	349 364	40.0 38.0	13.8 -
I/M ⁽¹⁾ Alloy A	693-723	25:1	497 498	344 344	24.9 23.3	17.9 17.5
I/M Alloy A	693-723	25:1	499 497	379 371	23.6 21.8	10.8 13.3
I/M Alloy B	693-723	25:1	474 462	371 377	38.6 40.0	13.3 15.0

(1) 7 h 464 K

Table 15 Artificial aging response of P/M and I/M 2024-T6 aluminum alloy extrusion products manufactured with a 25:1 extrusion ratio and various extrusion-preheat temperatures. P/M 2024 extrusion products were made from alloy E powder.

Charge No.	Processing Parameters		Mechanical Properties			
	Extrusion- preheat	Extrusion Ratio	UTS [MPa]	O.2%YS [MPa]	R.A. [%]	e
2024-T8510(1 $\frac{1}{2}$ % tensile deformation plus 11 h 464 K)						
longitudinal properties						
P/M 41	643	25:1	498 500	445 446	29.8 23.3	13.1 10.4
P/M 16	753	25:1	489 490	429 429	40.4 44.3	14.6 15.4
I/M-Control			512	464	34.5	11.8
Alloy C 61	643	25:1	502 510 514	455 461 465	27.3 37.4 34.6	16.3 13.8 11.9
I/M Alloy B	693-723	25:1	501 501	464 461	37.3 38.4	13.8 14.2
P/M 48B	643	10:1	483 490	424 432	21.7 27.5	10.0 10.6
I/M-Control Alloy C 62	643	10:1	518 507	490 474	32.4 35.1	15.0 15.0

Table 16 Artificial aging response of P/M and I/M 2024-T8510 aluminum alloy extrusion products manufactured with various extrusion-preheat temperatures and extrusion ratios. P/M extrusion products were made from alloy E powder.

Charge No.	Processing Parameters		Mechanical Properties					
	Extrusion-preheat	Extrusion Ratio	UTS [MPa]	O.2%YS [MPa]	R.A. [%]	e	NTS [MPa]	NTS/YS
2024-T8520(2 % plastic deformation plus 11h 464 K)								
longitudinal properties								
I/M Alloy C 54	643	10:1	528	497	24.0	10.6	684	1.38
			528	493	33.8	11.9	684	1.38
			transverse properties					
			518	483	9.4	4.4	691	1.44
2024-T8540(4 % plastic deformation plus 11h 464 K)								
longitudinal properties								
P/M 49	643	10:1	517	468	16.0	12.5	692	1.48
			515	465	18.9	11.9	697	1.50
P/M 40	643	25:1	505	457	46.1	14.7	-	-
			510	463	47.0	14.4	-	-
transverse properties								
P/M 49	643	10:1	501	453	22.8	12.5	690	1.52
			500	457	31.5	11.9	690	1.52

Table 17 Response of P/M and I/M 2024 aluminum alloy extrusion products manufactured with 643 K extrusion-preheat and various extrusion ratios, to thermal mechanical treatments (TMT) of 2 and 4 % tensile plastic deformation before artificial aging. P/M extrusion products were made from alloy E powders.

Charge No.	Processing Parameters		Mechanical Properties			
	Extrusion- preheat	Extrusion Ratio	UTS [MPa]	O.2%YS [MPa]	R.A. [%]	e
			2024-T8570(7-8 & plastic deformation plus 8h 464 K)			
			longitudinal properties			
P/M 16	753	25:1	522 522	481 479	44.9 41.1	14.2 13.8
I/M Alloy B	693-723	25:1	534 534	504 506	34.9 36.9	12.9 12.9

Table 18 Response of P/M and I/M 2024 aluminum alloy extrusion products manufactured with a 25:1 extrusion ratio and various extrusion-preheat temperatures, to thermal mechanical treatment (TMT) of 7-8 & tensile plastic deformation before artificial aging. P/M extrusion products were made from alloy E powders.

Effect of Initial APD on Longitudinal Mechanical Properties of P/M 2024-T4
(753 K Extrusion-Preheat with 25:1 Ratio)

Alloy (APD)	Charge No.	UTS [MPa]	0.2%YS [MPa]	R.A. [%]	e (in 4D) [%]	NTS [MPa]	NTS/YS	oxygen content [wt.%]	density 10^3 [kg·m ⁻³]
D (117 μm)	19	556	398	24.3	22.5	535	1.34	.273	2.796
		559	400	29.2	20.0	539	1.35		
E (82 μm)	22/16	553	393	21.1	20.0	610	1.54	.316	2.793
		561	401	17.7	16.7	603	1.52		
F (44 μm)	48A	533	384	19.7	20	581	1.50	.566	2.796
		540	391	16.1	14.6	598	1.54		
G (36 μm)	26	549	391	28.1	20.4	522	1.39	.343	2.800
		545	390	27.6	22.1	523	1.38		

Table 19 Longitudinal mechanical properties of P/M 2024-T4 extrusion products.
Alloys D and G were sieved from alloy E

Effect of Initial APD on Transverse Mechanical Properties of P/M 2024-T4
(753 K Extrusion-Preheat with 10:1 Ratio)

Alloy (APD)	Charge No.	UTS [MPa]	0.2%YS [MPa]	R.A. [%]	e (in 4D)	NTS [MPa]	NTS/YS
D (117 μ m)	58	516	354	25.0	23.1	614	1.73
		532	355	28.7	25.6	620	1.75
E (82 μ m)	49	507	356	23.7	23.1	620	1.75
		505	353	28.4	23.8	617	1.74
F (44 μ m)	48B	513	366	20.6	20	599	1.64
		508	362	17.9	19.4	647	1.78

Table 20 Transverse mechanical properties of P/M 2024-T4 extrusion products.
Alloy D powder particles > 63 μ m.

2024 Aluminum Alloy Extrusions

Charge	Alloy	\bar{L}_p ^{1.} [μ m]	VPCP ^{2.} [vol. %]	lattice constant [10^{-10} m]	time [h]	homogenization treatment ^{3.} temperature [K]
41	P/M E	0.329	2.6 \pm 0.44	4.0512	TREATMENT A: 24 h at 766 K (Standard I/M 2024 homogenization treatment)	
44	I/M C	0.611	3.3 \pm 0.64	4.0500		
-	I/M A	0.895	3.9 \pm 0.49	4.0489		as received from supplier - VAW
65	P/M E	0.409	6.5 \pm 0.46	-	TREATMENT B: (short time homogenization) 7 h at 766 K	
64	P/M E	0.442	2.7 \pm 0.41	-	TREATMENT C: (high temperature homogenization) 4 h at 766 K plus 5 h at 793 K with 1 h heating rate between the two temperatures	

Note: 1. mean particle intercept length after [42].
 2. VPCP values based on a 95 % confidence limit, after [35].
 3. all times plus 1 h solution heat treatment at 743 K after extrusion.
 4. for P/M products, the homogenization treatment was accomplished during outgassing of the green compact.

Table 21 Quantitative metallographic characterization of the coarse intermetallic (soluble and insoluble) particles for P/M and I/M 2024 aluminum alloy 25:1 extrusion products.

Alloy	Grain Structure		Substructure $\bar{\lambda}$ [μm]	Remarks*
	\bar{L} [μm]	G_L / G_L [μm]		
P/M E	6.7	3.9	2.2	extrusion preheat 643 K
P/M E	7.1	4.9	-	" 643 K (1)
P/M G	7.2	5.2	-	" 753 K
P/M E	8.6	6.0	2.4	" 753 K
P/M E	10.0	8.8	-	" 613 K
P/M F	10.8	6.5	-	" 753 K
P/M D	14.6	7.9	-	" 753 K
P/M E	5.1	11.8	-	" 753 K (2)
P/M E	63.5	44.4/200	-	" 643 K (3)
I/M C	178.0	137.0	-	" 643 K
I/M A	187.0	176.0	-	" 693 - 723 K

*all products were given homogenization treatment A and produced as round (ϕ) products manufactured with a 25:1 extrusion ratio unless otherwise specified
(1) ϕ 16 product given homogenization treatment B (short time homogenization)

(2) equal angle extrusion product (flange 30 mm x thickness 4 mm) with a 22.44:1 extrusion ratio
(3) channel product (depth 40 mm x width 25 mm x thickness: flange 2.5 mm and web 2.0 mm) with a 25.78:1 extrusion ratio.

Table 22 Quantitative metallographic values for the grain morphology of P/M and I/M 2024-T3510 aluminum alloy extrusion products.

Alloy	$\bar{L}^{(1)}$ [μm]	$G_L^{(2)}$ [μm]	Structure	UTS [MPa]	0.2%YS	e [%]
(P/M)E	6.7	3.9	partially recrystallized (2%)	598 576 618 620	467 453 486 488	15.0 16.3 15.0 16.3
(P/M)E	8.6	6.0	unrecrystallized	581 582	440 440	15.8 16.7
(P/M)E	10.0	8.8	partially recrystallized (50%)	498 493	381 377	20.8 21.3
(P/M)E ⁽³⁾	63.5	44.4 200.	completely recrystallized	443 442	349 344	17.6 18.6
(I/M)C	178.	137.	completely recrystallized	491 491	377 361	24.6 25.2

- (1) average linear intercept on a plane parallel to the extrusion axis
(2) grain width perpendicular to extrusion direction on same plane as for \bar{L}
(3) channel product, with a long and short transverse perpendicular grain width

Table 23 Effect of microstructure on longitudinal mechanical properties of 2024-T3510 extrusion products, with 25:1 ratio for round (ϕ 16) and 25.78:1 for the channel.